MSC THESIS

STABILITY OF ROCK ON MILD SLOPES UNDER WAVE ATTACK

Delft University of Technology

Faculty of Civil engineering, Department of Hydraulic Engineering

Name: Roy Kramer

Student number: 4022246

Date: 8 December 2016

TU Delft Delft University of Technology

de Vries & van de Wiel
Dredging & Environmental Solutions

GRADUATION COMMITTEE

CHAIR

Prof. Dr. Ir. W.S.J. Uijttewaal
Professor of Experimental Hydraulics
Delft University of Technology

BOARD MEMBERS

Ing. C. Kuiper
Guest lecturer
Delft University of Technology

Dr. Ir. B. Hofland
Assistant Professor of Coastal Engineering
Delft University of Technology

Ir. D. Jumelet
Project Engineer
De Vries & van Wiel

PREFACE

The thesis is part of the curriculum at the Technical University of Delft, faculty of Civil Engineering. This research is in continuation of the research of Marieke Wit [2015] and Mark Postma [2016]. Both have done numerical testing on the subject, with X-Beach G, their research forms the starting point of my research.

This research has come together with the help of my graduation committee, who have kept me on the right track during the writing of my thesis. I would like to thank Daan Jumelet, for the daily supervising and warm welcome at the company 'de Vries en van de Wiel'. Your positive criticism has helped me through the process of writing my thesis. From Delft University of Technology, I would like to thank Coen Kuiper for helping me get on the right track in the beginning of my thesis and keeping me on track during the rest of my thesis. Furthermore, I would like to thank Bas Hofland for his endless enthusiasm and helping me out with the processing of all the data that was gathered during the tests in the laboratory. Also, I would like to thank Wim Uijttewaal for his guidance in the committee meetings. Furthermore, I want to thank Sander de Vree, who supervises the fluid mechanics lab, for his help and guidance throughout the experiments and at last all the other staff in the lab who helped me out during the experiments.

During my experiments, I have had the help of my brother, Tim Kramer, who helped me clean the stones for my experiments and Yueqian Shen, who has helped me with the 3D scans of the slopes. Yueqian also helped out with the pre-processing of the data gathered by the 3D scanner. Therefore, I would also like to thank you both.

The writing of this thesis is done with the support and facilities of both the Delft University of Technology as well as the company 'de Vries & van de Wiel'.

Roy Kramer

8 December 2016

ABSTRACT

Momentarily the determination of the static stability of rock on mild slopes can be split in roughly two paths, the empirical and the physical approach. However, both the approaches have their limitations from which one could conclude that neither approach is currently an accurate description of the stability of rock on mild slopes under wave attack. The empirical approach by van der Meer [1988] has to be extrapolated outside its validity region and is deemed to be too conservative by Schiereck and Fontijn [1996]. The physical approaches on which the software XBeach-G[1], runs are capable of globally determining dynamic profile response reasonably well however they cannot accurately determine static stability.

Wit [2015] looked into the applicability of XBeach-G on the design of rock armour coastal protections. She examined the use of XBeach-G on homogeneous structures. Wit [2015] found promising good results for homogeneous structures. Postma [2016] further examined XBeach-G, looked into the applicability to inhomogeneous structures and different modelling approaches within XBeach-G. The results of Postma [2016] showed irregularities and raised more question marks. Inconsequently good results were found for Xbeach-G's two different physical approaches, the Nielsen [2006] and the Van Rijn [2007] approach. From this lack of an accurate approach to determine the stability of rock on mild slopes under wave attack, follows the research question of this thesis: *"How should the stability or rock on mild slopes be described?"*

To determine how to describe the stability of rock on mild slope under wave attack, a test plan was set up. The test plan was split into two parts, firstly the empirical approach and secondly the physical approach. The empirical approach is based around the formula of Van der Meer [1988] for plunging waves. The key principle of the tests is to measure the change of profile, over the duration of a wave series consisting of 3000 irregular waves. A 3D scanner, a Leica C10, scanned the slope pre- and post-wave series. By evaluating the differences in the slope between the two scans, damage characteristics were determined. The damage level 'S' as used in the Van der Meer [1988] formula and the damage depth 'E_3' as was proposed by Hofland et al [2011]. Three different slopes were tested (cotα=5, 10 & 15), with for each slope two wave series.

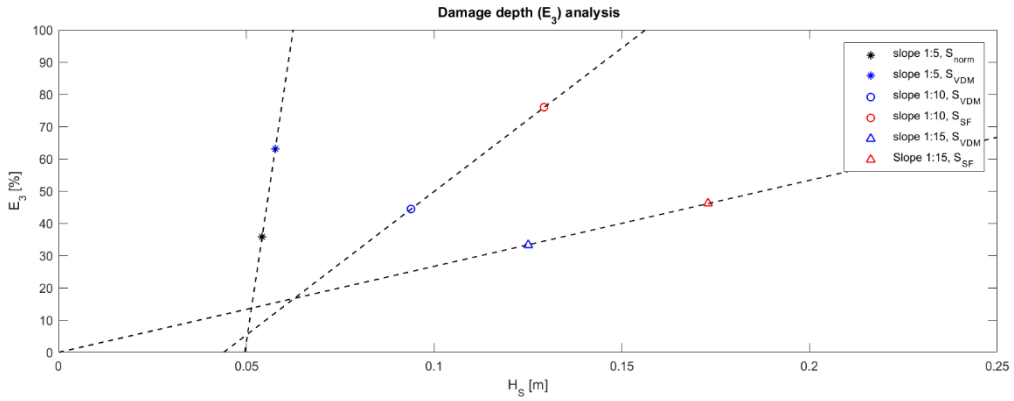

FIGURE 1 - DAMAGE DEPTH E_3 [-] VS. WAVE HEIGHT [M]

With the research was found that for very mild slopes (in this research cotα= 15), the damage level 'S' does not suffice to describe the damage. For the 1:15 slope the damage level did not increase with the wave height, profile change was scattered randomly and did not form an erosion profile. For the other mild slope (cotα= 10), it was found that the Van der Meer [1988] indeed is too conservative for mild slopes. More useful was the damage depth 'E_3', that did increase with

[1] XBeach-G is a side branch of XBeach, developed by Robert McCall [2015]. XBeach-G uses the one-layer, depth averaged, non-hydrostatic extension of the XBeach model.

increasing wave height. See figure 1. Trendlines have been drawn for each slope that was tested in the figure. These trendlines indicate that the damage depth increases with increasing wave height. However this ratio is different per slope angle. This difference in ratio can be explained by the spreading of the wave energy dissipation, as on milder the slopes the wave energy spreads out over a longer part of the profile than it does on steeper slopes. Therefore also the trendlines are milder for the mild slopes and steeper for the steep slopes.

Secondly tests to examine the two physical approaches have been done. Here a combination of BIV and PIV has been used. The use of this combination of techniques allows to get detailed flow patterns close to the bottom throughout the entire wave cycle. From these flow patterns the parameters for the two physical approaches, Nielsen [2006] and Van Rijn [2007] can be determined. Both formulae will have exactly the same input. Furthermore, where Xbeach-G uses fixed values for certain parameters, these parameters can now exactly be determined. The BIV/PIV tests will be done on three different slopes ($\cot\alpha$= 5, 10 & 15), with regular waves. The wave characteristics are chosen such that they represent the waves under which incipient motion is found.

With all the parameters accurately determined, as was done during this analysis, the results of Nielsen [2006] and Van Rijn [2007] were both analysed quantitatively and qualitatively. The Van Rijn [2007] approach gives Shields values of roughly 0.055, which coincides with Shields's stage 6 transport. Whereas the approach based on Nielsen [2006] results in Shields values of around 0.035 (i.e. Shields's stage 1). This would indicate occasional movement at some locations.

The Nielsen [2006] approach results in Shields value just around the Shields's first stage of movement, which is an underestimation of the displacement. This conclusion is based on the visual observations during the profile change tests, in which significant movement was observed during the highest waves of the spectrum. The Van Rijn [2007] approach does describe this type of movement and therefore, based on the visual observations together with test results, gives the most reliable results. Note that, the results of the Nielsen [2006] formula also strongly depend on the accuracy of the input parameters; the phase lag angle (φ) and the sediment friction factor (f_s). In Xbeach-G these paramaters are commonly based on standard values, when substituing these values in the Nielsen [2006] formula the results strongly differ and give an unrealistic outcome.

Concluding on the test results, the empirical Van der Meer [1988] gives good results for slopes up to 1:10. For slopes milder than 1:10, the damage should no longer be described by the damage level 'S'. A good alternative seems to be the damage depth 'E_3'. The fact that 'S' no longer is a proper way to determine the damage, suggests that the Van der Meer [1988] formula should not be used for mild slopes any more. However, for all cases the extrapolation of Van der Meer [1988] results in (very) conservative approach and can therefore still be used in this form. The Van Rijn [2007] approach seems to be preferable over the Nielsen [2006] approach, because the Van Rijn [2007] approach aligns with the visual observations and profile change measurements. Apart from better results, the Van Rijn [2007] is more pragmatic than the Nielsen [2006] approach. This is because the parameters used in Van Rijn [2007] can easily be determined with basic details of the slope, whereas the Nielsen [2006] approach significantly depends on the accuaracy of the parameters (φ and f_s), which both have been proven hard to determine.

Keywords

- Mild slopes
- Rock protection
- Wave attack
- Damage definition
- Xbeach-G
- 3D profile scans
- BIV/PIV analysis
- Van der Meer [1988]
- Nielsen [2006]
- Van Rijn [2007]

LIST OF SYMBOLS AND ACRONYMS

SYMBOL	DESCRIPTION	UNIT	SYMBOL	DESCRIPTION	UNIT
A_e	Eroded Area	[m^2]	α	Slope angle	[-]
A	Exposed area	[m^2]	$\boldsymbol{\beta}$	Slope angle	[-]
c	Coefficient	[-]	Δ	Relative weight	[-]
c_f	Friction coefficient	[-]	ρ	Density	[kg/m^3]
D	Stone size diameter	[m]	ξ	Surf simularity	[-]
D_{50}	Average stone diameter	[m]	$\boldsymbol{\theta}$	Shields value	[-]
D_{n50}	Nominal stone diameter	[m]	$\boldsymbol{\theta'}$	Slope corrected Shields value	[-]
d_e	Erosion depth	[m]	$\boldsymbol{\tau}$	Shear stress	[N/m^2]
E_3	Damage depth	[m]	$\boldsymbol{\varphi}$	1. Angle of repose	[-]
E_{wave}	Wave energy	[Nm]		2. Phase lag angle	[-]
f_s	Sediment friction factor	[-]			
g	Gravitation acceleration	[m/s^2]			
h	Water depth	[m]			
H	Wave height	[m]			
H_s	Significant wave height	[m]			
$H_{1\%}$	Highest 1% waves	[m]			
L	Length	[m]			
N	Number of waves	[-]			
P	Notional Permeability	[-]			
S	Damage level	[-]			
T	Wave period	[s]			
T_m	Mean wave period	[s]			
T_p	Peak wave period	[s]			
u	Velocity	[m/s]			
u_∞	Free stream velocity	[m/s]			
u_*	Shear velocity	[m/s]			
V	Volume	[m^3]			

ACRONYM	DESCRIPTION
BIV	Bubble Image Velocimetry
DOF	Depth of Field
FOV	Field of View
fps	Frames per second
PIV	Particle Image Velocimetry
RGB	Red Green Blue
ROI	Region of Interest
SWL	Still Water Level

CONTENTS

1. INTRODUCTION

In this chapter a brief introduction to this report shall be presented. Starting with a concise elaboration of background information and the problem analysis. From this problem analysis follows the objective and thereafter the approach of this research. In order to specify further what will and what will not be part of this research in the last paragraph the scope will be elaborated.

1.1 BACKGROUND INFORMATION

De Vries & van de Wiel, a Dutch contractor, was assigned to install a rock coastal protection on the foreshores of the Eastern Scheldt. These foreshores have a mild slope. The contract had strict requirements concerning the design, the design formulae that was prescribed was the Van der Meer [1988] formula. This resulted in a coastal protection with rather large rocks. This was the reason that further research has started regarding the stability of rock on mild slopes. In which the definition of mild slopes are slopes of 1:5 and milder, thus steep slopes are defined as steeper than 1:5 slopes.

In order to protect the coastline and coastal structures against erosion, many forms of protection have been used over the years, one of those shore line protection methods is the use of rocks. For these kinds of structures stability can be described in statically and dynamically. Static stability means that none or very little damage is allowed, whereas dynamically stable entails that the profile is allowed to change to its equilibrium profile under storm conditions. The latter can only be applied with a significant layer thickness of the slope protection. This thesis focusses on the static stability.

Many researchers have already dedicated their time to research the static stability (as well static as dynamic) of gravel/rock on slopes (e.g. Van der Meer [1988], Hudson [1953]). Of those methods van der Meer [1988] is the methodology that is most frequently used for rock slopes under wave attack. However, the Van der Meer [1988] formula is only validated for relative steep slopes, for this reason the formula is extrapolated towards the milder slopes. The validity of this extrapolation is questionable, and results of Schiereck & Fontijn [1996] suggests that this extrapolation is indeed too conservative.

In order to get into more depth on this subject two students from the Delft University of Technology dug in to this matter. Both Marieke Wit and Mark Postma wrote their master thesis on the stability of rock on mild slopes under wave attack. Marieke Wit [2015] looked into the applicability of XBeach-G[2] on the design of rock armour coastal protections. She examined the use of XBeach-G on homogeneous structures. For these cases the model appeared to give reasonably good results, this was the reason to continue research with Mark Postma [2016]. Postma [2016] further examined XBeach-G, looked into the applicability to inhomogeneous structures and different modelling approaches within XBeach-G. Whereas the results of Wit [2015] were promising, the results of Postma [2016] showed irregularities and raised more question marks. With these results the decision was made that 'the stability of rocks on mild slopes under wave attack' should be further investigated.

[2] XBeach-G is a side branch of XBeach, developed by Robert McCall [2015]. XBeach-G uses the one-layer, depth averaged, non-hydrostatic extension of the XBeach model.

1.2 PROBLEM ANALYSIS

Momentarily the determination of the stability of rock on mild slopes can be split in roughly two paths, the empirical and the physical approach. However, both the approaches have their limitations from which one could conclude that neither approach is currently an accurate description of the stability of rock on mild slopes under wave attack. The empirical approach by van der Meer [1988] has to be extrapolated outside its validity region and the physical approaches on which the software XBeach-G runs are capable of globally determining profile changes reasonably well however they cannot accurately determine stability.

Van der Meer [1988] has a validated range for slope angles up to 1:6 (inhomogeneous) and 1:2 (homogeneous). Currently when designing rock protections on slopes milder than the above-mentioned slopes, the Van der Meer formulae [1988] are extrapolated. Schiereck & Fontijn [1996] already found that for a decreasing surf similarity (ξ) the stability increased. Wit [2015] also found these results when she derived the stability from the damage factor (S) in XBeach-G. See the results Schiereck & Fontijn [1996] as well as the results of Wit [2015] in Figure 1.1.

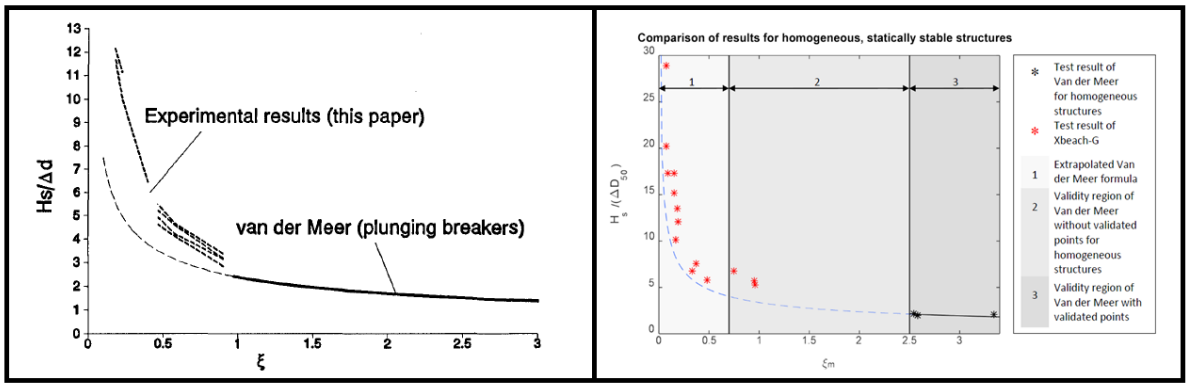

FIGURE 1.1 – RESULTS OF SCHIERECK & FONTIJN [1996] (LEFT) AND RESULTS OF WIT [2015] (RIGHT)

When applying the model XBeach-G one should on the first-hand note that the aim of the programme is to determine the profile response of the beach in question under certain (storm) conditions. From this however the eroded area can determine the damage factor ($S = A_e/d_{n50}^2$). When implementing this into the van der Meer formula [1988], the results can be compared. This method was applied by Wit [2015] and showed reasonably good results for homogeneous structures.

Furthermore, difficulties arise when zooming into the physical background of Xbeach-G. The morphodynamics are modelled in two ways, a choice can be made between the sediment transport formula of van Rijn [2007] or Nielsen [2006]. Both methods were adapted from their original purpose to fit the situation of rock on mild slopes under wave attack. Postma [2016] found that both methods give inconsequently better or worse results. Van Rijn [2007] uses a morphodynamic approach which starts with the forcing i.e. the bed shear stress, van Rijn [2007] states that this bed shear stress is caused by two components, the drag part and the inertia part. This approach originally written for the sediment transport of sand under uniform flow, hence it is arguable that when applying to rock on a slope under wave forcing this is still valid. Nielsen [2006] defined the forcing of the sediment by the shear velocity. The shear velocity in this case is defined by roughly determined parameters which have a significant influence on the outcome. Therefore, the results greatly depend on the accuracy of these parameters.

1.3 OBJECTIVE

The aim of this research is to determine a more accurate way to formulate and design a rock armour on a mild slope under wave attack. In order to do so both physical and empirical approaches will be examined, ultimately leading towards a comparison between the different approaches. Rewriting the aim of this research into separate research questions results in the following, with the main research question boxed in followed by 3 sub-questions.

How should the stability of rock on mild slopes under wave attack be described?

- Is the extrapolation of van der Meer [1988] an accurate way to define stability of rock on mild slopes under wave attack?
- How do Nielsen [2006] and Van Rijn [2007] combined with the modified Shields parameter, as used by McCall [2015] comply with the test results?
- Could the previously mentioned methodologies (i.e. Van der Meer [1988], van Rijn [2007] and Nielsen [2006]) be improved based upon the data gathered from the test series?

1.4 APPROACH

In order to answer the research questions a solid approach should be made. A concise version of the approach will be given here, whereas a more elaborated break down is given in chapter 3, Methodology. In rough lines the test series are split into two different phases, the first phase focusses on the empirical Van der Meer [1988] approach. Whereas the second part of the research, emphasizes the physical processes around the movement of stones.

For this research on the stability of rock on mild slopes under wave attack, three different slopes will be submitted in a series of tests. Per slope two different wave heights will be tested, both creating a different amount of damage. For phase one a laser scanner will be used to measure the profile pre- and post-wave series. By comparing the two scans directly, a 3D image of the erosion and accretion on the slope can be produced. From this, the average profile change can be determined, which can be translated to the damage characteristics. With the damage characteristics, the results from the test can be directly compared with the theory, i.e. the Van der Meer [1988] formulae.

Phase two will done by the means of a combination of Bubble Image Velocimetry (BIV) and Particle Image Velocimetry (PIV). Using these techniques gives a good insight of the flow patterns, velocity and acceleration near the bottom, where conventional velocity measurements are unable to measure close to the bottom. Using the combination of BIV and PIV results in an accurate measurement in the aerated state of the water as well as the non-aerated state during the return flow. PIV as well as BIV measurements result in a vector-field in the field of view (FOV). By aiming the camera, the FOV can be altered and set to the region of interest. Bubbles as well as the particles are visualized by the means of powerful LED lights.

2. LITERATURE REVIEW

In this chapter a concise review of the existing literature and knowledge on this subject will be given, in a discussion of this literature will be reviewed. From this discussion, a list of governing variables shall be derived.

2.1 EXISTING LITERATURE

In this paragraph a concise break-down of the most relevant existing literature shall be given. Starting with a general introduction the rest shall be done in chronological order.

The stability of stones is all about the balance of forces, however every stone is of different shape, size and protrudes in a different way. From this first notion one can describe the balance of stones in two different ways, Izbash [1935] reasoned that all stones must have a critical value of velocity at which the stone is no longer in equilibrium, i.e. the stones start to move. Where Izbash looked at the balance of forces on a single grain, Shields [1936] approach considered a larger area. He considered the friction forces caused by the water on the bed, thus the area to be significantly larger than for a single grain. Shields value stated that when this friction force exceeds a certain value the bed will start to erode, hence the grains will start to move.

Van der Meer [1988] is the most common way to describe the stability of rock on slopes under wave attack. Van der Meer divided the profile stability into two parts, static stability and dynamic stability. This research relates to the static stability. Static stability is determined by the amount of damage, which is defined in the damage level, see Equation 2.1. Static stability is defined by the occurrence of acceptable damage, which defined as S<2, for steep slopes. For milder slopes Van der Meer already suggests that the acceptable damage level might be higher than two.

$$S = \frac{A_e}{D_{n50}^2} \qquad \text{Equation 2.1}$$

Van der Meer described the stability, with dependence on the type of wave breaking. Different formulae for plunging and surging type of wave breaking, however no formula for the spilling type of wave breaking. Since surging type of waves are only occurring on steeper slopes, the formula for plunging type of wave breaking is most relevant and given in Equation 2.2.

$$\frac{H_s}{\Delta \cdot d_{n50}} = 6.2 \cdot P^{0.18} \cdot \left(\frac{S}{\sqrt{N}}\right)^{0.2} \cdot \xi^{-0.5} \qquad \text{Equation 2.2}$$

The Van der Meer [1988] formula for plunging waves has a validated range from 1:2 to 1:6 slopes for inhomogeneous structures. The same type of structures that is used in this research.

Schiereck & Fontijn [1996] found that for breaking waves no existing relations can be used to describe the describe the stability on mild slopes. They tried to connect a physical description of the occurring phenomena with the test results. The experimental results on stability on mild slopes from Sistermans [1993] and Ye [1996] were used by Schiereck & Fontijn [1996]. A provisional empirical design rule was established. The data results of the research used by Schiereck & Fontijn, used a different definition of damage. They used coloured strips and counted the amount of stones that displaced over the entire slope, they stated that 0,5% of displacement of the stones would indicate incipient motion (comparable with S=2). The results were consistent with the existing Van der Meer [1988] formula, but are not accurate enough to be applied as design formula.

Tromp [2004] did research on the influence of acceleration on the threshold of motion. He found that the acceleration plays a significant role in the incipient motion of rocks on mild slopes. By altering the wave steepness and keeping the wave height constant, he created situations with constant velocities but altering accelerations. A critical value for the acceleration was found for which stones starting moving, with constant velocity. It appeared that stones started moving roughly 0.05-0.15 seconds before passing of the wave top. This is also the moment on which both velocity and acceleration have high values. He described the forces by the means of a Morison-like formula, see

$$F = \frac{1}{2} \cdot C_B \cdot \rho \cdot A \cdot U \cdot |U| + C_M \cdot V \cdot \frac{dU}{dt} \qquad \text{Equation 2.3}$$

With U is the horizontal velocity, C_B represents the friction coefficient and C_M is a bulk constant, that represents shape of the stones, coefficient of added mass and a coefficient for number of stones per unit of area. Furthermore, A and V are the horizontal exposed surface and the volume derived from the stone.

McCall [2015] did research on the morphological response of gravel beaches and barriers to storm events. He did so by adapting numerical model XBeach to XBeach-G, which is a morphodynamic, depth averaged, cross-shore profile model. The model is basically split into three parts, the hydrodynamics, the groundwater dynamics and the morphodynamics. The morphodynamic response can be determined by the model along the line two different approaches, Van Rijn [2007] and Nielsen [2006]. Both theories are based around Shields [1936], however both have been adapted from their original purpose to fit to the characteristics of gravel beach. See equation 2.4 to 2.7.

Van Rijn [2007] states that the bed shear stress is caused by two components, the drag part and the inertia part. This approach originally written for the sediment transport of sand under uniform flow, hence it is arguable that when applying to rock on a slope under wave forcing this is still valid. Furthermore, van Rijn [2007] defines the initiation of motion by the hand of a modified Shields, the modification is to account for bed slope effects and is according to Fredsøe and Deigaard [1992]. See equation 2.3 and 2.4.

$$\theta' = \theta \cos\beta \left(1 \pm \frac{\tan\beta}{\tan\phi}\right) = \frac{\tau_b}{\rho g \Delta_i D_{50}} \cos\beta \left(1 \pm \frac{\tan\beta}{\tan\phi}\right) \qquad \text{Equation 2.4}$$

$$\tau_b = \tau_{bd} + \tau_{bi} = \underbrace{c_f \rho \frac{u|u|}{h}}_{drag} + \underbrace{\rho c_m c_v c_n D_{50} \frac{\partial u}{\partial t}}_{inertia} \qquad \text{Equation 2.5}$$

McCall [2015] simplifies the Van Rijn [2007] formula for his use in Xbeach-G. McCall [2015] simplifies with respect to the inertia term, in which he merely uses $\frac{\partial u}{\partial t}$ instead of $\frac{Du}{Dt} = \frac{\partial u}{\partial t} + u \frac{\partial u}{\partial x}$. As he states "that the inertia component of the bed shear stress does not represent the actual inertia of the particles but refers to the force on particles in the bed due to pressure gradients, as well as due to the disturbance of the accelerating flow, following the potential flow theory (c. Morison et al. [1950], O'Brien and Morison [1952]. It should be noted that the implementation of this modification has little impact on the hydrodynamic results of McCall et al [2014]" – McCall et al [2015].

Nielsen [2006] defines the forcing on the sediment by the shear velocity, which he defined by the hand of a number of parameters, amongst others the sediment friction factor and the phase lag angle. The phase lag angle is between the free stream velocity and the bed shear velocity. The phase lag angle is based upon an approximation and the friction factor is also empirically determined. As these roughly determined parameters have a significant influence on the outcome, accuracy in this case is essential, which at the moment is not possible. Furthermore, Nielsen [2006] can just as Van Rijn [2007] approach be split into two parts, a velocity term and an acceleration term (i.e. drag and inertia). Furthermore, the Nielsen approach also uses a modified Shields approach, modified for bed slope effects, in order to determine the initiation of motion. This modification is also according to Fredsøe and Deigaard [1992]. See equation 2.5 and 2.6.

$$\theta' = \theta \cos\beta \left(1 \pm \frac{\tan\beta}{\tan\phi}\right) = \frac{u_*^2}{\Delta g D_{50}} \cos\beta \left(1 \pm \frac{\tan\beta}{\tan\phi}\right) \qquad \text{Equation 2.6}$$

$$u_* = \sqrt{\frac{f_s}{2}} \left(\cos\varphi \cdot u + \frac{T_{m-1.0}}{2\pi} \sin\varphi \frac{\partial u}{\partial t}\right)$$

$$= \underbrace{\sqrt{\frac{f_s}{2}} \cdot \cos\varphi \cdot u}_{velocity} + \underbrace{\sqrt{\frac{f_s}{2}} \cdot \frac{T_{m-1.0}}{2\pi} \cdot \sin\varphi \cdot \frac{\partial u}{\partial t}}_{acceleration} \qquad \text{Equation 2.7}$$

The most generic way to describe the damage on slopes due to wave impact, is to analyse the profile change and determine the total erosion area. Van der Meer [1988] uses this methodology to define the damage parameter 'S', defined as the damage level. Hofland et al. [2011] proposes a different damage description parameter, see equation 2.8, the damage depth.

$$E_3 = \frac{\langle d_e \rangle_{3Dn50}}{D_{n50}} \qquad \text{Equation 2.8}$$

This description uses the eroded depth as key variable in quantifying the damage. The eroded depth (d_e) averaged in a circle with diameter of $3D_{n50}$, divided by the nominal stone size. Hofland et al. [2011] proposes a tentative classification, which states that initial damage occurs if E_3 = 0.2-0.3 for a layer thickness of $2D_{n50}$. Intermediate damage occurs between E_3 = 0.5-0.6 and failure would be between E_3 = 1.5-1.6.

Wit [2015] used the numerical model XBeach-G to simulate tests on mild slopes for homogeneous structures. In these results, she found that on mild slopes the Van der Meer [1988] formula for plunging waves is too conservative, this is in line with the results from Schiereck & Fontijn. As it looked like the model XBeach-G gave a good representation of the reality.

Postma [2016] continued with this model. He went in to more depth on the software, and switched to the more relevant inhomogeneous structures. Postma recreated exact Van der Meer [1988] tests in XBeach-G, therefore allowing him to directly compare numerical against physical results. However, he found some irregularities in the results. He concluded that both Nielsen [2006] as well as Van Rijn [2007] were both inconsistent in giving accurate representations of reality. It appears that for Van Rijn [2007] the balance between drag and inertia is disturbed because of the larger stone size that it is applied to with gravel. Whereas Nielsen [2006] appears to be more consistent in accurate results, still is inconsequently accurate.

Postma suggests that this is caused by the constants, the phase lag angle and the sediment friction factor. These constants are not accurately determined/modelled in XBeach-G but appear to have a significant influence on the results.

For the tests in the wave flume the scaling laws need to be checked, this is done by the hand of the Schiereck [2007], as tests in the wave flume can have scaling effects. Sources of scaling effects can be the water viscosity, surface stress and air entrainment in breaking waves. The waves will be greater than 0.05 meter meaning that the breaking characteristics will be maintained according to Weber, the Weber number indicates the ratio between inertia and surface stress. Furthermore,. The particle Reynolds number indicates the dependency on viscosity, if the particle Reynolds number is greater than 600 the flow around the stones can be considered turbulent. This minimal Reynolds value coincides with a minimal stone size diameter of 7 mm. As the stones are larger (D_{n50} =16.2 mm, results in $Re_* \approx 1500$) the flow can be considered turbulent. The wave flume at Delft University of Technology is because of these relations considered as a physical reality during the tests.

2.2 DISCUSSION LITERATURE

Concluding from the breakdown of these approaches one can say that all methods are insufficient to determine the stability of rock on mild slopes under wave attack accurately. The empirical van der Meer [1988] approach is not validated for mild slopes and is based on an extrapolation of a test series. The extrapolation that is commonly made is too conservative according to Schiereck & Fontijn [1996] and Wit [2015]. From the research of Postma [2016] followed that the results gained from XBeach-G are promising but lacks consistency. Van Rijn [2007] originally describes the stability of sand on a flat bottom by the means of drag and inertia terms, these terms seem out of balance when applied to rocks. And at last the Nielsen [2006] approach in XBeach-G shows promising results, however doesn't consequently give good results. This inconsistency appears to be because roughly determined parameters as the phase lag angle and the sediment friction coefficient.

2.3 GOVERNING PARAMETERS

From the literature review of the three-important formula came forward, Van der Meer [1988], Van Rijn [2007] and Nielsen [2006]. Zooming in on these formulae gives a list of parameters and constants. These parameters are split into dimensional parameters and non-dimensional parameters. General forms of these dimensional parameters are listed below.

- Significant wave height H_s [m]
- Water depth h [m]
- Mean wave period T_m [s]
- Water velocity u [m/s]
- Water acceleration $\frac{\partial u}{\partial t}$ [m/s^2]
- Slope angle α [rad]
- Stone size diameter D_{n50} [m]
- Shear velocity u_* [m/s]
- Shear stress τ [N/m^2]
- Density ρ [kg/m^3]

The governing non-dimensional parameters are

- Stability parameter $H_s/\Delta D_{n50}$ [-]
- Wave steepness s_{0m} [-]
- Damage level S [-]
- Damage depth E_3 [-]
- Surf similarity parameter ξ_m [-]
- Relative weight under water Δ [-]
- Sediment friction factor f_s [-]
- Friction factor c_f [-]

3. METHODOLOGY

From the previous chapter a list of governing parameters was derived; this list of governing parameters is input for the chapter Methodology. From this list of parameters, a list of variables and constant input parameters is presented in the first paragraph. This list forms the input for the test series. The test set up and methodology will be elaborated in the second paragraph of this chapter. The input together with the methodology, will result in the output parameters that are necessary to answer the research questions. The latter will be elaborated in the third and final paragraph of this chapter. A more thorough and elaborate breakdown of the methodology is presented in Appendix A.

3.1 INPUT PARAMETERS AND VARIABLES

In this paragraph the input parameters together with the variables will be presented. The range of the variables will be discussed, together with other main characteristics in the test. This paragraph will be, just as the next two, split in to two parts: The profile change tests and the BIV/PIV tests.

3.1.1 PROFILE CHANGE

The input for the tests regarding the profile change, is split in constant input parameters (see Table 3.1) and input variables (see Table 3.2 and Table 3.3). A more elaborate description of and reasoning behind the parameters can be found in Appendix A.

Input constants			
h	Water depth	[m]	0.65
[-]	Wave spectrum	[-]	JONSWAP
N	Number of waves	[-]	3000
D_{n50}	Nominal stone size diameter	[mm]	16.20
Δ	Relative density	[-]	1.69
s_{0m}	Steepness	[-]	0.04
P	(notional) Permeability	[-]	0.10

TABLE 3.1 – CONSTANT PARAMETERS FOR PROFILE CHANGE TEST SERIES

The wave characteristics are derived from the existing theory of Van der Meer [1988] and Schiereck & Fontijn [1996]. Van der Meer [1988] states that the beginning of damage occurs at different values of 'S' for different slopes, with an increasing 'S' for milder slopes. Wit [2015] made an extrapolation of this increase of 'acceptable' damage levels. This extrapolation of the definition of the beginning of damage is used as input for the wave height. This extrapolation is denoted as S_{VDM} throughout this report. Since all other variables are constant and known the wave height which is, theoretically, responsible for this amount of damage can be calculated by equation 3.1.

$$H_s = 6.2 \cdot P^{0.18} \cdot \left(\frac{S}{\sqrt{N}}\right)^{0.2} \cdot \xi^{-0.5} \cdot \Delta \cdot D_{n50} \qquad \text{Equation 3.1}$$

Variables based on Van der Meer [1988]			1:5	1:10	1:15
S_{VDM}	Damage (Based on Van der Meer [1988])	[-]	3.000	5.910	8.840
H_s	Significant wave height	[m]	0.062	0.089	0.133
T_m	Mean wave period	[s]	0.995	1.266	1.458
ξ_m	Iribarren Value	[-]	1.00	0.5	0.33

TABLE 3.2 - INPUT VARIABLES BASED ON THE EXTRAPOLATION OF VAN DER MEER [1988] AS DONE BY WIT [2015]

The second wave characteristics are based on the results used by Schiereck and Fontijn [1996] for their research. Based on those results, see Figure 1.1, the dimensionless stability parameter has been derived for the relevant Iribarren value. The stability parameter is rewritten to derive the wave height. Note that for the 1:15 slope, the wave height has been adjusted downward to H_s = 0.2 m for two reasons. Firstly, the data used by Schiereck & Fontijn [1996] for ξ = 0.33, are based on a milder slope (cotα= 25) and secondly the size of the wave would become too big for the flume (breaking of the wave on the horizontal bottom). For the 1:5 slope (i.e. ξ =1.0), where the results used by Schiereck and Fontijn [1996] are not represented, the original definition of acceptable damage by Van der Meer [1988] is used, i.e. S=2.

Variables based on Schiereck & Fontijn [1996]			1:5[3]	1:10	1:15
$H_s/\Delta D_{n50}$	Stability parameter	[m]	-	5	8
H_s	Significant wave height	[m]	0.057	0.135	0.200
T_m	Mean wave period	[s]	0.955	1.470	1.790
ξ_m	Iribarren Value	[-]	1.00	0.5	0.33

TABLE 3.3 - INPUT VARIABLES BASED ON SCHIERECK & FONTIJN [1996]

Concluding; per slope, two different wave heights are tested. The first one is based on the extrapolation of tolerable damage as was suggested by Van der Meer [1988]. The second test is based on the data used for the research of Schiereck & Fontijn [1996], except for the steepest slope (cotα= 5) where the standard tolerable damage level (S=2) was used.

3.1.2 BIV/PIV

For the BIV/PIV tests roughly the same constants are applicable for this set of tests. The same slopes will be used in the tests and with the same stones. See Table 3.4.

Input constants			
h	Water depth	[m]	0.65
D_{n50}	Nominal stone size diameter	[mm]	16.2
Δ	Relative density	[-]	1.69
P	(notional) Permeability	[-]	0.1

TABLE 3.4 – CONSTANT PARAMETERS FOR BIV/PIV TEST SERIES

The waves are based on tests using the extrapolation of tolerable damage of Van der Meer [1988] done by Wit [2015]. For the wave input, the highest one percent waves will be used. For the BIV/PIV tests regular waves are used. Since the Field of View (FOV) is limited by the camera characteristics, it is favourable to place the camera exactly in the Region of Interest (ROI), i.e. where the most stone movement is found. By repeating the exact same wave over and over, i.e. regular waves, this location is constant in time. Furthermore, since the same situation is created in every wave, the repeatability of the test is great.

[3] Note that these input values are not based Schiereck & Fontijn [1996].

Statistically a wave distribution of a JONSWAP wave spectrum can be described by a Rayleigh-distribution. For the highest one percent of the waves the wave height can described as approximately 1.5 times the significant wave height. The highest one percent of the waves is chosen because these waves generate the highest velocities, i.e. wave induced forces on the bed. Hence around the moment of incipient motion of the stones, the motion will be caused by these waves (the highest one percent).

To create the same type of wave breaking the steepness was kept constant. Only for the 1:5 slope, a second test has been done. For that test the steepness of the waves is also changed. This is done in order to exactly represent the highest 1% of the wave spectrum. Whereas for the rest of the tests the wave steepness has been kept constant, with s=0.04. See Table 3.5.

Wave parameters			**1:5**		**1:10**	**1:15**
H	Wave height	[m]	0.093	0.093	0.133	0.200
T	Wave period	[s]	0.995	1.220	1.459	1.790
s	Steepness	[-]	0.06	0.04	0.04	0.04
ξ_m	Iribarren value	[-]	0.82	1.0	0.5	0.33

TABLE 3.5 - INPUT WAVE DATA FOR THE BIV/PIV TEST SERIES

Concluding, for the BIV/PIV tests per slope one test has been done, except for the steepest slope (cotα= 5)

3.2 TEST SET UP AND METHODOLOGY

Paragraph 3.2 elaborates on the test methodology, the used measuring devices and gives a sketch of the test set up. For further elaboration on the methodology, see Appendix A.

3.2.1 PROFILE CHANGE

With all input variables and constants known, the test plan can be finalized. For constructional reasons from the lab, the first slope to be tested is the 1:15 slope. The slope was constructed in a sturdy way, i.e. the slope is very stiff, such that upon wave impact the slope construction will not significantly vibrate. (see the left picture in Figure 3.1 on the next page, in which the slope construction is partly visible). This way the stones placed on the slope will not be influenced by wave induced vibrations. The layer thickness was indicated with tape on the side of the flume, which was used during the construction of the armor layer as reference for the layer thickness. A plumb rule was used to make sure the same layer thickness was applied over the entire width of the flume. See the middle picture in Figure 3.1). Using this methodology, a layer thickness of 2 D_{n50} was constructed, i.e. 32 mm.

Once the slope was fully constructed and aligned to the design layer thickness, the first scan can be made. The scans were made with a 3D laser scanner, a Leica C10. For each profile measurement two scans are made, one before and one after the wave series. This results in two separate pointclouds. These two pointclouds will be fitted together with the use of three (as required) especially placed trackers. These trackers will remain in the exact same position, with these stationary points the two pointclouds can be exactly aligned. See Figure 3.1 (right picture) with the red square indicating the scanner and the red circles the trackers.

FIGURE 3.1 - CONSTRUCTION OF SLOPE (LEFT & MIDDLE) AND SCANNER AND TRACKERS (RIGHT)

With the first scan done, the water can be pumped into the flume. This has to be done slowly in order for the rising water level not to influence the stones on the slope. A final check on the position of the wave gauges and the EMS has to be made, in order to verify that all are in the correct position. The setup of the profile measurement tests is depicted in Figure 3.2. The wave gauges are represented with the bold vertical lines crossing the water level, whereas the EMS is represented by the dashed line. Furthermore, the Leica C10 laser scanner is depicted by the circle on the left side of the flume.

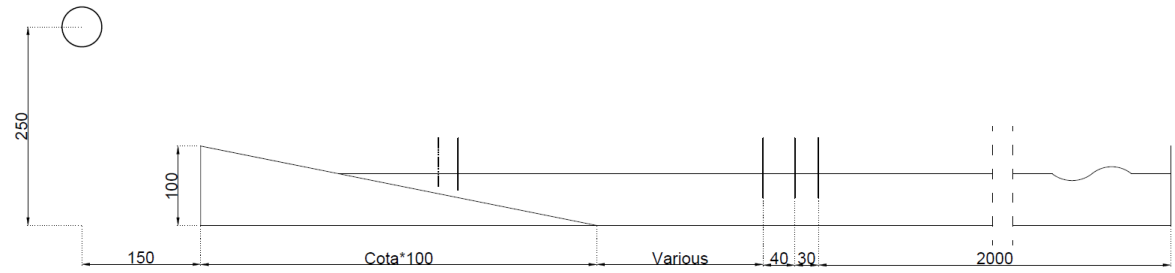

FIGURE 3.2 - TEST SET UP FOR PROFILE CHANGE TESTS. (LENGTHS IN CM)

Once this is verified, the wave gauges are calibrated. The calibration is done by moving the gauges 5cm upward and downward over time. The change in voltage can then be used to calculate the ratio volt to centimeter. Which is later used to translate the voltage signal produced by the wave gauge to a wave signal. At last the input values for the wave board are checked before the start of the test.

Once all input values and set up characteristics are checked and verified, the test can commence. The wave board can be activated and the set wave conditions created. A total number of 3000 waves will be created. This represents a storm event. After the wave series, the flume will be carefully drained, in order to make sure the stones do not move.

After the stones are dry, which is necessary for accurate laser measurement of the slope, another scan is made of slope using the same principal. This scan forms the post measurements of the slope. By analyzing the cloud to cloud distances, the profile change caused by the wave series can be determined.

By averaging over the width of the flume, the mean profile change along the flume can be determined. With the mean profile change the damage level can be determined, which is derived from the erosion area. Furthermore, from this average profile change the maximum and mean erosion depth are determined.

After all the scans are done, the slope can be restored and prepared for the next test. After doing all the checks and calibration again, the second test can be done. After both tests are done for each slope, the BIV/PIV tests for that particular slope will be done. Once also these tests are completed for the 1:15 slope, the slope will be adjusted to the 1:10 to do the same routine followed by the 1:5 slope.

3.2.2 BIV/PIV

After the tests for the profile change were finalized, the BIV/PIV tests were executed. For this BIV/PIV test series the stones in and around the Field of View (FOV) have to be replaced with black stones. This was done because of the reflection of the lights on the stones.

For the BIV/PIV test series, a strip of glued stones is used, this way the stones will not move through the FOV during the measurements. This strip is placed in the FOV. The rest of the black stones will be placed around the strip of glued stones. The stones are spread out and aligned to a layer thickness of 2 D_{n50}. This layer thickness is realized in the same manner as was done in the profile change test series, i.e. with an indication line and a plumb rule. Once all the black stones are placed the lights can be put in position.

The lights are placed on top of a wooden structure that holds the LED lights into position (see Figure 3.3, the right figure). This structure holds the lights 30 centimetres above a plank with a gap of 5 mm in the direction of the flume. The lights shine through the gap and create a beam of light, which limits the Depth of Field (DOF). See Figure 3.3.

FIGURE 3.3 - DEPTH OF FIELD (LEFT AND MIDDLE) & LIGHTING SET UP (RIGHT)

When the DOF is large, there is difference in width of the FOV and the close edge of the DOF compared to the far edge. This is explained in Figure 3.4**Error! Reference source not found.**. As the camera creates 2D images, one cannot derive from the picture whether a particle moved in the front or in the back of the FOV, this creates an uncertainty in the measurement.

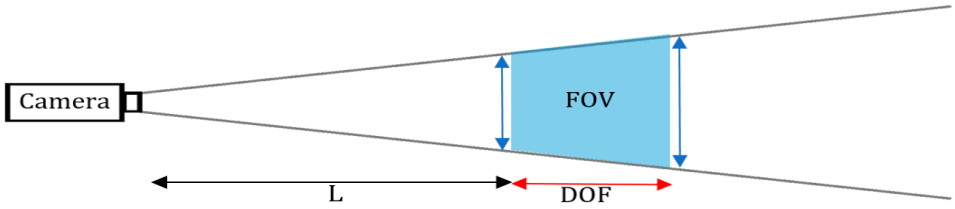

FIGURE 3.4 - SCHEMATIC OVERVIEW DOF AND FOV FOR BIV/PIV TESTS

A larger DOF results in more inaccurate results, the relations between the DOF and the error can be directly calculated by the means of

$$error = \frac{{}^{1}/_{2}\,DOF}{L} \qquad \text{Equation 3.2}$$

With 'L' is the distance of the camera to the FOV and DOF is the Depth of Field, Figure 3.4. This error can be visualized, by the increasing of the size of the FOV when increasing 'L'.

The size of the DOF can be regulated by either camera settings or by the lighting. With the camera and lens available for this research it was not possible to create a sufficiently small DOF. Therefore, the option to regulate the DOF with the lighting set up was used in this research. This resulted in a DOF of 4.5 centimetre (see Figure 3.3), which results in an error of 2.8 %.

In front of the flume the camera will be placed 75 cm from the flume. With the FOV 5 centimetres removed from the inner side of the flume this gives a total distance of the camera to the FOV of 80 centimetres. At this distance the FOV has the desired dimensions, roughly 12 by 9 centimetre.

First assumption is that the velocities are in the order of 1 m/s. Combining the resolution of the camera (720x480) with the size of the FOV gives a pixel density of 28 pixels per mm^2 (each pixel is roughly 0.2x0.2 mm). With 132 frames per second that comes down to a movement of 7.6 mm in between two consecutive frames. This is appeared to be a proper amount of movement to be able to analyse the velocity distribution within the FOV.

Once the camera is installed and focussed on the FOV the entire set up is covered in a blanket to exclude as much of the external light as possible. With everything in place, the water can be pumped into the flume. This has to be done slowly in order for the rising water level not to influence the stones on the slope. A final check on the position of the wave gauges and the EMS has to be made, in order to verify that all equipment is in the correct position. See Figure 3.5 on the next page. The same indicators have been used, i.e. a bold line for the wave gauges and a dashed line for the EMS. The FOV is depicted by the shaded square on the slope.

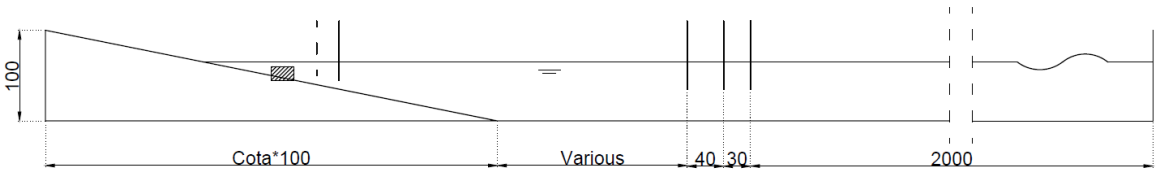

FIGURE 3.5 – SCHEMATIC OVERVIEW TEST SET UP BIV/PIV TESTS (LENGTHS IN CM)

Once all this is done, a calibration image of the camera was made. This was done by holding a ruler in the FOV. These images together with the set framerate are later used to transform the vectors from the unit pixel/frame to meter/second.

Once all previous steps have been completed, final step is to check and verify the input for the wave board. With this verified the wave board can be turned on. Since bubbles are not always present in the FOV, for example during the run-down of the wave, particles have been added to the water prior to the camera recording. The particles have a size of 100 µm (= 0.1 mm) which comes down to 25% of the size of a pixel. This was assumed to be enough to alter the colour signal in the pixel. With this difference in colour the particle can be traced by the software PIVLab. Once the waves are rolling and have reached the FOV, carefully the particles can be strewn just in front of the breaking waves and mixed into the water. Once this is done short videos will be made, each video is roughly 10 seconds long. As the wave period is in the order of a 1-2 seconds, each video covers at least five waves.

The videos are made with a camera from the imaging source, the DFK 23GP031. This camera shoots at a framerate of 132 frames per second (fps). At this framerate, the output of the camera is set to a resolution of 720x480 pixel. First assumption is that the velocities are in the order of 1 m/s. Combining the resolution of the camera (720x480) with the size of the FOV gives a pixel density of 28 pixels per mm^2 (each pixel is roughly 0.2x0.2 mm). With 132 frames per second that comes down to a movement of 7.6 mm in between two consecutive frames. With this resolution, this translates to a movement of roughly 35-40 pixels per time step. This gave satisfactory results, thus was used for all BIV/PIV measurements.

The video file will be broken up into separate frames for the analysis with PIVLab. During the analysis with the software PIVLab, two following (frame n and frame n+1) will be cross-referenced in order to determine the flow velocities in the FOV. The analyzation process is elaborated in the next paragraph.

3.3 OUTPUT PARAMETERS & ANALYZATION PROCESS

This paragraph will describe the processing of the raw results from the test plan as described above. Firstly, the profile change tests will be elaborated, followed by the test of BIV/PIV tests. For a more elaborated version of the processing of the data see Appendix B. In this Appendix, the general procedure of the processing will be described in further detail.

3.3.1 PROFILE CHANGE

Firstly, the .txt files containing the data gathered by the Leica C10 (.txt files with XYZ values, RGB values and an intensity value) are imported in Matlab. Because the dimensions of the pointclouds don't overlap for a full 100%, the inner-boundaries are used for the grid definition. This way, both pre- and post-wave series scan will have the same coordinates. The pointclouds are than fitted into a grid with $\Delta x = \Delta y = 3\ D_{n50}$. This size is chosen to align with the damage description by

Hofland et al. [2011], they proposed to take the average over a circle with diameter 3 D_{n50}. For pragmatic reasons a square is used in this research. Per grid the median z-value of all the data points within the grid will be taken, the median is taken instead of the average to exclude the extreme values. Since the scanner scans from 1 single point per scan, the density of the points in the pointclouds decreases with the distance from the scanner. (The scanner creates a data point every 60 µrad, both horizontally and vertically)

The scans are made from the topside of the slope, because the pointcloud density is higher close to the scanner than it is further away, see Figure 3.6. As the damagezone is closer to the topside of the slope, this will create a more detailed scanning result. Note that, as is further elaborated in Appendix B, the accuracy of the measurement is not significantly influenced by a lower amount of points.

Figure 3.6 represents the pointcloud density of the pre-waves scan on the extrapolation of tolerable damage of Van der Meer [1988] done by Wit [2015] test on the 1:10 slope. The results of this test will be used throughout this whole paragraph, as this is example gives clear results.

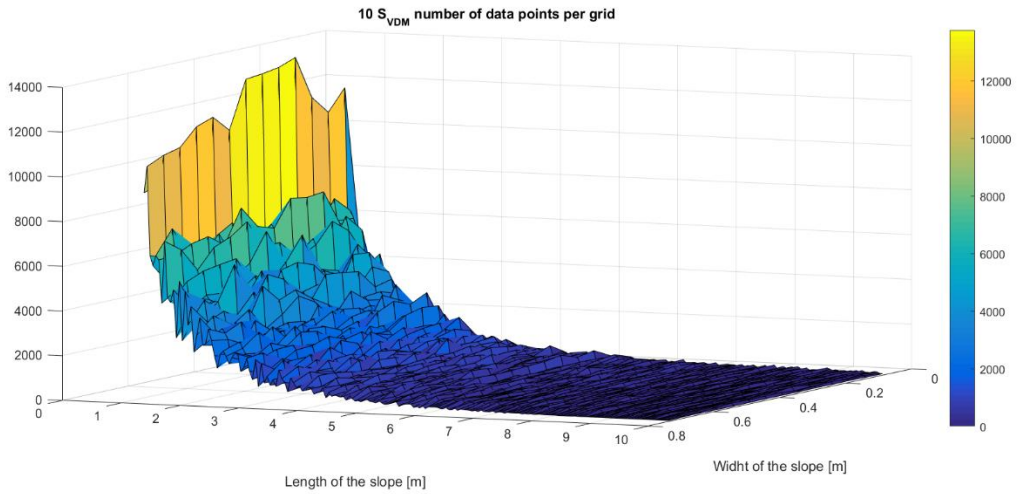

FIGURE 3.6 - POINTCLOUD DENSITY (COTA=10, WAVES BASED ON VAN DER MEER [1988])

Both scans (pre- and post-waves) have been fitted over the grid, the median of the data per grid is taken for both scans. The post wave series scan is then subtracted from the pre-wave scan. This results in the profile change per grid, this profile change is plotted in a 3D figure, see Figure 3.7. The still water level (SWL) is depicted in the figure together with the wave direction.

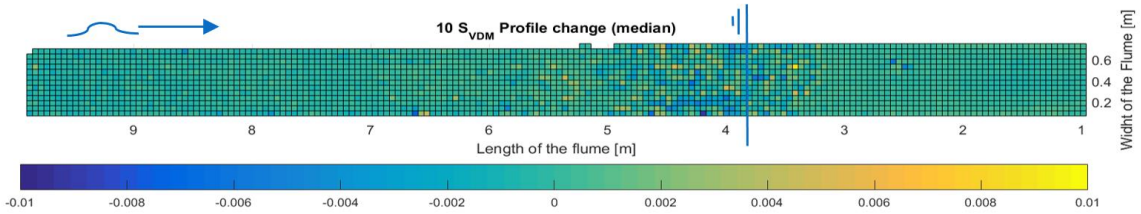

FIGURE 3.7 - 3D PLOT PROFILE CHANGE FOR SLOPE 1:10, WAVES BASED ON VAN DER MEER [1988]

If you examine Figure 3.7, you can conclude that all the damage occurs at one specific area. This area is around SWL. The conservation of mass states that the amount of stones will stay the same during the tests, which can be translated to that the sum of the profile change should be zero. The area over which the sum has been taken has been diminished to the area where profile change is found. This results in Figure 3.8.

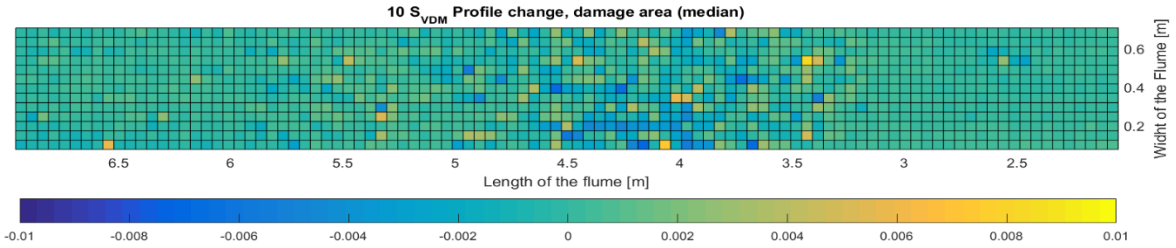

FIGURE 3.8 - 3D PLOT PROFILE CHANGE, DAMAGE AREA (SLOPE 1:10, WAVES BASED ON VAN DER MEER [1988])

The profile change is averaged over the width of the flume, resulting in an average profile change over the length of the flume. When integrating the entire averaged profile change, the balance of the profile change should be zero. ($\sum A_e = 0$). In most of the scans the sum of the erosion was however significant. In order to account for this, a correction factor (c_f) was applied to the average profile, either shifting the average profile up or down. This was done iteratively until the total erosion area was in the order of 10^{-6} (=O(mm²)), which is roughly relates to 0 and 4 % of one D_{n50}^2. With these final adjustments, the profile change can be plotted, this is done in Figure 3.9.

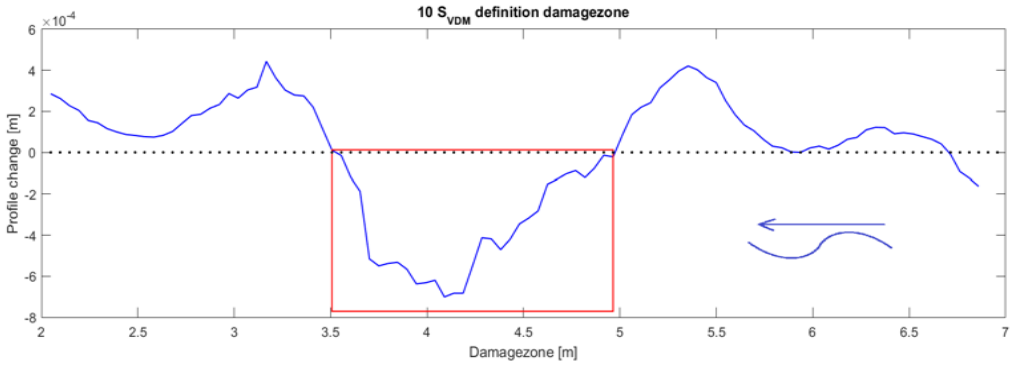

FIGURE 3.9 - AVERAGE PROFILE CHANGE AND DEFINITION OF THE DAMAGEZONE (SLOPE 1:10, WAVES BASED ON VAN DER MEER [1988])

In this profile the erosion area can be identified, this erosion area will be called the damage zone as this area will be representative for the derived damage characteristics. The damage zone is defined as a part of the profile, which is *continuously* below zero (i.e. represents erosion). The boundaries of the damagezone are marked by the zero crossings of the average profile (i.e. the shift from erosion to accretion and vice versa) In Figure 3.9 this average profile is depicted together with a visualization of the damagezone, the red square.

From the damage zone, as defined in Figure 3.9, the damage characteristics can be derived. From the average profile zoomed in on the damagezone, the total erosion area is determined. This erosion area translates to the damage level Van der Meer [1988] uses to describe the damage level, $S = \frac{A_e}{D_{n50}^2}$. Furthermore, the average and maximum erosion depth are determined. The latter will be related to the nominal diameter of the rock protection, as proposed by Hofland et al. [2011].

The damage characteristics are summarized in Table 3.6. The average erosion depth is defined as the total erosion of the damagezone (A_e) divided by the length of the damagezone. The maximal erosion depth is maximal erosion depth represented by a grid cell, where each grid cell represents the median of the data points in that grid cell. The size of the grid cell corresponds with a square of 3 x 3 D_{n50}. This grid size corresponds with the by Hofland et al. [2011] suggested damage characteristic damage depth 'E_3'.

Slope	Test	H_s [m]	A_e [m²]	$d_{e;av}$	$d_{e;max}$	S [-]	$d_{e;av}/D_{n50}$ [-]	$D_{e;max}/D_{n50}$ [-]
1:10	S_{VDM}	0.100	-5.29E-4	-3.5E-4	-7.2E-3	2.01	2.2%	44.4 %

TABLE 3.6 - DAMAGE CHARACTERISTICS (COTA=10, WAVES BASED ON WIT [2015])

This table is derived for all test scenarios and further elaborated in Appendix B. The results of this analysis will be evaluated in the next chapter.

3.3.2 BIV/PIV

In this subparagraph, the procedure regarding the processing of the raw data for the BIV/PIV tests will be elaborated. For an elaboration on the test program and the test set up, see Appendix A. The images will be processed with the software 'PIVLab', a plugin for Matlab. This is a graphical user interface application, which can be downloaded and implemented in Matlab. PIVLab has been developed by Thielicke [2014], for his PhD research.

In the previous paragraph, the camera and lighting set up has been elaborated. With this set up merely a small beam of light has been used, in order to create a narrow Depth of Field (DOF). There within the Field of View (FOV) only the bubbles and particles within the DOF are lit and therefore visible. The camera shoots a video with a resolution of 720*480 pixels and a frame rate of 132 frames per second (fps). In order to analyze the video with PIVLab, the video has to be broken up into separate frames. This was done by writing a Matlab script, that reads an .avi file and returns .bmp files.

The .bmp files are imported in to PIVLab, where the first steps are to create a mask over the stones in the FOV. The stones are excluded from the analysis because there will be no movement in this layer, that is of interest for this research. Furthermore, image enhancement is applied in three forms, CLAHE, Intensity highpass and intensity capping (See Appendix B).

The frame analysis is done by the DFT (Discrete Fourier Transform) PIV algorithm, this algorithm is chosen as it, according to Thielicke [2014], results in the most accurate results and has the lowest computational time. The frame analysis is done in three passes, firstly a rather large interrogation area has been used.

This results in a reliable first estimate of the displacement, with a high signal-to-noise ratio. The displacement information of the first pass, forms the offset of the second pass. The same applies for the third pass. By using three passes (128x128 pixel, 64x64 pixel and finally 32x32 pixel) results in a high vector resolution but remains reliable with a high signal-to-noise ratio.

The calibration is done by the means of a calibration image, that is made with the exact same camera settings and set up as the tests. In this image a ruler is hold in the FOV. This image can then be used in PIVLab in order to translate numbers of pixels to distances. Furthermore, since the framerate of the camera is known (132 fps) the time difference between two frames is also known. Based on a scatter the most extreme vectors are ignored, see Appendix B.

Finally, the vectors are set to represent the velocity magnitude. During the processing the vectors have been smoothed (least squares smoothing technique, which is standard implemented in PIVLab) and the background is color graded to represent the velocity magnitude with a range between 0 and 2 meter per second. Lacking data is interpolated in PIVLab, and represented by red arrows. See Figure 3.10, which represents an arbitrary frame of the slope 1:10 BIV test. Note that the boundaries of the FOV have a higher frequency of interpolated vectors, and is therefore less reliable.

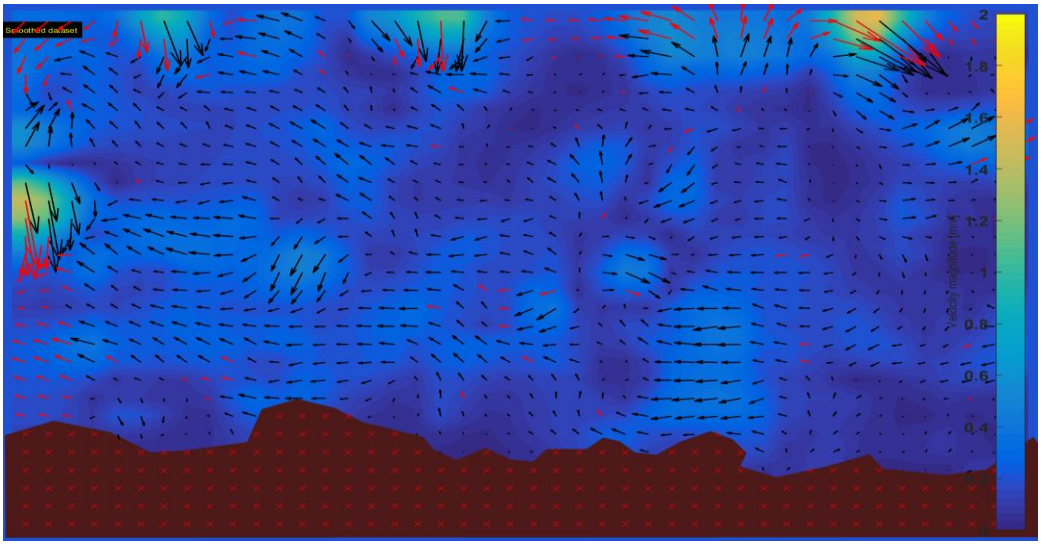

FIGURE 3.10 – ARBITRARY FRAME FROM SLOPE 1:10, BIV ANALYSIS

The PIVLab results are exported in .mat files, which are further processed in Matlab. In Matlab, a Region of Interest (ROI) is defined with the size of $2D_{n50}$ wide and 1 D_{n50} high (which results in 11x5 vectors, the size of this ROI is arbitrary chosen). Over the ROI the average velocity near the bottom is derived. This area is located above a protruding stone within the FOV. The area close to the bottom is chosen because the velocity and acceleration in this area are responsible for the forces on the stones. The ROI is depicted in Figure 3.11, the frame used for the picture is an arbitrary frame. The red circles indicate the vectors in the ROI. The ROI is far enough removed from the boundaries of the FOV to be significantly

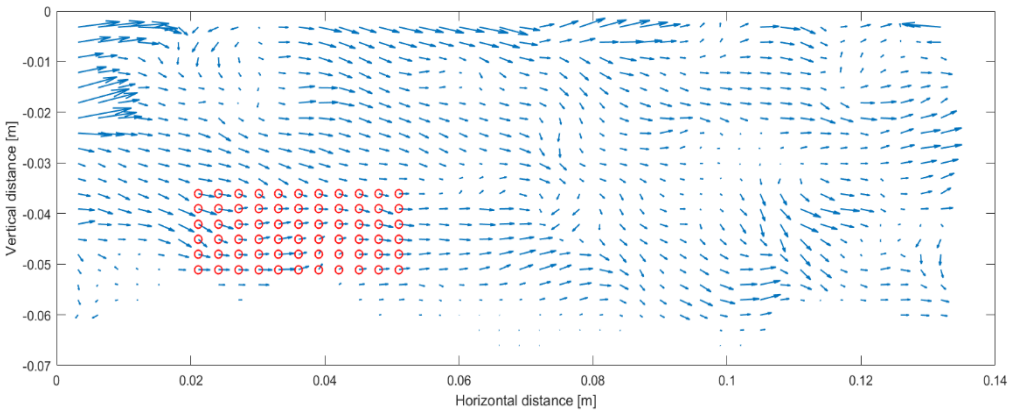

FIGURE 3.11 - DEFNITION OF THE ROI FOR THE BIV ANALYSIS (SLOPE 1:10)

From this ROI, the velocity and acceleration profile over time are derived. This forms the input for the comparison of the test results with the XBeach-G methodology. The output of the velocity signal from the ROI is smoothed over time and the derivative is taken (i.e. the acceleration over time), this is represented in Figure 3.12. The blue dots represent the actual measurement whereas the red line represents the fitted smoothed output. This smoothed output will from the input for the further analysis.

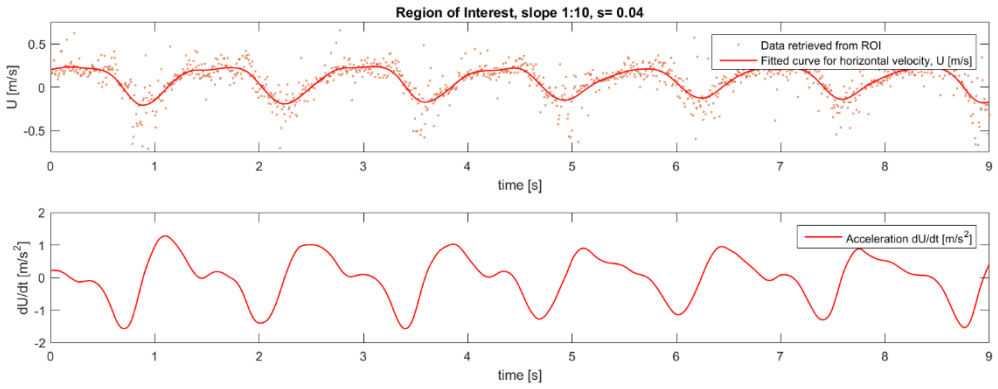

FIGURE 3.12 – VELOCITY & ACCELERATION SIGNAL DERIVED FROM THE BIV/PIV ANALYSIS (SLOPE 1:10)

The velocity and acceleration signal will be substituted in the different physical methodologies applied in XBeach-G, i.e. Van Rijn [2007] and Nielsen [2006]. Both methods are combined with a Shields [1936] approach to determine the initiation of motion. This evaluation will be presented in the chapter 4, Results.

4. RESULTS

In this chapter the results and the analysis of the results will be presented. This chapter will be split into two parts, firstly the results from profile change and secondly the results from the BIV/PIV tests. For a more comprehensive elaboration of the analysis and a breakdown of the results see Appendix B.

4.1 PROFILE CHANGE

In this paragraph the results from the profile change tests will be elaborated. The elaborated breakdown of the results is presented in Appendix B. The tests have followed the methodology that was presented in chapter 3, and elaborated in detail in Appendix A.

For each slope two profile scans were made, one pre- and one post-wave series. These scans were subtracted from each other in order to retrieve the profile change for each test. The profile change (3D) has been averaged over the width of flume, to gain the average profile change (2D). From this profile the damage zone was defined, and at last from this damage zone the damage characteristics were derived. A summary of the results derived from all the profile scans is presented in Table 4.1. With the damage characteristics in the last 3 columns.

Slope	Test	H_{m0}[4] [m]	S_{theory} [-]	A_e [m²]	$d_{e;max}$ [m]	S [-]	E_3 [-]
1:5	S_{VDM}	0.057	2.00	-2.77E-4	-1.02E-3	1.06	63.0 %
	S_{norm}	0.054	1.47	-1.44E-4	-5.80E-3	0.55	35.8%
1:10	S_{VDM}	0.094	4.04	-5.29E-4	-7.20E-3	2.01	44.4 %
	S_{SF}	0.129	20.02	-9.22E-4	-1.23E-2	3.51	75.9%
1:15	S_{VDM}	0.125	5.98	-2.76E-4	-5.40E-3	1.05	33.3%
	S_{SF}	0.173	30.38	-1.85E-4	-7.50E-3	0.70	46.3%

TABLE 4.1 - DAMAGE CHARACTERISTICS FOR ALL TEST SCENARIOS

The damage level S is defined as the eroded area (A_e) divided by the square of the nominal stone size diameter. The damage depth, as proposed by Hofland et al. [2011], is defined by the maximal damage (median value per grid with $\Delta x = \Delta y = 3D_{n50}$) divided by the nominal stone size diameter. The same has been done for the average erosion depth in the damagezone.

4.1.1 DAMAGE LEVEL - VAN DER MEER [1988]

In order to compare the test results with the Van der Meer [1988] formula, the test results have to be processed. Van der Meer [1988] formulae plots, stability number vs the Iribarren value, are based on a constant damage level (S=2). However, the test results have different damage levels. Therefore, the test results are inter- and extrapolated in order to find the wave height, which is theoretically (based on the test results) responsible for a damage level of S=2. This is explained in this paragraph.

[4] H_{m0} is assumed to be representative for $H_{1/3}$ and is used in this research. Note that Van der Meer [1988] uses $H_{1/3}$, and that in shallow water these definitions are not equal. Using H_{m0} leads to a more conservative approach (as $H_{m0} < H_{1/3}$).

SLOPE 1:5

The damage curve for slope 1:5, based on the Van der Meer [1988] formula, has been plotted against the wave height in Figure 4.1. Furthermore, the two test results for slope 1:5 are depicted in Figure 4.1. The two test results depicted with a blue circle (S_{norm} & S_{VDM}). The results are linearly inter- and extrapolated with respect to the wave height, this leads to a damage curve based on our results.

Furthermore, in Figure 4.1, the constant damage line of S= 2 is depicted. The intersection of this line with the inter- and extrapolation line represents the wave height that is theoretically (based on our results) responsible for a damage level S= 2.

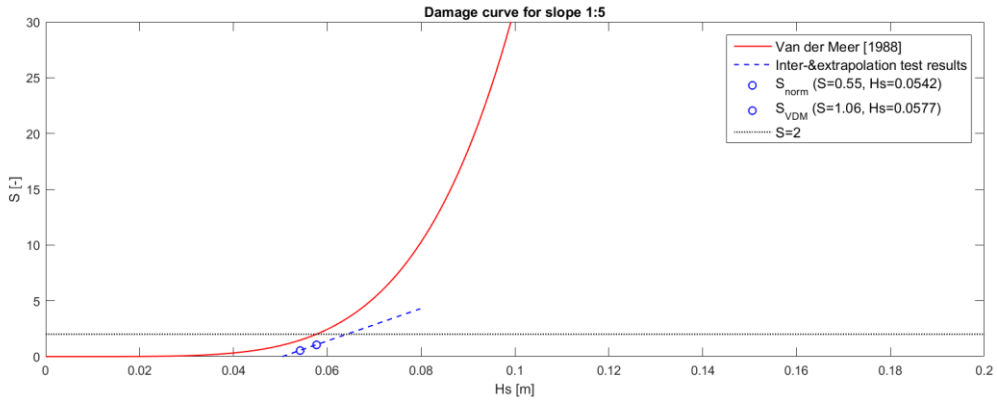

FIGURE 4.1 – DAMAGE CURVE ANALYSIS FOR SLOPE 1:5

For slope 1:5 this results in a significant wave height of 0.0628 meter. Van der Meer [1988] states that for the conditions in this research a damage of S= 2 would occur under a significant wave height of 0.057 meter, in other words the results of this research indicate that the wave height can be roughly 10% higher. Furthermore, the damages that were measured are significantly lower than Van der Meer [1988] suggests, for the 1:5 slope approximately only 30%. This percentage even further diminishes for milder slopes.

SLOPE 1:10

This approach has been done for the other slopes too, which for the 1:10 slope resulted in an inter-extrapolated significant wave height of 0.0939 meter. Whereas Van der Meer stated S= 2 would occur under waves of 0.082 meter. For the 1:10 slope that entails that the test results suggest that wave height can be roughly 14 % higher. Note that Van der Meer [1988] already suggest that damage levels higher than 2 are deemed to be acceptable.

SLOPE 1:15

For the 1:15 slope, the results were not as clear as for the previous slopes. For 1:15 the test S_{VDM} showed a higher damage level than the test S_{SF}, whilst the latter has had a higher significant wave height. From visual observations during the test series, was noticed that significantly more stones were in movement during the S_{SF} test, than during the S_{VDM} test. However, the displacements do not appear to have dominant direction. Stones frequently move up but also down the slope, therefore resulting in a net transport very close to zero. This leads to a scattered profile change plot, see Figure 4.2. This figure shows the area with the most profile change of the slope.

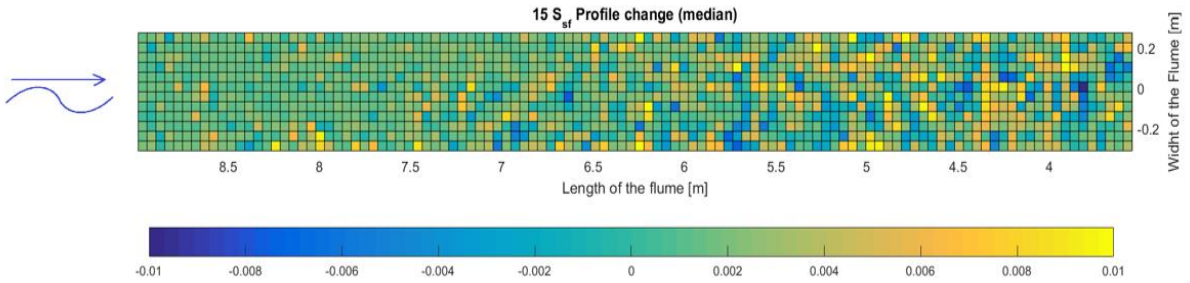

FIGURE 4.2 - 3D PROFILE CHANGE (COLORBAR IN METER) (COTA= 15, S_{SF})

In Figure 4.2 significant profile change is measured, and plotted, but when averaged over the width of the flume almost balances out.

The wave heights derived from the tests are rewritten into stability parameters (i.e. divided by the effective weight times the nominal diameter) and plotted against the surf similarity number. As was also done by Van der Meer [1988] and Schiereck & Fontijn [1996]. The results of this test are plotted together with the results of the latter and presented in Figure 4.3. As can be seen in the figure both interpolated test results lie above the plotted Van der Meer [1988] formula. The points represent a higher stability value than Van der Meer [1988] provides, indicating that despite a greater wave height this theoretically results in the same damage level (S= 2).

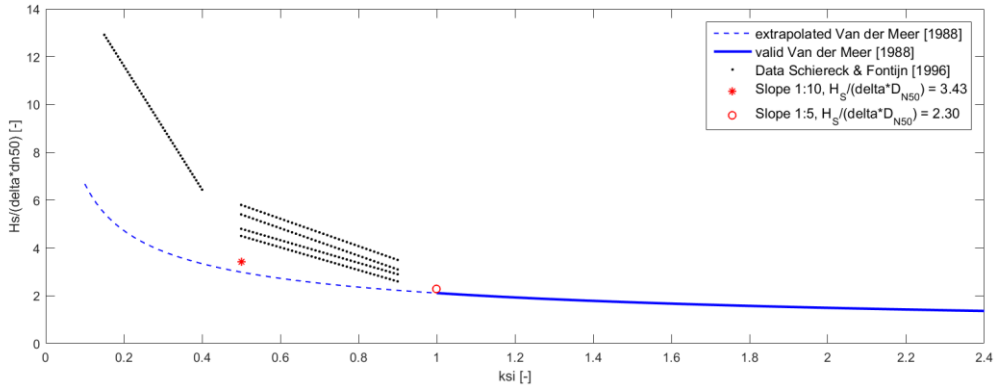

FIGURE 4.3 - TEST RESULTS, PLOT OF VAN DER MEER [1988] FORMULA AND THE DATA SET SCHIERECK & FONTIJN [1996] USED.

DAMAGE LEVEL AS FUNCTION OF SLOPE

The results in Figure 4.3 are based on the design damage level S= 2, however as this research suggests that these damage levels are too conservative. Higher damage levels are ought to be acceptable, which resulted in the extrapolation by Wit [2015] of the tolerable damage based on Van der Meer [1988] (denoted as S_{extrap}). Using the higher damage levels, gives different results. The blue lines in Figure 4.4, will shift upward, indicating higher stability.

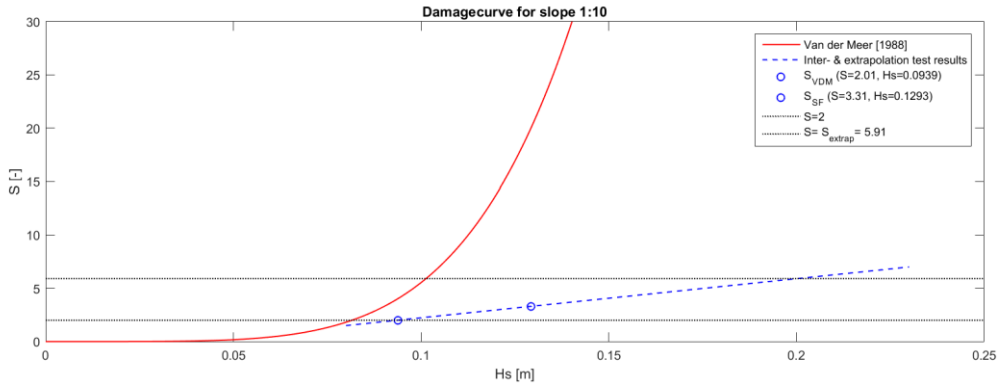

FIGURE 4.4 - DAMAGE CURVE ANALYSIS FOR EXTRAPOLATED DAMAGE LEVEL (SLOPE 1:10)

For this slope the damage level, S_{extrap}= 5.91, intersect the extrapolation of the test results at a wave height of H_s=0.202 (102% higher than the Van der Meer [1988] formula suggests). Translating this to the stability parameter results in a stability parameter of $H_s/\Delta D_{n50}$= 7.33.

Combining all previous results and implementing them in a stability parameter vs. Iribarren number plot results in Figure 4.5. The blue line (solid) represent the conventional Van der Meer [1988] approach with S= 2, this formula is extrapolated (blue dashed line) outside its validity region. The black circles represent test results Van der Meer [1988] based his results on. The black dots indicate the test results Schiereck & Fontijn [1996] based their research on. Furthermore, the inter- & extrapolated results from this results are represented with the asterisks. The blue asterisks represent the extrapolation to S= 2, and the red asterisks represent the extrapolation to S= S_{extrap}.

Furthermore, in this Figure 4.5, the red dashed line depicts the Van der Meer [1988] formula with the damage level 'S' as function of the slope angle. As derived in Figure 4.3, does the stability number increase when higher damage levels are deemed acceptable, i.e. red asterisks compared to the blue asterisks.

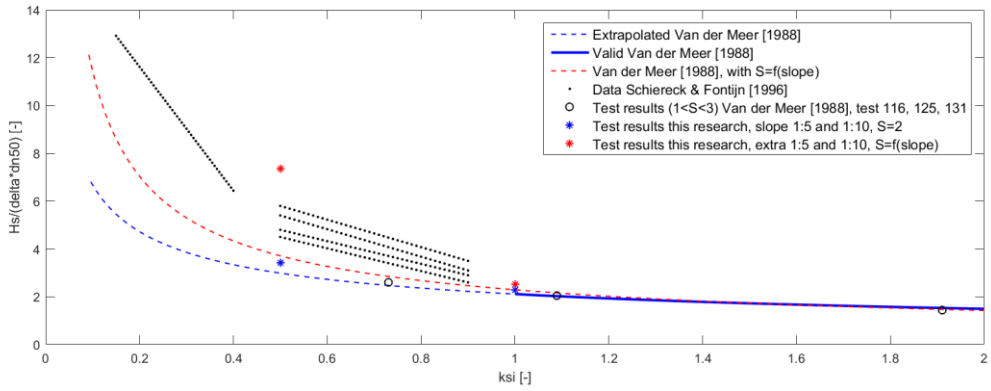

FIGURE 4.5 – STABILITY PARAMETER VS IRIBARREN NUMBER PLOT, WITH DAMAGE LEVEL AS FUNCTION OF THE SLOPE

Based on these results one can conclude that the stability of the stones on mild slopes is higher than the Van der Meer [1988] formula for plunging waves suggests. Especially with the extrapolation of tolerable damage by Wit [2015]. Significantly lower damage levels were measured in the test series. All test results are more stable than the extrapolation of the Van der Meer [1988] formula suggests.

4.1.2 DAMAGE DEPTH – HOFLAND ET AL [2011]

Hofland et al [2011] proposed the damage depth, which is defined as $E_3 = \frac{\langle d_e \rangle_{3dn50}}{D_{n50}}$. This will be elaborated in this paragraph.

The eroded depth, denoted as d_e, was the average depth taken in a circle of $3D_{n50}$. In this research, for pragmatic reasons the median depth over a square with sides of $3D_{n50}$. These results appear to give reasonable results, even for the 1:15 slope. The results are plotted in Figure 4.6. The different shapes indicate different test inputs, which are specified in the legend of the figure. Subscript 'norm' indicates the test on slope 1:5 with the normal damage level S=2. The subscript 'VDM' represent the test based on the extrapolation of Van der Meer [1988] as was done by Wit [2015] and at last the subscript 'SF' represents the test based on the data that was used by Schiereck & Fontijn [1996].

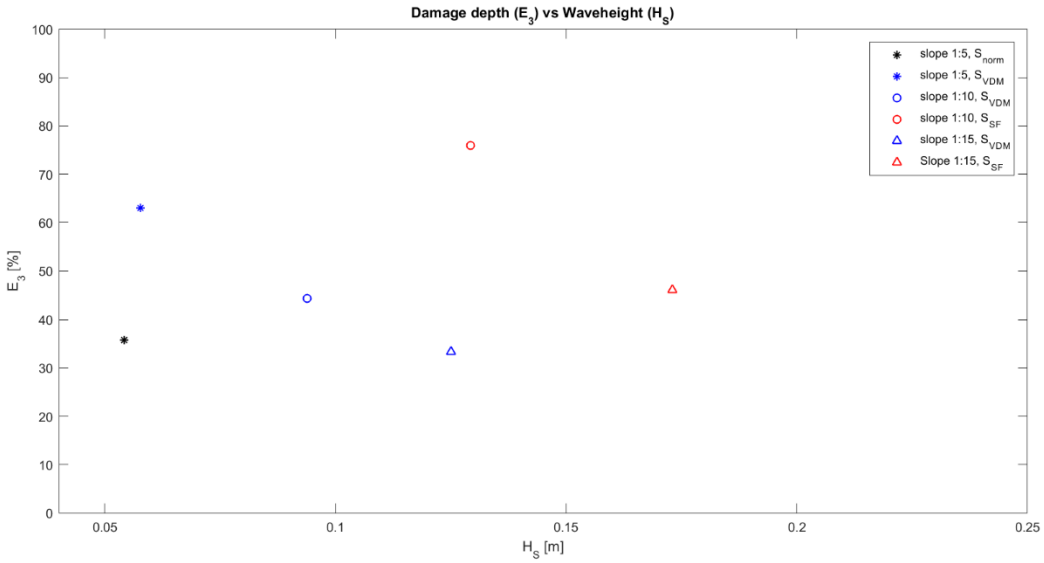

FIGURE 4.6 - DAMAGE DEPTH VS. THE SIGNIFICANT WAVE HEIGHT.

When closely examing Figure 4.6, and relating the damage depth to the slope angle. A trendline can be drawn through the data points per slope, resulting in one trendline for each slope. This is presented in Figure 4.8. One can see that the influence of the waveheight, with respect to the damage depth, decreases for milder slopes.

This can be explained by the spreading of the wave energy. Under constant steepness, the type of wave breaking changes with the changing of the slope angle. The different type of wave breaking are related to the surf simularity parameter or Iribarren number 'ξ'.The energy dissipation of waves can be significantly different, as is sketched in Figure 4.7.

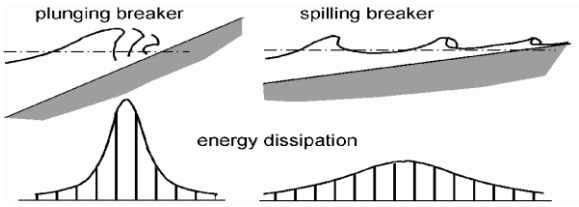

FIGURE 4.7 - ENERGY DISSIPATION UNDER PLUNGING AND SPILLING WAVES (SCHIERECK ET AL. [2012])

Therefore on one particular slope, the damage depth increases with increasing wave height. However this ratio is different per slope angle. This difference in ratio can be explained by the spreading of the wave energy (which is defined as $E_{wave}=1/8 \cdot \rho \cdot g \cdot H_S^2$). More tests should be done to derive a proper trend line through the data.

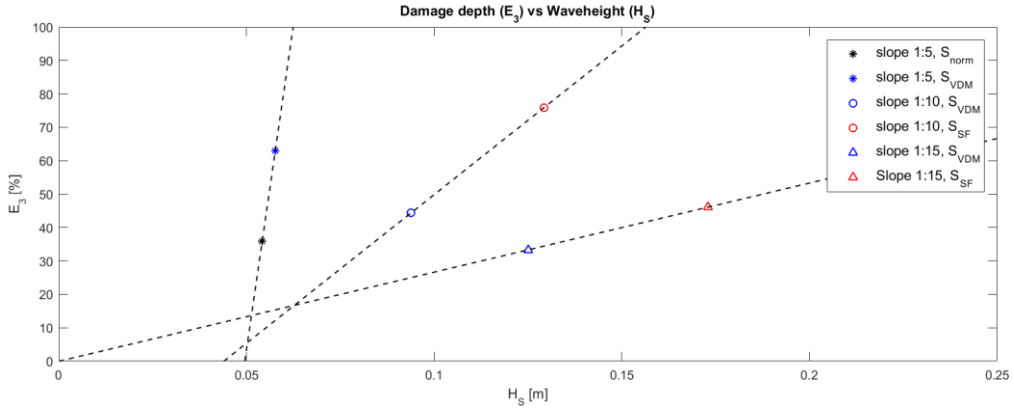

FIGURE 4.8 - DAMAGE DEPTH VS WAVEHEIGHT WITH TRENDLINES PER SLOPE

When multiplying the results with the tangent of the slope all the results cluster together, see Figure 4.9.This appears to represent that the damage depth is a function of the wave height times the tangent of the slope angle ($E_3 = f(H_S \cdot \tan\alpha)$). Noted should be that the effect of the slope still is represented in the trendlines, as the milder slopes have a lower inclination than the steeper slopes. Further research should be done in order to determine the shape of this formula, in which more variables should be examined.

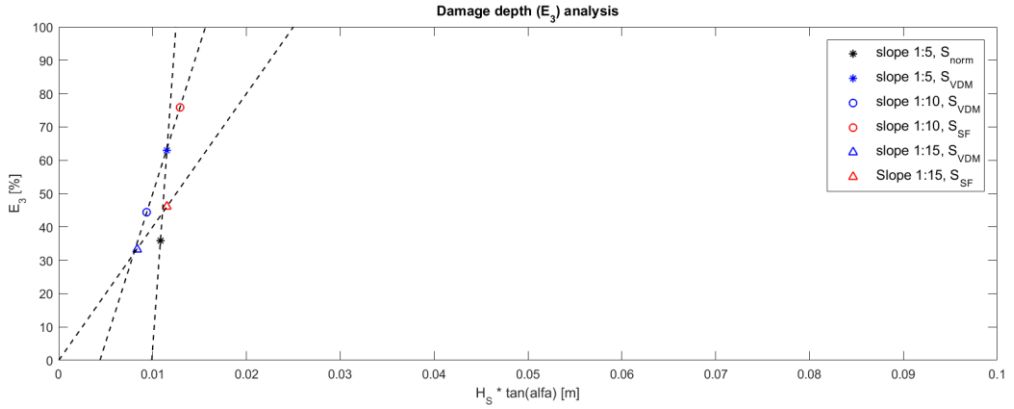

FIGURE 4.9 - DAMAGE DEPTH VS WAVEHEIGHT * TANGENT ALFA

4.2 BIV/PIV

In this paragraph the results of the BIV/PIV tests will be elaborated. The key results from the BIV/PIV are the velocity 'U' and acceleration 'dU/dt', which have been derived in paragraph 3.3. The results will be substituted in two physical approaches of the Shields value, the Nielsen [2006] and Van Rijn [2007] approach. Which will be elaborated in this paragraph. Firstly, the other parameters in the approaches are derived, followed by the substitution of the parameters. And finally, the shields values for both approaches are compared and evaluated. The results are elaborated in more detail in appendix B.

4.2.1 PARAMETER DERIVATION

The velocity and acceleration signal will be substituted in the different physical methodologies applied in XBeach-G, i.e. Van Rijn [2007] and Nielsen [2006]. Both methods are combined with a Shields [1936] approach to determine the initiation of motion. This approach is modified to account for the slope effect. As both the Van Rijn [2007] and the Nielsen [2006] approach are used in this form, they can be directly compared in this form. Both approaches are elaborated in chapter 2, Literature. A brief recap of the formulae will be given, with a brief derivation for the values for the slope dependent parameters.

VAN RIJN [2007]

XBeach-G applies the Van Rijn [2007] formula in the following way, see equation 4.1 and 4.2.

$$\theta = \frac{\tau_b}{\rho g \Delta D_{50}} \cdot \cos\beta \cdot \left(1 \pm \frac{\tan\beta}{\tan\emptyset}\right) \qquad \text{Equation 4.1}$$

$$\tau_b = \tau_{bd} + \tau_{bi} = \underbrace{c_f \rho \frac{u|u|}{h}}_{drag} + \underbrace{\rho c_m c_v c_n D_{50} \frac{\partial u}{\partial t}}_{inertia} \qquad \text{Equation 4.2}$$

The velocity and the acceleration over time are derived from the BIV/PIV analysis. The rest of the parameters still need to be determined, for the Van Rijn [2007] formula this results in the following parameters.

h – the water depth. The water depth is measured at the location of the ROI in the FOV. The FOV is located at the location of the most significant erosion after the irregular waves series. As the wave height changed per slope, so did the location of the erosion compared to SWL. See

Test	1:5, s= 0.04	1:5, s= 0.06	1:10, s= 0.04	1:15, s= 0.04
Water depth at ROI – h [m]	0.035	0.035	0.059	0.077

TABLE 4.2 - WATER DEPTHS FOR THE BIV TESTS

C_f - the friction factor. The Van Rijn [2007] methodology uses the method of Chezy. [1775].

$$c_f = \frac{g}{\left(18\log\left(\frac{12h}{k}\right)\right)^2} \qquad \text{Equation 4.3}$$

$$with\ k = 3\,d_{90}$$

Test	1:5, s= 0.04	1:5, s= 0.06	1:10, s= 0.04	1:15, s= 0.04
Friction factor – c_f [-]	0.054	0.054	0.031	0.025

TABLE 4.3 - FRICTION FACTORS VAN RIJN [2007] FORMULA

c_x – coefficients. Three coefficients, apart from the friction coefficient, are used in the Van Rijn [2007] approach. For convenience, the shape of the stones is considered spherical. The coefficient for the added mass is defined as $c_m = 1 + c_a$, with c_a is 0.5 for spheres with zero autonomous acceleration. The volume shape factor c_v is $\pi/6$ for spheres. At last the coefficient for the number of grains (i.e. stones) that is influenced by the acceleration per unit of area. All these coefficients can also be replaced with one calibration coefficient $c_i = c_m \cdot c_v \cdot c_n \approx \mathcal{O}(1)$.

D_{50} – the characteristic stone size. The characteristic stone size in this research is 19.2 mm, as follows from the sieve curve presented in Appendix A.

The derived parameters are presented in Table 4.4.

Parameter	C_f [-]	ρ [kg/m³]	h [m]	C_m [-]	C_v [-]	C_n [-]	g [m/s²]	Δ_i [-]	D_{50} [m]
Value	variable	1000	variable	1.5	0.52	1	9.81	1.685	0.0192

TABLE 4.4 - PARAMETERS VAN RIJN [2007] METHODOLOGY

NIELSEN [2006]

Xbeach-G uses the Nielsen [2006] formula in the following way, see equation 4.4 and 4.5

$$\theta = \frac{u_*^2}{\Delta g D_{50}} \cdot \cos\beta \cdot \left(1 \pm \frac{\tan\beta}{\tan\emptyset}\right) \qquad \text{Equation 4.4}$$

$$u_* = \sqrt{\frac{f_s}{2}}\left(\cos\varphi \cdot u + \frac{T_{m-1.0}}{2\pi}\sin\varphi\frac{\partial u}{\partial t}\right)$$

$$= \underbrace{\sqrt{\frac{f_s}{2}} \cdot \cos\varphi \cdot u}_{Velocity} + \underbrace{\sqrt{\frac{f_s}{2}} \cdot \frac{T_{m-1.0}}{2\pi}\sin\varphi\frac{\partial u}{\partial t}}_{Acceleration} \qquad \text{Equation 4.5}$$

The velocity and acceleration are derived from the BIV/PIV analysis, the most significant parameters are derived below and will be summarized in Table 4.8.

f_s - sediment friction factor. This value can be calculated by the means of the standard wave friction factor. In the research of Postma [2016] this friction factor was kept constant at f_s=0.025. However, with the BIV/PIV measurements it this friction factor can be determined. This is done by the means of equation

$$f_s = \exp\left(5.5\left(\frac{2{,}5\,D_{50}}{A}\right)^{0.2} - 6.3\right) \qquad \text{Equation 4.6}$$

$$with\ A = \frac{\sqrt{2}}{\omega_p}\sqrt{var\ \{u_\infty(t)\}}$$

The angular peak frequency is known, as regular waves are used during the BIV/PIV analysis, T_p=T. With this the angular velocity is defined as 2π/T. Since the wave characteristics alter per slope, the angular velocity also changes. The variance of the free stream velocity follows from a Matlab analysis which is further elaborated in Appendix B. By plotting multiple time steps of a wave (e.g. t=0.1T, t=0.2T, t=0.3T…), the depth at which the profile approximately reaches the free stream velocity can be determined or approximated. At this depth, a velocity and acceleration profile has been derived, representing the free stream flow characteristics. From the free stream velocity, the variance has been derived and presented in Table 4.5

This results in values of $f_{s,}$ see Table 4.5.

Test	1:5, s= 0.04	1:5, s= 0.06	1:10, s= 0.04	1:15, s= 0.04
Var {u_∞(t)}	0.0284	0.0355	0.0846	0.0430
Sediment friction factor - f_s [-]	0.3611	0.3215	0.2091	0.2914

TABLE 4.5 – SEDIMENT FRICTION VALUES FOR NIELSEN [2006] FORMULA.

Xbeach-G [2016] used the suggests a value of sediment friction factor, which is set at f_s = 0.025. The values found with the BIV/PIV tests are about a factor 10 higher.

φ – Phase shift angle. The phase shift angle is defined as the phase difference between the free stream velocity and the shear velocity. For pragmatic reasons this value is determined by plotting both the free stream velocity and the shear velocity on the same time scale. For each zero crossing (up- and downward) the phase lag of the shear velocity is determined in seconds. The phase lag for all zero crossings are summed and divided by the number of zero crossings. The phase lags are then transferred to degrees by dividing the phase lag (in seconds) by the wave period and multiplying by 360°. An example of a plot of both the shear velocity and the free stream velocity is presented in Figure 4.10.

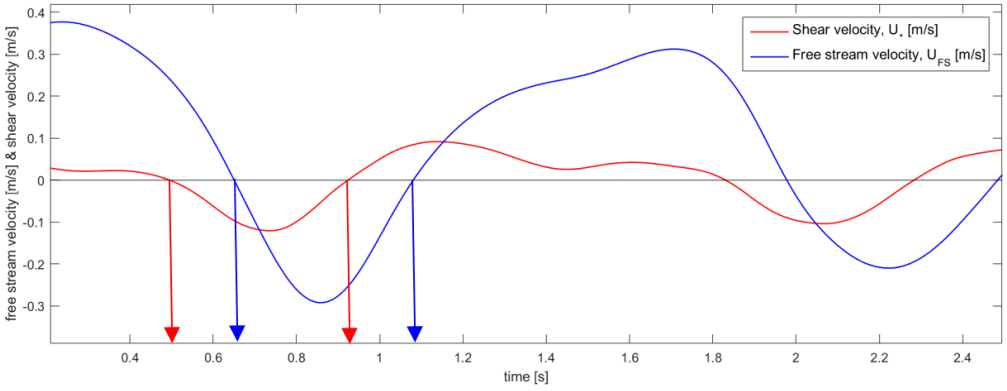

FIGURE 4.10 - DETERMINATION OF THE PHASE LAG ANGLE (ARBITRARY EXAMPLE OF SLOPE 1:10)

Figure 4.10 shows an arbitrary determination of the phase lag of the shear velocity compared to the free stream velocity. The blue arrow represents the zero crossing of the shear velocity, whereas the red arrow represents the zero crossing of the free stream velocity. The time difference is here roughly 0.15 seconds. This method is applied for all zero crossings for each BIV/PIV analysis and then divided by the number of zero crossings. This results in Table 4.6.

Test	1:5, s= 0.04	1:5, s= 0.06	1:10, s= 0.04	1:15, s= 0.04
Phase shift – φ_{time} [s]	0.247	0.195	0.280	0.346
Phase shift angle - φ[°]	72.8	70.5	65.0	69.6

TABLE 4.6 - PHASE SHIFT ANGLE VALUES FOR NIELSEN [2006] FORMULA

Note that this phase lag is significantly higher than the value given as standard in Xbeach-G and as used by Postma [2016], who used a phase lag angle of 25°. This higher phase lag increases the dominance of the acceleration term in the Nielsen [2006] approach.

$T_{m-1.0}$ – spectral wave period. As regular waves were used, the spectral wave period is equal to the mean wave period which has been derived for all tests and presented in Table 4.7

Test	1:5, s= 0.04	1:5, s= 0.06	1:10, s= 0.04	1:15, s= 0.04
Wave period – T [s]	1.2196	0.9948	1.5503	1.7900

TABLE 4.7 - WAVE PERIOD VALUES FOR NIELSEN [2006] FORMULA

Summarizing the previously presented values for the Nielsen [2006] formula results in Table 4.8. all the variable parameters are specified in their respective tables, as presented above.

Parameter	f_s [-]	φ [rad]	$T_{m-1.0}$ [s]	g [m/s²]	Δ [-]	D_{50} [m]
Value	variable	Variable	variable	9.81	1.685	0.0192

TABLE 4.8 - PARAMETERS NIELSEN [2006] METHODOLOGY

4.2.2 PARAMETER SUBSTITUTION

With the parameters from the previous sub-paragraph, all the input values have been derived. The substitution of the parameters in both the Nielsen [2006] and the Van Rijn [2007] formula, results into two approaches of the Shields value. Firstly, the shear velocity (i.e. Nielsen [2006]) and shear stress (i.e. Van Rijn [2007]) are derived. Both methodologies can be split into two terms, a velocity and an acceleration term (i.e. respectively drag and inertia for Van Rijn [2007]). By plotting the separate terms in time, the relative dominance of either term can be determined, see Figure 4.11.

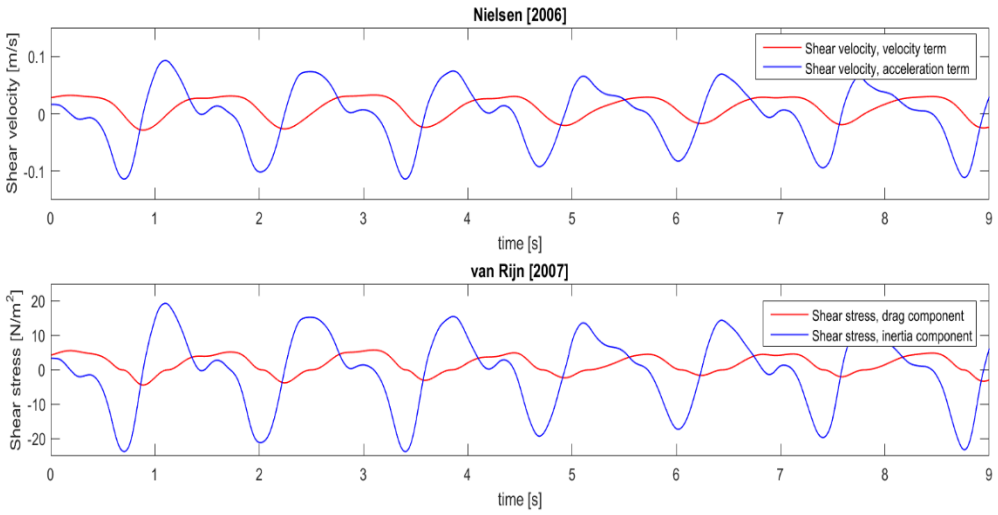

FIGURE 4.11 - DRAG AND INERTIA TERM, FOR BOTH NIELSEN [2006] AND VAN RIJN [2007], BASED ON THE RESULTS OF THE 1:10 SLOPE

From this plot one can see that for both the Nielsen [2006] and the Van Rijn [2007] formula, the acceleration (i.e. inertia) term is dominant. Furthermore, the direction of the shear velocity (negative is upslope and positive represents downslope) seems to be equally great, indicating that there is no dominant direction for this slope. Per approach both terms are summed, processed into the Shields value and multiplied by the slope correction factor of Fredsøe and Deigaard [1992]. This results into a plot of Shields value in time for both the Nielsen [2006] and the Van Rijn [2007] formula, see Figure 4.12.

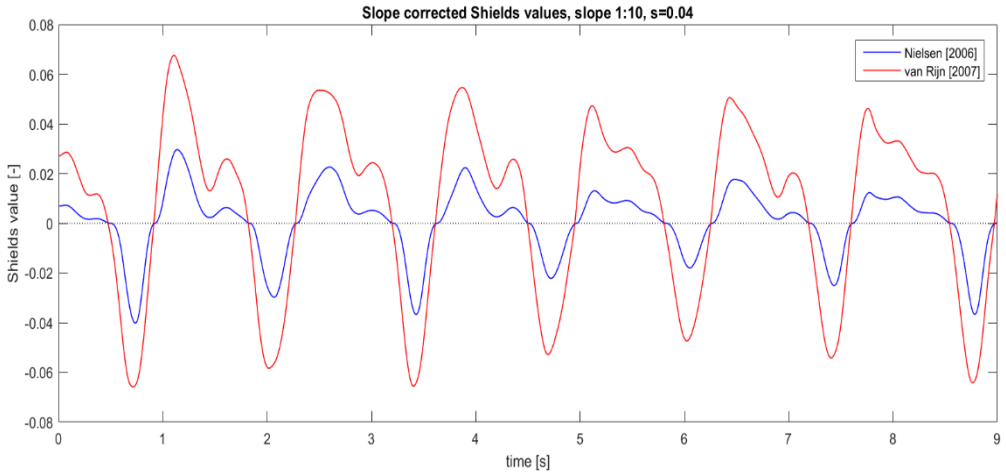

FIGURE 4.12 - SLOPE CORRECTED SHIELDS VALUES, FOR SLOPE 1:10

As Figure 4.12 shows, do the Nielsen and Van Rijn formula generate almost exactly the same answers. Noted should be that, this is only the case when the phase lag angle (φ) and the sediment friction (f_s) values are used that are based on the BIV/PIV measurement, rather than the standard approximated values (φ= 25°, f_s=0.025). The difference is plotted in Figure 4.13, where the blue and red line are the same as plotted in Figure 4.12 and represent the respective the Nielsen [2006] and Van Rijn [2007] formula with derived parameters. The black line however represents the Nielsen [2006] formula with standard approximated values.

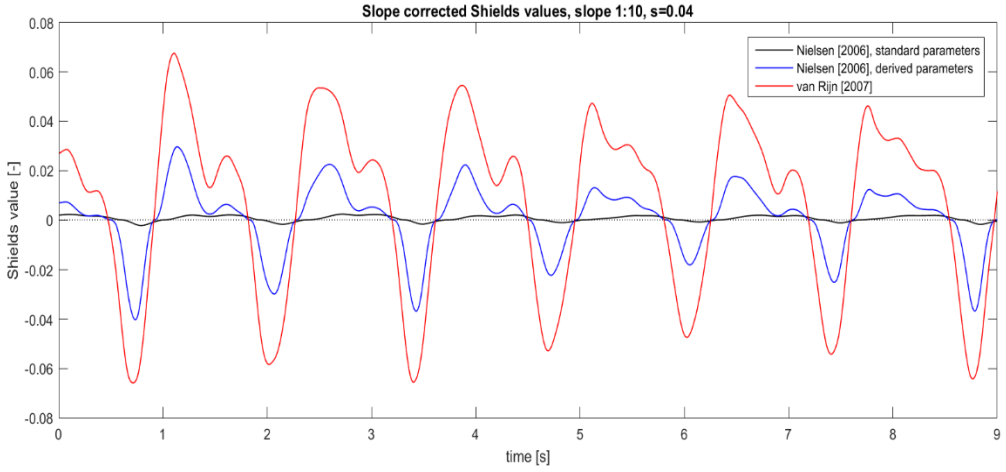

FIGURE 4.13 - DEPENDENCY ON THE ACCURACY OF THE PARAMETERS IN NIELSEN [2006]

All the slopes are analysed in the same manner as has been presented in Figure 4.11 and Figure 4.12, for a more elaborate presentation on all the results see Appendix B. The characteristic values, the mean, maximum and minimum, have been derived from the slope corrected Shields values.. These results are plotted against the Iribarren value.

Test	1	2	3	4
Slope angle – cotα [-]	5	5	10	15
Wave steepness – s [-]	0.04	0.06	0.04	0.04
Iribarren value - ξ [-]	1.00	0.82	0.50	0.33

TABLE 4.9 – IRIBARREN VALUES FOR EACH TEST.

The characteristic results of all the BIV/PIV tests are presented in the tables below, Table 4.10 which represents the Shields values based on the Nielsen [2006] approach and Table 4.11 which respectively represents the Van Rijn [2007] approach.

Nielsen [2006]	Slope 1:5		Slope 1:10	Slope 1:15
	ξ= 1.00	**ξ= 0.82**	**ξ= 0.50**	**ξ= 0.33**
Mean	-0.0001	-0.0006	0.0013	-0.0025
Max	0.0207	0.0264	0.0297	0.0338
Min	-0.0324	-0.0475	-0.0402	-0.0758

TABLE 4.10 – SHIELDS VALUE CHARACTERISTICS, BASED ON NIELSEN [2006] FOR ALL TESTS.

Van Rijn [2007]	Slope 1:5		Slope 1:10	Slope 1:15
	ξ= 1.00	**ξ= 0.82**	**ξ= 0.50**	**ξ= 0.33**
Mean	-0.0025	-0.0014	0.0087	-0.0008
Max	0.0482	0.0659	0.0676	0.0410
Min	-0.0470	-0.0779	-0.0658	-0.0511

TABLE 4.11 - SHIELDS VALUE CHARACTERISTICS, BASED ON VAN RIJN [2007] FOR ALL TESTS.

Seven different stages of movement can be described, starting from stage 0. no movement at all, to 1. occasional movement at some locations, to 2. Frequent movement at some locations… to eventually 6. Continuous movement of at all location and 7. General transport of grains. See Figure 4.14, the Re_* value for this research is roughly 1500, which indicates that the critical shields values become constant. And that stage 6 is represented by the critical Shields value of 0.055.

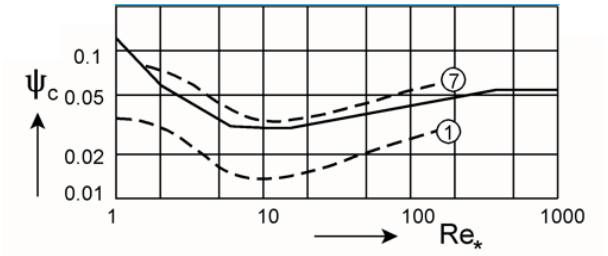

FIGURE 4.14 – QUALITATIVE PLOT OF SEVEN STAGES OF MOVEMENT WITH RESPECT TO THE CRITICAL SHIELDS VALUE (SCHIERECK ET AL. [2012])

The stage 1 of movement are found at critical Shields values of 0.035. This roughly coincides with the peaks found in the plots of the Shields value based on the Nielsen [2006] approach. This indicates that the Shields values that are derived from the BIV/PIV measurements indeed suggest that there is movement of stones.

However, during the irregular wave series, the profile change tests, visual observations concluded that there was significant movement under the highest waves of the spectrum. The regular waves in the BIV/PIV measurements are based on the highest one percent waves of the spectrum that was applied in the irregular wave tests. Therefore, significant movement should be present during the BIV/PIV tests. Hence, the Shields values based on the Nielsen [2006] approach are too low. The Shields values found by applying the Van Rijn [2007] methodology seem to agree with the visual observations, as they represent Shields's stage 6-7 movement.

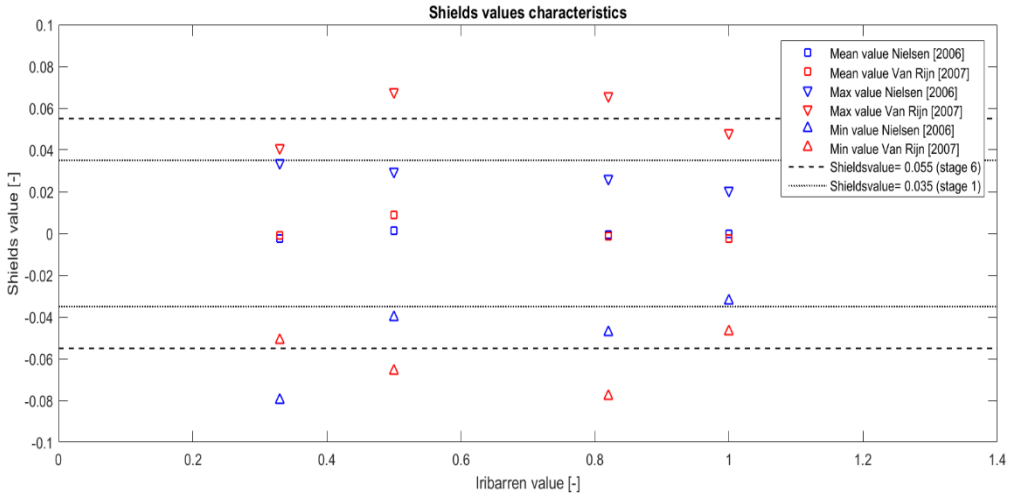

FIGURE 4.15 - CHARACTERISTIC SHIELDS VALUES

Furthermore, when comparing Nielsen [2006] with the Van Rijn [2007], the uncertainty of the Nielsen approach comes forward. This was briefly outlined in Figure 4.13. The accuracy of the Nielsen [2006] approach depends significantly on the accuracy of two parameters, the phase lag angle (φ) and the sediment friction factor (f_s). In this controlled environment, that is the wave flume, together with the BIV/PIV measurement these parameters have been relatively well derived. Which has led to reasonably good results. However, in a natural environment these parameters become very hard to accurately determine. Whereas on the other hand, the Van Rijn [2007] approach uses variables that are easily determined and only need basic design details.

5. CONCLUSION AND RECOMMENDATIONS

In this chapter the conclusion on this research will be presented, the conclusion will be elaborated by answering of the research questions. With the conclusion in mind a review of the research is done in the final paragraph, in which recommended additional or successive research will be elaborated.

5.1 CONCLUSION

In this paragraph the research question will be answered and sub-questions will be elaborated.

How should the stability of rock on mild slopes under wave attack be described?

Based on this research the stability of rock on mild slopes under wave attack it seems that should be described by the Van Rijn [2007] formula for the shear stress and rewritten into a slope adjusted Shields value. Of the three investigated methodologies, the Van Rijn [2007] approach resulted into the most accurate and most consistent answers.

The damage description by the means of the damage level 'S', that Van der Meer [1988] uses to describe damage, appears to be insufficient in characterizing the occurring damage on mild slopes. Applying the Van der Meer [1988] approach results in a too conservative outcome, but could be used as a first indication. The Nielsen [2006] approach overestimates the stability and is highly dependent on the accuracy of two parameters, which have proven to be hard to accurately determine.

- *Is the extrapolation of van der Meer [1988] an accurate way to define stability of rock on mild slopes under wave attack?*

Based on the results of this study the Van der Meer [1988] formula for plunging waves is not an accurate way to describe the stability of rock on mild slopes. As suggested by Schiereck & Fontijn [1996] the extrapolation of Van der Meer [1988] to mild slopes is indeed too conservative. For all tests that were done, the damage levels derived from the 3D profile change plots were (significantly) lower than the Van der Meer [1988] suggests. With the difference increasing towards milder slopes.

Furthermore, the method that van der Meer [1988] used to describe damage (i.e. the damage level 'S') does not suffice on mild slopes. On mild slopes was found that the type of damage differs from a general formation of an erosion pit, on the mildest slope (cotα= 15) despite significant move of the stones no pit was found. The stones move up and down the slope arbitrary, without a dominant direction. The damage depth, as proposed by Hofland et al. [2011] was found to be a good replacement for the damage definition. With this in mind and based on these test results, the Van der Meer [1988] formula should not be used on slopes milder than 1:10.

- *How do Nielsen [2006] and Van Rijn [2007] combined with the modified Shields parameter, as used by McCall [2015] comply with the test results?*

Both the approach based on Nielsen [2006] as well as the approach based on Van Rijn [2007] give consistent results. However, Nielsen [2006] gives results that coincide with Shields's first stages of movement, whereas Van Rijn [2007] results in Shields values that comply with Shields's stage 6-7 of movement.

Based visual observations during the irregular wave series, which form the basis of the regular waves series, significant movement was observed in the damage zone during the highest segment of waves. The definition of Shields's sixth stage is "significant movement at most locations", this does to comply with the results of Van Rijn [2007]. The results of the approach based on Nielsen, which result in Shields's stage 1 to 2, defined as "occasional to frequent movement at some locations". It seems that based on these results that the Nielsen [2006] approach therefore overestimates the stability.

Furthermore, when comparing Nielsen [2006] with the Van Rijn [2007], the uncertainty of the Nielsen approach comes forward. This was briefly outlined in Figure 4.13. The accuracy of the Nielsen [2006] approach depends significantly on the accuracy of two parameters, the phase lag angle (φ) and the sediment friction factor (f_s). In this controlled environment, that is the wave flume, together with the BIV/PIV measurement these parameters have been relatively well derived. Which has led to reasonably good results. However, in a natural environment these parameters become very hard to accurately determine. Whereas on the other hand, the Van Rijn [2007] approach uses variables that are easily determined and only need basic design details. Therefore, based on the results found in this research, it is advised to always use the Van Rijn [2007] Methodology.

- *Could the previously mentioned methodologies (i.e. Van der Meer [1988], van Rijn [2007] and Nielsen [2006]) be improved based upon the data gathered from the test series?*

Yes, the methodologies could be improved based on the results found in this research, in particular the Van der Meer [1988] approach to mild slopes and the Nielsen [2006] approach used in Xbeach-G.

The extrapolation of the Van der Meer [1988] formula, based on the results of this study and the results of Schiereck & Fontijn [1996], is confirmed to be too conservative. Consistently less damage was found in the analysis of the test results than was predicted by the Van der Meer [1988] formula. Note that this is a different discussion than that on mild slopes, a higher damage level should be tolerable. Furthermore, the description of the damage by the damage level 'S' appeared to be unsuitable for mild slopes. An improved empirical approach, written specially for mild slopes, should therefore not use the damage level 'S' as the damage parameter but the damage depth, as was proposed by Hofland et al. [2011].

The Van Rijn [2007] approach appears to have been giving quantitatively good results for all slopes. Furthermore, the advantage of the Van Rijn [2007] approach is that all the parameters are easy to determine, resulting in a very accessible approach to determine the stability of rock on mild slopes. Based on this research no points of improvement were found.

5.2 RECOMMENDATIONS

The test results have been analysed and the conclusion drawn, now the recommendations on extension of the research, improvements to this research and potential successive research will be elaborated in this paragraph. The recommendations are split into two parts, recommendations considering the test procedure and recommendations regarding further research. This division has been made because relatively new measuring techniques have been used throughout this research.

5.2.1 TEST PROCEDURE

In this research two relatively new (for this kind of research) measuring techniques have been used. For the profile change analysis, a 3D laser scanner has been used and for the physical analysis BIV/PIV measurements have been done. This subparagraph elaborates the recommendations for each measuring technique separately.

3D PROFILE ANALYSIS

- During the profile change measurements, scans were made from the entire slope. However, as the pointcloud density (i.e. the amount of measuring points per surface area) decreases with distance from the scanner, it is better to optimize this distance and only focus on the Region of Interest (ROI).

- During the profile change test, create a beacon in the measurement for reference. It has proven hard to, e.g. determine the exactly location of the waterline in the pointcloud after the measurement.

- The scans and pre-processing were done by somebody with extensive knowledge of the scanner and pre-processing software. Despite the great help and support received, it has the preference to do the scans yourself. Such that you exactly keep track of what happens with the data. The help of a third party in this case, results in sort of a 'black-box'[5] effect.

BIV/PIV ANALYSIS

- The BIV/PIV analysis was done with the resources available in the fluid mechanic laboratory of Delft University of Technology. There is an optimization possible in the hardware used in this research. The framerate of the camera could be higher, as well as the resolution.

- The lights used during the tests were 50 W LED lights. The LED were grouped together in a square of lightbulbs. Preferably one would create a line of LED lights. Such that over the width of the Field of View (FOV) equal light is distributed.

- The Depth of Field (DOF) was limited by the means of a gap in a wooden construction on top of the flume, see chapter 3 or Appendix A. The width of this gap, together with the height of the lights above this gap determine the DOF. For this research, merely one set up has been tested. Optimization of the gap, the height of the lights and the configuration of the lights (see previous bullet point) can increase the accuracy of the results.

[5] In science, computing, and engineering, a black box is a device, system or object which can be viewed in terms of its inputs and outputs (or transfer characteristics), without any knowledge of its internal workings.

- During the processing of the video material in PIVLab, the standard recommended image pre-processing settings have been used. As the combination of both bubbles and particles has been used in the analysis, and PIVLab normally is only used for particles of constant size, it is likely that an optimization can be made here.

- In the analysis of the BIV/PIV results a curve has been fitted through the velocity data points derived from the ROI. As regular waves were used during the tests, ensemble averaging could be applied to the data. This would lead to a more accurate fitted curve, as more data points would be available, and therefore a more accurate analysis.

5.2.2 FURTHER RESEARCH

In this sub-paragraph recommended further research is elaborated. In this research the focus has been on both the empirical description as well as the physical description of the stability of rock on mild slopes under wave attack. However, on both sides further research should be done in order derive a proper way to describe the stability of rock on mild slopes under wave attack.

- It is advised to do further research on this subject, as due to limited number of tests these results are promising but remain merely indications. When more tests are done, it is advised to stick to one slope (suggested cotα= 10), and apply more variables.

- From the empirical point of view. Based on this research the Van der Meer [1988] formula does not suffice anymore for the mild slopes (cotα > 10), because the damage level 'S' is not sufficient as damage description anymore. Suggested is to use the damage depth 'E_3' as was proposed by Hofland et al. [2011]. First trendlines based on the results have been plotted against the wave height. Furthermore, the damage depth appears to be a function of the significant wave height times the tangent of the slope angle. More test should be done regarding this damage description with respect to the wave height, such that these trendlines can be evaluated.

- The relation between the wave height and the damage depth 'E_3', is suggested to be within the wave energy. Differences in trendline between different slopes is provisionally explained by the spreading of the wave energy dissipation on slopes. This should however be further investigated in order to check and maybe even quantify these trends.

- The physical analysis based on the BIV/PIV results, should be repeated for more slopes and wave conditions in order to make sure the results of Van Rijn [2007] indeed consistently show good results. This should confirm or alter the view on whether the Van Rijn [2007] is still the preferred approach. This is emphasized because Postma [2016] found, while using Xbeach-G, that Nielsen [2006] gave the more accurate results for milder slopes.

- Postma [2016] suspects that the hydrodynamics in Xbeach-G are not properly modelled. He states that the slope correction factor is not accurate enough for rock on slopes, as the correction factor is originally derived for sand on a slope. Furthermore, he states that the infiltration effects have a significant influence on the stability of the stones. These suggestions have not been part of this research, and should therefore still be investigated in order to determine whether XBeach-G can be used as a design tool.

- The tests that were done in this research should be modelled numerically in the Xbeach-G software to see if the Van Rijn [2007] methodology indeed predicts the same amount of erosion that was found in profile change tests.

- The derived Shields values should be linked to a damage parameter. As when this is possible, one could use the Shields value as a design parameter. This way, the results of the two separate test programmes, the empirical tests with irregular waves and the physical tests with regular waves can be connected and directly compared.

REFERENCES

In this section the references will be presented, firstly the literature and secondly the software that has been used in this research.

LITERATURE

Bosboom, J. & Stive, M.J., 2013. *Coastal Dynamics 1*, version 0.4 ed. Delft University of Technology, VSSD

CIRIA, CUR, CETMEF, 2007. '*The Rock Manual. The Use of Rock in Hydraulic Engineering (2nd edition)'.* C683, CIRIA, London.

Hofland, B., Van Gent, M.R.A., Raaijmakers, T. & Liefhebber, F., 2011. '*Damage evaluation using the damage depth*.' Coastal Structures 2011. Yokohama, Japan.

Holthuijsen, L.H., 2007, *'Waves in oceanic and coastal waters',* Cambridge University press, New York

McCall, R., 2015. *Process-based modelling of storm impacts on gravel coasts*, s.l.: PhD, Plymouth University, United Kingdom.

Nielsen, P., 2006. *Shear stress and sediment transport for swash zone modelling*. Coastal Engineering, Volume 45 (1), pp. 54.60

Postma, M.G., 2016. *'Xbeach as a design tool for rock on mild slopes under wave loading'* Delft: Delft University of Technology.

Rivillas-Ospina G., Pedrozo-Acuña, A., Silva, R., Torres-Freyermuth, A., Gutierrez, C., 2012, *'Integrated study on the velocity field induced by plunging breakers',* Coastal engineering

Ryu, Y.U., 2006, *'Extreme wave impinging and overtopping',* Texas A&M University

Sistermans, P. G., 1993. '*Stability of rock on beaches'*, Delft: Delft University of Technology.

Schiereck, G., Fontijn, H. L., Grote, W. V., & Sistermans, P. G. J., 1994. '*Stability of Rock on Beaches'*,1553–1567.

Schiereck, G. J., & Fontijn, H. L., 1996. '*Pipeline protection in the surf zone'*, 4228–4241.

Schiereck, G. J. & Verhagen, H. J., 2012. '*Introduction to Bed, bank and shore protection'*. 2nd edition ed. Delft: VSSD.

Schiereck, G.J., 2007. '*Concise overview of scale rules in coastal engineering'.* Delft University of Technology, MSc community, Hydraulic Engineering.

Shields, A., 1936, '*Anwendung der Aenlichkeitsmechanik und der Turbulenzforschung auf die Geschiebebewegung'*, Preußischen Versuchsansalt für Wasserbouw

Thielicke, W. & Stamhuis, E.J., 2014**.** *'PIVlab – Towards User-friendly, Affordable and Accurate Digital Particle Image Velocimetry in MATLAB'*. Journal of Open Research Software

Tromp, M., 2004. *'Influences of fluid accelerations on the threshold of motion'* Delft: Delft University of Technology

Van der Meer, J. W., 1988. '*Rock slopes and gravel beaches under wave attack',* s.l.: TU Delft, Delft University of Technology.

Van Rijn, L.C., 2007. '*Unified view of sedient transport by currents and waves. Part 1: Initiation of motion, bed roughness and bed load transport*'. Journal of hydraulic engineering, volume 6, pp. 649-667

Wit, M., 2015. '*Stability of gravel on mild slopes in breaking waves*', Delft: Delft University of Technology

Ye, L., 1996. '*Stability of Rock on Beaches*'. Delft: Delft University of Technology.

SOFTWARE

Thielicke, W. & Stamhuis, E.J., 2014**.** *PIVlab - Time-Resolved Digital Particle Image Velocimetry Tool for MATLAB* (version: 10.4). Retrieved from http://pivlab.blogspot.nl/

Girardeau-Montaut, D., 2009. *'CloudCompare'* (version 2.7.0) [GPL software]. (2016). Retrieved from htp://www.cloudcompare.org/

FIGURES AND TABLES

Here a list of figures and tables is presented.

LIST OF FIGURES

LIST OF TABLES

APPENDIX A – TEST PHASE RECAP & RECOMMENDATIONS

In this appendix, the realization of the test plan will firstly be elaborated, in which the focus will be on the reasoning behind the test plan. In paragraph A.2 the final test plan is presented, whereas A.3 gives an evaluation of the test phase. The content of this appendix is presented below.

A.1. BASE OF THE TESTPLAN

In this paragraph the reasoning and decision making of the test plan will be elaborated. From the aim and scope of the research, follows the necessary and preferred output parameters. Once these are known the test plan can be developed, deciding on which parameters to vary and which ones to keep constant. Furthermore, the measuring techniques will need to be investigated and evaluated. Once all this is done the test plan can be finalized.

A.1.1 PROBLEM ANALYSIS

Momentarily the determination of the stability of rock on mild slopes can be split in roughly two paths, the empirical and the physical approach. However, both approaches have their limitations from which one could conclude that neither approach is currently an accurate description of the stability of rock on mild slopes under wave attack. The empirical approach by Van der Meer [1988] has to be extrapolated outside its validity region and the physical approaches on which the software XBeach-G runs are capable of globally determining profile changes reasonably well however they cannot accurately determine stability.

Van der Meer [1988] has a validated range for slope angles up to 1:6 (inhomogeneous) and 1:2 (homogeneous). Currently when designing rock protections on slopes milder than the respective slopes, the Van der Meer formulae [1988] are extrapolated. Schiereck & Fontijn [1996] already found that for a decreasing surf similarity (ξ) the stability increased. Wit [2015] also found these results when she derived the stability from the damage factor (S) in XBeach-G. See the results Schiereck & Fontijn [1996] as well as the results of Wit [2015] in Figure A.1

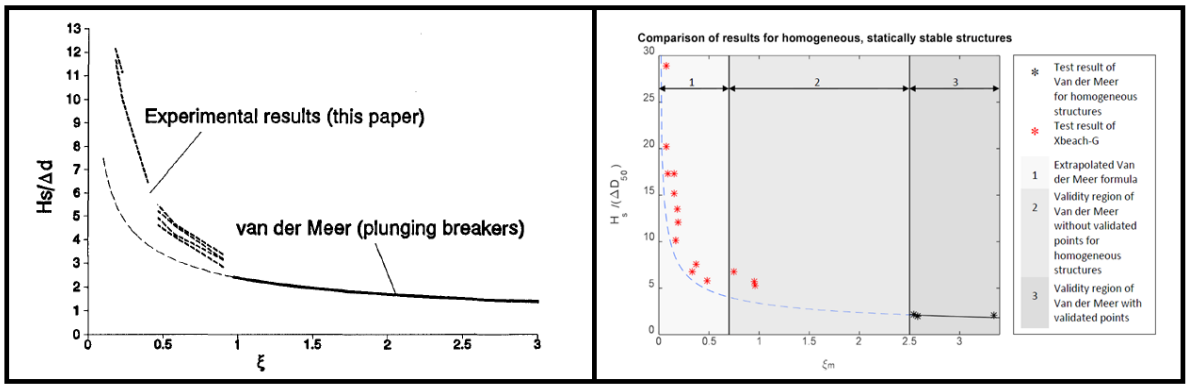

FIGURE A.1 - RESULTS OF SCHIERECK & FONTIJN [1996] (LEFT) AND RESULTS OF WIT [2015] (RIGHT)

When applying the model XBeach-G as a design tool one should on the first-hand note that the aim of the programme is to determine the profile response of a particular gravel beach, under certain (storm) conditions. From this however the eroded area can determine the damage factor ($S = A_e/d_{n50}^2$). When implementing this into the van der Meer formula [1988], the results can be compared. This method was applied by Wit [2015] and showed reasonably good results for homogeneous structures.

Furthermore, difficulties arise when zooming into the physical background of Xbeach-G. The morphodynamics are modelled in two ways, a choice can be made between the approach of Van Rijn [2007] or Nielsen [2006]. Both methods were adapted from their original purpose to fit the situation of rock on mild slopes under wave attack. Both methods give different results. Van Rijn [2007] uses a morphodynamic approach which starts with the forcing i.e. the bed shear stress, van Rijn [2007] states that this bed shear stress is caused by two components, the drag part and

the inertia part. This approach originally written for the sediment transport of sand under uniform flow, hence it is arguable that when applying to rock on a slope under wave forcing this is still valid. Nielsen [2006] defined the forcing of the sediment by the shear velocity. The shear velocity in this case is defined by approximated parameters which have a significant influence on the outcome. Therefore, the results greatly depend on the accuracy of these particular parameters.

A.1.2 OBJECTIVE & RESEARCH QUESTION

The aim of this research is to determine a more accurate way to formulate and design a rock armour on a mild slope under wave attack. In order to do so both physical and empirical approaches will be examined, ultimately leading towards a comparison between the different approaches. Rewriting the aim of this research into separate research questions results in the following, with the main research question boxed in followed by 3 sub-questions.

How should the stability of rock on mild slopes under wave attack be determined?

- Is the extrapolation of van der Meer [1988] an accurate way to define stability of rock on mild slopes under wave attack? And how do they relate to the provisional Schiereck and Fontijn [1996] formula?
- How do Nielsen [2006] and Van Rijn [2007] combined with the modified Shields parameter, as used by McCall [2015] comply with the test results?
- Could the previously mentioned methodologies (i.e. Van der Meer [1988], van Rijn [2007] and Nielsen [2006]) be improved based upon the data gathered from the test series

A.1.3 IN- AND OUTPUT PARAMETERS

To determine the in- and output parameters, the current methodology should be examined. This will be done by zooming in on the formulae used to describe the stability of rocks on mild slopes under wave attack. Firstly, the empirical formulae of Van der Meer [1988] will be elaborated, followed by the physical input used in XBeach-G, i.e. Van Rijn [2007] and Nielsen [2006]. The formulae will be broken down into their variables, which will be concisely described. From this elaborated list the preferred output shall be determined. Once the output is known variables and constants are determined, with this list the final test programme can take shape.

A.1.3.1 ENVIRONMENTAL PARAMETERS

The environmental parameters describe the characteristics of the water motion in front of the structure. Noted should be that in reality the structure does not influence these parameters and therefore the designer of a coastal structure has no influence on them.

WAVE HEIGHT

The wave height is one of the most important parameters, is this is one of the main parameters that determines the forcing on the slope. Over the years many definitions of the wave height have been given. Most commonly used is the significant wave height, noted as H_s. It is important to be consistent in the use of the terminology, since H_s is commonly used this definition shall be used most frequently.

When a visually estimated wave height (H_{visual}) is compared to recordings of the wave data, is appears that this visual estimated value is equal to the average height of the $1/3$ part of the highest waves ($H_{1/3}$). By the means of a wave spectrum which is than denoted as $H_{m_0} \approx 4\sqrt{m_0}$ with m_0

being the zeroth moment of the wave energy density spectrum. This being said is despite differently defined in deep water they are considered all the same.

$$H_s = H_{visual} = H_{\frac{1}{3}} = H_{m_0}$$ Equation A.1

Wave heights in a random sea state in deep water can be described by the Rayleigh probability distribution, i.e. with one value of a wave height the probability of exceedance of other values can be calculated. Commonly H_s is used.

As stated the validity of the Rayleigh distribution is merely in deep water, because the bigger waves start breaking when they approach the shoreline. With this assumption, also the highest 1% of the waves in deep water can be determined, which is approximately equal to 1.5 times H_s

WAVE PERIOD

For wave periods three characteristic wave periods are used. The peak period of the wave spectrum (T_p), the significant wave period (T_s)and the average period of zero crossings (T_m). This last value can also be calculated from the spectrum by $T_m = \sqrt{m_0/m_2}$. Depending on the shape of the wave spectrum these different definitions of the wave period have a certain ratio. T_p/T_s, T_p/T_m and T_s/T_m roughly vary between 1.0 and 1.5. The ratio between peak period and mean period is in this thesis set to $T_p=1.07 \cdot T_m$.[6] , with the assumption that $T_m=T_{1/3}$, for JONSWAP spectra.

WATERDEPTH

The water depth plays an important role in the breaking process of waves. Miche [1944] described the breaking limit as $H_b/h = 0.88$, which follows from Miche's breaking criterion.

$$H_b = 0.142\, L \tanh(\frac{2\pi}{L} h)$$ Equation A.2

Solitary wave theory had a slightly different definition, where $H_b/h = 0.78$. When translating this to the significant wave height this results in $H_s/h = 0.4 - 0.5$. This corresponds with the breaking of larger waves (h=1.5-2 H_s). The depth of the water in front of the structure should be as high as possible, without the risk of waves overtopping the flume, to simulate deep water.

SPECTRAL SHAPE

The wave spectrum contains a lot of information, as mentioned both the period and the significant wave height are derivable from the spectrum. These variables however don't describe the shape of this spectrum nor the groupiness of the waves. Based on the bivariate Rayleigh probability density function the parameter κ was developed. This value describes the shape of the spectrum with theoretical boundaries 0 and 1. (respectively being white noise and a spectrum with only one frequency). Practical boundaries are $\kappa = 0.3 - 0.9$. In other words, the lower the kappa value, the narrower the spectrum is and thus the more regular the waves will be, see Figure A.2.

[6] Based on lecture 07 of the course 'Bed, bank & shoreline protection – CIE4310' at Delft university of College.

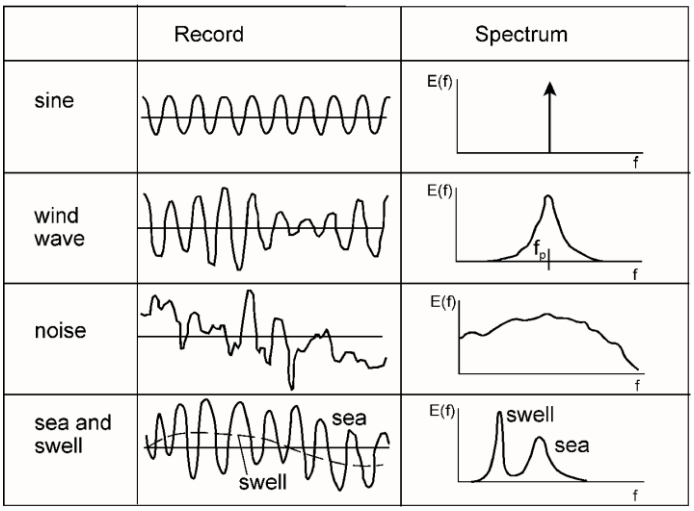

FIGURE A.2 – WAVE RECORDS AND SPECTRA – SCHIERECK ET AL [2012]

Commonly used wave spectra are the Pierson Moskowitz spectrum (PM-spectrum) and the JONSWAP spectrum (JOint North Sea WAve Project). The PM spectrum is assumed to represent fully developed conditions in deep water. Whereas the JONSWAP spectrum is limited by the fetch, hence the sea state was never fully developed. The spectra are closely related and can be rewritten (with some coefficients) into each other's shape. Since JONSWAP is applicable to the Dutch coast and is most commonly used, this spectrum chosen for this research.

STORM DURATION

Storm duration is normally taken into account by varying the number of waves in the test series. Especially when looking into the dynamic equilibrium than the number of waves will play an important rule. However, at some stage the equilibrium profile will be reached and the influence of the number of waves dies out. For the Dutch coast a representative storm duration is 5 hours according to Vellinga [1986], with an average of 6 seconds per wave this comes down to 3000 waves.

PHASE LAG ANGLE

The phase lag angle in this context is defined as the phase difference between the free stream velocity and the bed shear stress. This value is used as a constant in the Nielsen [2006] formula and is caused by the asymmetry of waves. According to Nielsen [2006] the phase lag angle is related to the wave period and the size of sediment. He states that bigger wave period lead to smaller phase lags as does bigger sediment.

A.1.3.2 STRUCTURAL PARAMETERS

The structural parameters describe the shape and features of the structure. Structural parameters have to withstand the loads but also play a major role in how the loads on the structure are characterized. For example, the size, shape and grading of the armour stones have influence on the roughness of the slope and therefore on the run-up and run-down.

STONE SIZE DIAMETER

The easiest way to measure a piece of rock/armour stone is its weight, M [kg]. The dimension of the equivalent cube size, D_n, better known as the nominal diameter is most commonly used in the design of bed protections. This nominal diameter is than related to the median mass of the stones, the M_{50}. This relation between weight and nominal diameter is given by the formula.

$$D_{n50} = \sqrt[3]{M_{50}/\rho_{stone}} \qquad \text{Equation A.3}$$

Another way to describe the stone size is by creating a sieve curve. In this case the median stone size is denoted as D_{50}. The D_{n50} is approximately equal to 0.84 times the D_{50}.

STONE SHAPE

The shape of the rock can be an important characteristic, it influences the shear strength, permeability and filtering properties. The shape of the stones should be taken into account when one does a lot of tests, because than the shape of the stone may vary over the experiments due to wearing of the stones. The shape of the stone could be examined in terms of for example the Length-to-thickness ratio, the blockiness, the roundness or the cubicity. All of which have been defined in the Rock Manual [2007]. This parameter is considered constant during the research, and will not be further implemented in the research.

GRADING OF THE STONE

The grading of the curve is an indicator for the diversity of stone sizes in a particular rock batch, they are normally depicted in a sieve curve. Steep curves represent narrow graded samples (i.e. low diversity) and gentle curves represent the wider graded samples (i.e. greater diversity in stone sizes).

Grading width	D_{85}/D_{15}	M_{85}/M_{15}
Narrow or single-sized gradation	Less than 1.5	1.7-2.7
wide	1.5-2.5	2.7-16
Very wide or quarry run	2.5-5.0	16-125+

TABLE A.1 - ARMOURSTONE GRADING – ROCK MANUAL [2007]

SLOPE

This research is about the stability of rock on mild slopes under wave attack. In this case, mild slopes are defined by slopes with cotα higher than 6. To determine the stability of the stones, the damage after a storm event will need to measured. This measurement is based on the profile difference between initial slope and the post storm event slope. The initial slope is the slope before the wave series have started, whereas the post storm event slope is the slope after the storm event. See storm duration for the definition of a storm event.

DENSITY OF THE STONE

Depending on the type of rock the density of rock can vary significantly, the range roughly lies between 2000 and 3000 kg/m^3. Most commonly the density of rock is 2650 kg/m^3, for this case the density of the stones has been determined at 2685 kg/m^3.

PERMEABILITY

The permeability of the structure is an important aspect in the stability of the structure. Permeability is dependent on most of the stone properties, the stone size diameter, grading, shape of the stones, but also on the way the structure has been built up. The presence of filter layers or not, the permeability of the core and how these layers relate to one another. Van der Meer [1988] used a notional permeability factor to describe certain types of structures, see Figure A.3. Most relevant structure for this type of research is the structure schematized top left of Figure A.3. This type of structure will be analysed in this research.

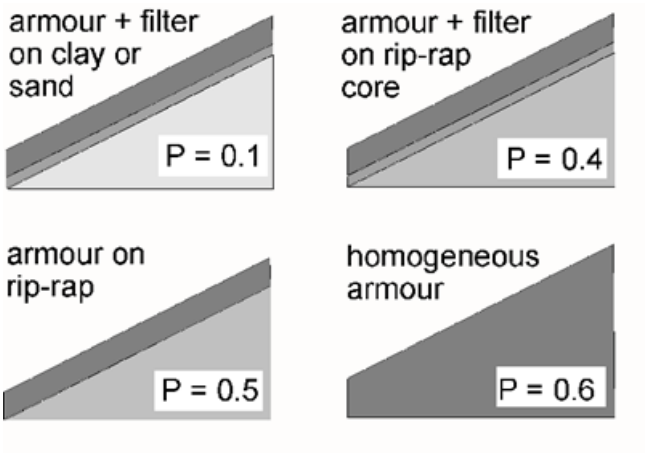

FIGURE A.3 - NOTIONAL PERMEABILITY - SCHIERECK ET AL. [2012]

FRICTION FACTOR

Friction factors are used in the Van Rijn [2007] as well as the Nielsen [2006] formula. However, both use a different definition of the friction. Van Rijn [2007] uses a dimensionless friction factor c_f and Nielsen [2006] uses the sediment friction factor f_s.

A.1.3.3 DIMENSIONLESS PARAMETERS

RELATIVE DENSITY

The relative density is defined as the density of the stones submerged in water. This is given by the equation:

$$\Delta = \frac{\rho_s - \rho_w}{\rho_w} \qquad \text{Equation A.4}$$

With the subscripts distinguishing between the density of the stone (ρ_s) and water (ρ_w).

WAVE STEEPNESS

The wave steepness is defined as the wave height over the wave length. The wavelength can be defined $L = gT^2/2\pi$. This gives for the wave steepness, which is generally defined as the ratio of wave height over wave length, to be described as equation A.5

$$s = 2\pi H/gT^2 \qquad \text{Equation A.5}$$

Normally the wave steepness is around a couple percent, 0.01-0.05. Fresh wind waves seldom being steeper than 0.05 and swell having a steepness of around 0.01 or less. The higher waves of spectrum typically have a higher wave steepness, in the order of 0.05-0.10.

IRIBARREN NUMBER

The Iribarren number, or sometimes called the surf similarity parameter, indicates the type of breaking on the structure. It is the ratio of the slope angle of the square root of the wave steepness. It is easy to imagine that differences in the type of breaking of a wave play a major role in the forces that act upon the structure, and thus on the design of a shore protection. The Iribarren number is defined, by Battjes [1974], as:

$$\xi = \frac{\tan\alpha}{\sqrt{H/L_0}} \qquad \text{Equation A.6}$$

DAMAGE

In the Van der Meer [1988] the damage is defined by the damage level 'S'. Where the damage level is defined as the erosion area divided by the square of the nominal diameter of the armor layer.

$$S = \frac{A_e}{D_{n50}^2} \qquad \text{Equation A.7}$$

A damage level of S= 2 is defined as the incipient damage. Hofland et al. [2011] proposes a different damage description parameter, see equation A.8, the damage depth.

$$E_3 = \frac{\langle d_e \rangle_{3dn50}}{D_{n50}} \qquad \text{Equation A.8}$$

This description uses the eroded depth as key variable in quantifying the damage. The eroded depth (d_e) averaged in a circle with diameter of $3D_{n50}$, divided by the nominal stone size. Hofland et al. [2011] proposes a tentative classification, which states that initial damage occurs if E_3 = 0.2-0.3 for a layer thickness of $2D_{n50}$. Intermediate damage occurs between E_3 = 0.5-0.6 and failure would be between E_3 = 1.5-1.6.

A.1.4 INPUT VARIABLES AND OUTPUT

With these parameters analysed choices with regard to the test plan should be made. What output is necessary to gain more insight in the stability of rock on mild slopes under wave attack? Which parameters are governing in the determination of stability? Which parameters should be varied and which should remain constant? When varying a parameter, how much should the variation be?

A.1.4.1 VARIABLES

When altering the variables, one should keep in mind that in order to represent a realistic model certain conditions have to be met. For example, the wave steepness should have a realistic value, this is the ratio between wave length and wave height, in which the wavelength can be determined by $L = gT^2/2\pi$ (under the deep-water assumption). In order to assume deep water, the wavelength compared to the depth may not be larger than half of the wavelength. Then the Iribarren number should be within the plunging/spilling wave range, in order to create the same kind of impact on the structure. And finally, the value for the stability $H_s/\Delta d_{n50}$ should not be too low, i.e. too stable because if that is the case than no damage will occur at all. This led to the following variables

Variable Parameter			Range
H_s	Wave height	[m]	Variable
T_m	Wave period	[s]	Variable
Cotα	Slope angle	[-]	1:5, 1:10 & 1:15

TABLE A.2 – VARIABLE PARAMETERS

A.1.4.2 OUTPUT PARAMETERS

The output parameters have been chosen in such a way that with the gathered data, a new formulation for stability of rock under mild slopes can be given. From the research of Tromp [2004] and Terille [2005] followed that both the velocity as well as the acceleration play a significant role in the initiation of motion of coarse particles.

Output Parameter			Data preferred/necessary?
u	Velocity	[m/s]	Necessary
$\delta u/\delta t$	Acceleration	[m/s²]	Necessary
u_b	Near bottom velocity	[m/s]	Necessary
S & E_3	Damage	[-]	Necessary (couple of cases)
φ	Phase lag angle	[rad]	Preferred

TABLE A.3 – PREFERED OUTPUT PARAMETERS

A.1.5 MEASURING TECHNIQUES

In order to gather the necessary and preferably the preferred data, a decent and adequate plan will need to be formulated. In the previous section the in- and output parameters were formulated. In this paragraph, a few measuring techniques will be elaborated in order to gain accurate data regarding the respective output parameters.

A.1.5.1 VELOCITY AND ACCELERATION

In order to measure the velocity over time (and thus also the acceleration in time, $\delta u/\delta t$) multiple techniques are possible. Here four techniques will be concisely elaborated; the EMS, the Vectrino II, Particle Image Velocimetry (PIV) measurements and a variant to PIV, the Bubble Image Velocimetry (BIV)

EMS (Electrical Magnetic Velocity) is used to measure the velocity of the water. This instrument is based on the principle that a conducting fluid will generate a voltage proportional to the flow velocity as it passes through the magnetic field created by the sensor.

Vectrino II (Acoustic Doppler Velocimeter, ADV) determines the velocity of particles along the theory of the Doppler shift effect. Advantageous of this measuring technique is that it allows for measurement close to the bottom. Output appears to less accurate and reliable.

PIV (Particle Image Velocimetry) is an optical method to determine visualize flow and the characteristics of the flow. Small traceable particles are placed in the water, so small that they are following the flow dynamics. These particles can be tracked and visualized by the measuring equipment such that the speed and direction of the particles can be determined. This technique gives results in a relative small area of interest.

BIV (Bubble Image Velocimetry) is a variant to the previously described PIV methodology. Instead of using suspended particles in the water the BIV tracks air bubbles in the water. This is an advantage over the PIV when measuring has to be done in the swash zone, where the water is aerated.

A.1.5.2 VELOCITY AT THE BED

The near bottom velocity, or velocity at the bed, is specified to the velocity in the first couple of centimetre to the bed. Since the EMS requires a certain distance above the bed in order to give accurate measurements, this distance is roughly 5 centimetres. The area in which the interest is located is closer to the bed than five centimetres, therefore the EMS measuring technique does not suffice the measurement for this case. PIV however, seems to be a good technique in order to determine this near bottom velocity. However, when applied to the swash zone, i.e. aerated water, the PIV technique cannot be used. In this case the BIV technique is the best option.

A.1.5.3 WAVE DATA

In order to determine the exact wave loading on the structure the waves will be measured along the flume, but in special just in front of the structure. This will be done by the means of wave gauges.

Wave gauges are used to measure the water surface elevation relative to the still water level. The waves are measured using an electrical resistance in the wire, the voltage output signal can on its turn be related to the wave signal. The wave signal gives the water level variation over time and thus contains information about both the wave height and the wave period. Two wave gauges will be placed together for increased accuracy. One pair of wave gauges will be placed just in front of the slope to measure the exact incoming wave height.

A.1.5.4 DAMAGE

In the past the damage has been defined in many different ways. Most commonly used is the damage factor S, which is defined as $S = A_e/d_{n50}^2$. Questionable however is whether that is the best definition to describe damage on a slope. It seems more logical to use the eroded depth over the d_{n50} as description of damage. Especially on mild slopes where the eroded area significantly increases due to a longer swash zone.

Bed profiler is used to measure the bed profile. It is a carriage that can move over the flume with a number of poles attached to the carriage, this poles can move up and down while the carriage is moving and in this way, they measure the profile.

Laser techniques can be used in order to evaluate the profile change of the slope after the wave forcing. Attention should be given on whether it is possible to read the bed level accurately under the water level. Within the laser measuring techniques the separation has to be made between 2D and 3D measuring techniques.

Coloured strips. By dividing the length of the slope into strips of equal width, the strips simulate equal depth contour lines, and giving each strip a different colour the damage can be determined by the means of counting displaced stones. In this case the width of the strips influences the accuracy of the measurement.

A.1.5.5 SCALING EFFECTS

For the tests in the wave flume the scaling laws need to be checked, this is done by the hand of the Schiereck [2007], as tests in the wave flume can have scaling effects. Sources of scaling effects can be the water viscosity, surface stress and air entrainment in breaking waves. The waves will be greater than 0.05 meter meaning that the breaking characteristics will be maintained according to Weber, the Weber number indicates the ratio between inertia and surface stress. Further the more particle Reynolds number indicates the dependency on viscosity, if the particle Reynolds number is greater than 600 the flow around the stones can be considered turbulent. This minimal Reynolds value coincides with a minimal stone size diameter of 7 mm. As the stones are larger the flow can be considered turbulent. The wave flume at Delft University of Technology is because of these relations considered as a physical reality during the tests.

A.2. TEST PLAN

In this chapter of Appendix A, the test plan will be elaborated. The test plan is split into two different kinds of tests, the profile measurements with irregular waves and the BIV/PIV tests with regular waves. However, before the tests were started the rock that was ordered had to be examined. As this material and its properties are the input for the rest of the tests, this part is elaborated first. After this is done the profile measurement tests will be explained, followed by the final part of the test plan in which the BIV/PIV tests will be elaborated.

A.2.1 STONE ANALYSIS

The characteristics of the stones play a significant role in the stability of the applied armour layer. Size, weight, density, shape and gradation are most important in this matter. All these aspects will be treated in this chapter. The stones used in this test are from a batch that was ordered especially for this research. This batch was specified as 'Yellowstone, 16-25 mm'. The range of the sizes of stones was further diminished by sieving out all the stones smaller than 15 mm. This was done during the washing of the stones. With the adjusted batch, further tests were done. The shape of the stones can have a large influence on the stability, as this batch consists of crushed rock it is naturally angular of shape. Whereas pebbles for example are a lot smoother and for that reason have less interlocking and are consequentially less stable than the stones used in this research. A lot of descriptions have been used to describe the exact shape of the stones, however this will not be part of this research.

A.2.1.1 SIZE AND GRADATION

For the size and gradation several sieve tests have been done. Three sieves have been constructed for this purpose, with openings of 15, 20 and 25 mm. (see Figure A.4) The determination of the sieve curve, i.e. the gradation of the stone sample has been done by analysing four samples of the batch. Each sample weighs approximately 12-13 kg. By weighing the total sample, as well as the fraction that surpasses the sieve, the fraction of the batch that is larger than 25 mm can be determined.

FIGURE A.4 - SIEVE (25 MM)

After analysis of the four batches, they resulted in roughly the same gradation of stones. Therefore, all batches were summed and the total was used as the representative gradation. The results are shown in Table A.4 and Figure A.5.5

	Weight [g]	Percentage [%]
D > 25 mm	5137	9.6%
20 mm > D > 25 mm	17468	32.7%
15 mm > D > 20 mm	26754	50.1%
15 mm > D	4017	7.5%
Total	53376	100.0%

TABLE A.4 - SIEVING RESULTS

From the results presented in the figure one can determine the gradation of the sample D_{85}/D_{15}. For the d15 this comes down to 15.7 mm and for the d_{85} the value is 24.4 mm, when combined these two values give a narrow gradation, with a D_{85}/D_{15} of 1.55. As can be seen in Table A.1 of in chapter 1 of this appendix, according to the Rock Manual [2007] this batch can indeed be qualified as a narrow graded stone batch.

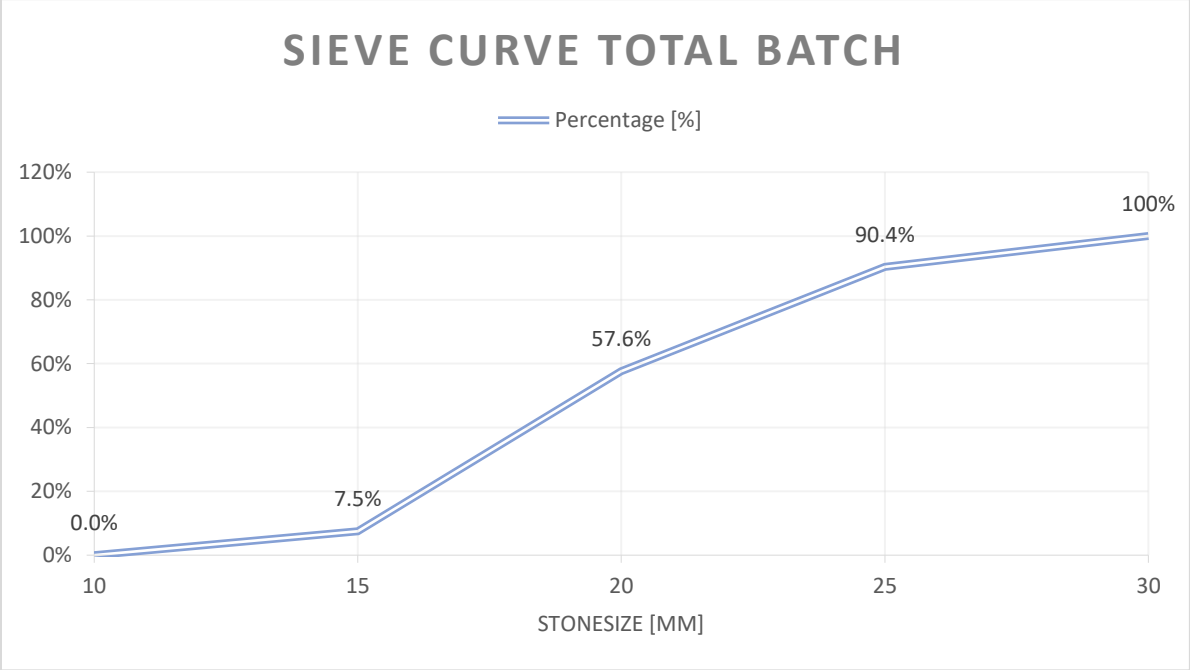

FIGURE A.5 - SIEVE CURVE STONE BATCH

From sieve curve, also the D_{50} can be determined, which in this case lies just below the middle sieve size (20 mm). When zooming in on the plot d_{50} corresponds with a value of 19.2 mm. However, in the literature mostly D_{n50} is used, according to Verhagen & Janssen [2014] D_{50} times a factor of 0.845 represents the D_{n50}. This is in line with what Laan [1996] said, he stated that this factor should be between 0.81-0.88, with for smaller stone sizes higher factors. Therefore, a D_{50} of 19.2 mm coincides with a D_{n50} of (19.2 x 0.845=) 16.2 mm

A.2.1.2 DENSITY

The density of the stones plays a significant role in the stability, as the density (multiplied with the volume of the stone) determines the gravity force on the stone. Especially since the gravity plays an increasingly important role for milder slopes, the density needs to be determined accurately. As the stone batch (Yellowstone 16-25 mm) consists of two different color stones (white and yellow), both colors will be determined separately. In order to make sure that both color stones have the same characteristics.

Four samples, roughly 0.8 kg each, of the stone batch have been taken and separated by color. Of each sample both the yellow and white stones were weighed, after the dry weight was determined the sample were submerged in a measuring cup filled with water. By measuring the volume change in the measuring cup, the volume of the stone sample can be determined. See Figure A.6.

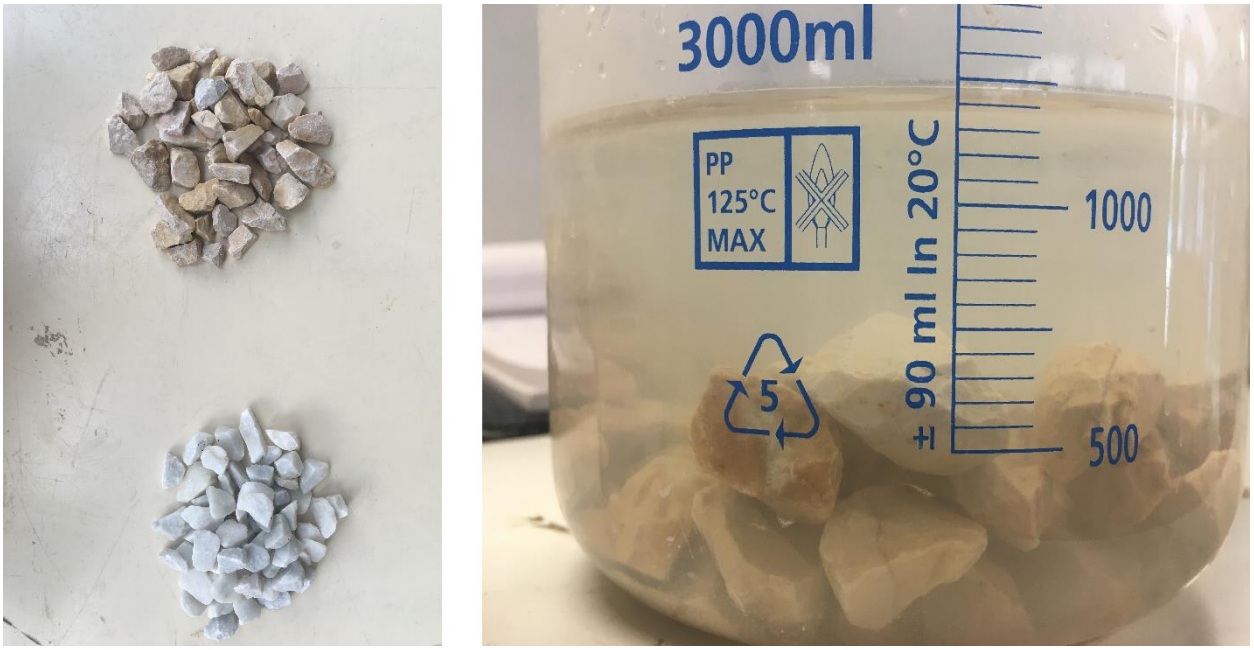

FIGURE A.6 - DENSITY DETERMINATION OF THE STONE BATCH

This was done per sample for both colors and both colors combined mixed. Results showed that the difference between yellow and white stones are negligible. After averaging over all four batches the following densities were found, see Table a.5. From Table a.5 can also be concluded that following from the samples that were taken from the batch, that the yellow stones are more dominantly present than white stones. However, since the difference in density is negligible this does not have any consequences on the batch as a whole.

	Mass [g]	Volume [ml]	Density [kg/m^3]
Yellow	1758	655	2684
White	1450	540	2685
Mixed	3208	1195	2685

TABLE A.5 - DENSITY DETERMINATION OF THE STONE BATCH

A.2.1.3 PERMEABILITY

For the energy dissipation of the wave on the slope the permeability of the rock sample plays a significant role. In order to quantify the permeability of the sample a Darcy type of test has been done. This test, just as the other tests, has been at the laboratory of the University of Technology in Delft. The test set up can be schematized as depicted in Figure A.7.

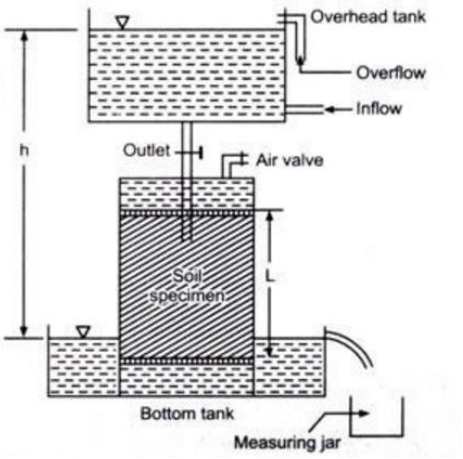

FIGURE A.7 - PRINCIPLE SKETCH PERMEABILITY SET UP

The sample of the rock is placed in the test set up with the dimension 0.26x0.26x0.30 m (LxBxH). This results in an area of 0.0676 m² (LxB=0.26x0.26) with a sample length, ΔL, of 0.30 metre. With the flowrate as an input value and the pressure difference, Δh, as ouput all the variables are determined in order to calculate the permeability 'k'.

$$\frac{Q}{A} = k \cdot \frac{\Delta h}{\Delta L} \quad \rightarrow \quad k = \frac{Q}{A} \cdot \frac{\Delta L}{\Delta h}$$

Equation A.9

The test was repeated thrice and is averaged over the three values. The results are presented in Table A.6

	A [m²]	ΔL	Q [m³/s]	h_1 [m]	h_2 [m]	Δh [m]	k [-]
Test 1	0.0676	0.30	0.0068	1.15	0.895	0.255	0.1183
Test 2	0.0676	0.30	0.0085	1.125	0.695	0.43	0.0877
Test 3	0.0676	0.30	0.0104	1.05	0.55	0.50	0.0923
						Average	**0.0995**

TABLE A.6 - PERMEABILITY TEST RESULTS

A.2.2 PROFILE CHANGE

This part of the tests series is purely based around the Van der Meer [1988] tests, these tests were done by measuring the eroded area after a storm event. Van der Meer [1988] used a bed profiler to measure the profile, since technique has evolved since than now a laser scanner will be used to make these measurements. Therefore, after the first slope results were analysed, and this problem arose, the choice was made to switch to a 3D scanner. The test programme remained the same. In the first two paragraphs the 3D scans will be elaborated. In the final paragraph, the evaluation of the test series, the 2D scans will be reviewed

A.2.2.1 INPUT

Three different slopes will be tested, namely a 1:5, 1:10 and a 1:15 slope. Whereas the last two (1:10 & 1:15) are considered mild slopes outside of the validity region of Van der Meer [1998], and the first steep slope (1:5) is within this validity region. These test results should therefore agree with the theory of van der Meer [1998]. Per slope two tests will be done, both with different wave characteristics.

The wave characteristics are derived from the theory. The first wave height per slope is derived from the extrapolation of tolerable damage defined by Van der Meer [1988] done by Wit [2015]. Whereas the second wave height is based on the results of Schiereck and Fontijn [1996].

Firstly, Van der Meer [1988] states that a damage level of S=2 (for steep slopes) coincides with the start of damage. Therefore, if S < 2 than the armor layer remains stable. Van der Meer [1988] however in his research already mentions that for milder slopes the acceptable damage level is higher than for steep slopes. This is because the erosion area will spread out over a longer length, therefore the erosion depth can be the same for a steep and mild slope but the damage level would be significantly higher for a mild slope. Therefore, higher damage levels are acceptable for mild slopes. Wit [2015] made an extrapolation of this increase of acceptable damage levels, based on Van der Meer [1988]. See equation A.10.

$$S(\alpha) = S_{start}{}^{\sin(\alpha_{start})}\Big/_{\sin(\alpha)} \qquad \text{Equation A.10}$$

For this research the starting value of S =3 for slopes of 1:5 is chosen, then from this starting point one can derive the acceptable damage levels. This results for slopes with cot α = 10 and 15 in acceptable damage levels of 6 and 8.8 respectively. This results in a Figure A.8, in which the extrapolated damage is represented by the red dashed line. As the wave steepness is constant during the test, the damage level is merely a function of the slope angle.

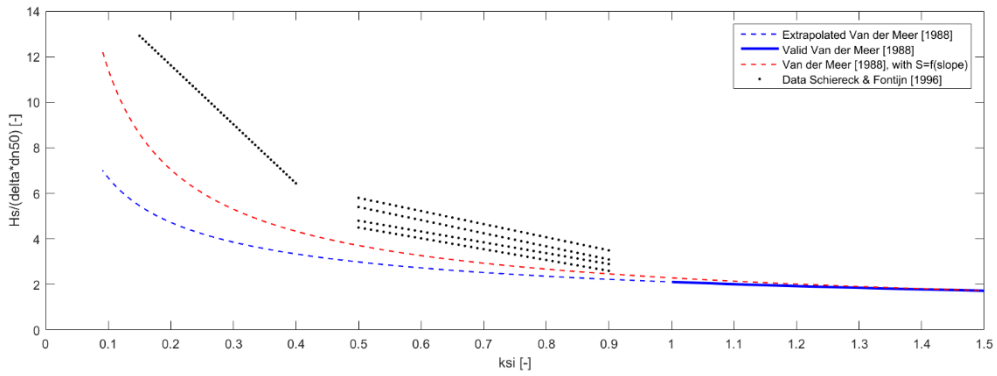

FIGURE A.8 - EXTRAPOLATION OF TOLERABLE DAMAGE FOR VAN DER MEER [1988]

Rewriting the formula of Van der Meer [1988] with all other variables substituted, results in a wave height which theoretically leads to the damage level stated, rewriting Van der Meer [1988] results in, see equation A.11.

$$H_s = 6.2 \cdot P^{0.18} \cdot \left(\frac{S}{\sqrt{N}}\right)^{0.2} \cdot \xi^{-0.5} \cdot \Delta \cdot d_{n50} \qquad \text{Equation A.11}$$

Because wave steepness will be will be constant, the Iribarren number per slope will not change. Resulting in that the only two variables for these tests are the wave height and damage level, as the rest will all be constant throughout the tests. For the 1:15 slope this will result in a significant wave height of 0.133 meter. The wave heights on their turn determine the wave period, this is because the wave steepness is kept constant, in this case the mean wave period would be 1.46 seconds.

The second wave height for the tests is based on the results of Schiereck & Fontijn [1996], as the wave steepness will be constant (s=0.04) and the slope angle is known the Iribarren number can be determined for each slope. From there the dimensionless stability number can be determined, from which the wave height can be determined. This is possible because again the other variables are known and remain constant throughout the tests. See Figure A.9 for an example of the determination of the stability number, this is done for the slope 1:15. This slope has an Iribarren value of 0.33, from which the stability parameter is derived leading to the derivation of the wave height.

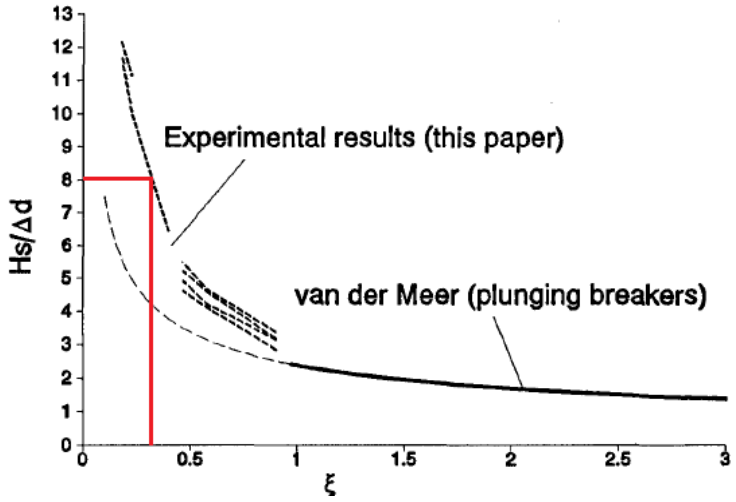

FIGURE A.9 - WAVE HEIGHT DETERMINATION SCHIERECK & FONTIJN [1996]

In Figure A.9 one can see that the Iribarren value of 0.33 coincides with a stability number of 8. Rewriting the stability number into the wave height, results in a significant wave height 0.215 meter. However, since this part results of Schiereck & Fontijn [1996] are based on slope of 1:25, the wave height is slightly adjusted to a significant wave height of 0.2 meter. This results in a mean wave period of 1.79 seconds.

For the 1:5 slope the input slightly varied from the above presented approach. This is done because on this slope the Van der Meer [1988] is valid again, therefore the starting point of the extrapolation of Wit [2015] can be used again, S=3. As Schiereck & Fontijn [1996] does not analyze this slope and has no coinciding Iribarren value to compare. Therefore, it is chosen to do a test with a wave height which theoretically results in a damage level of S=2.

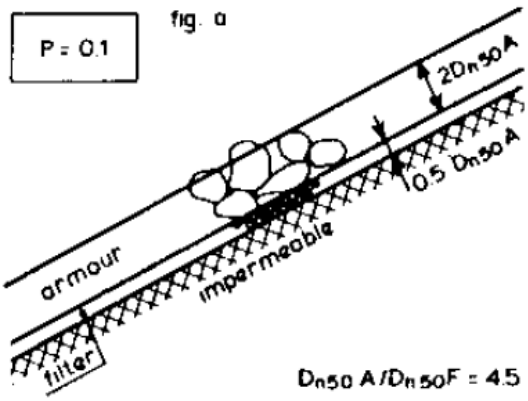

FIGURE A.10 - P=0.1 - VAN DER MEER [1988]

Van der Meer [1988] assumed notional permeability values for different kind of structures. Most realistic and relevant for cases in the Netherlands, is an inhomogeneous structure on top of an impermeable core, e.g. sand. In order to replicate these conditions a wooden understructure will be used. Upon this wooden structure a layer of stones will be placed. This layer will be 2 times the nominal stone size diameter thick. Van der Meer [1988], officially accounts for a filter layer which is not used in this test series. The test set up used is assumed to coincide with a notional permeability value of P=0.1. (see Figure A.10)

With the preceding elaboration and the following constants as presented in Table A.7, form the constant input for each test regarding the profile change.

Variable			1:5	1:10	1:15
h	Water depth	[m]	0.65	0.65	0.65
[-]	Wave spectrum	[-]	JONSWAP	JONSWAP	JONSWAP
N	Number of waves	[-]	3000	3000	3000
D_{n50}	Nominal stone size diameter	[mm]	16.20	16.20	16.20
Δ	Relative density	[-]	1.69	1.69	1.69
s	Steepness	[-]	0.04	0.04	0.04
P	(notional) Permeability	[-]	0.10	0.10	0.10
ξ	Iribarren value	[-]	1.00	0.50	0.33

TABLE A.7 - CONSTANTS PROFILE CHANGE TEST SERIES

The input for each test as presented in Table A.8 and Table A.9, represents the variable input. The wave data for each test and the theoretically expected damage. According to the lectures of the course 'Bed, bank, and shoreline protection, CIE4310' given at DUT. the peak period relates to the mean wave period with a factor of 1.07. The peak period together with the significant wave height forms input for the wave board in the wave flume, when applying a JONSWAP spectrum. For the test duration, the number of waves 'N' times the mean wave period 'T_m' is used.

Variables based on Wit [2015]			1:5	1:10	1:15
H_s	Significant wave height	[m]	0.062	0.089	0.133
T_m	Mean wave period	[s]	0.995	1.266	1.458
T_p	Peak wave period	[s]	1.065	1.355	1.560
S_{theor}	Damage (Based on Van der Meer [1988])	[-]	3.000	5.910	8.840

TABLE A.8 - INPUT VARIABLES BASED ON WIT [2015]

Variables based on Schiereck & Fontijn [1996]			1:5[7]	1:10	1:15
H_s	Significant wave height	[m]	0.057	0.135	0.200
T_m	Mean wave period	[s]	0.955	1.470	1.790
T_p	Peak wave period	[s]	1.022	1.570	1.915
S_{theor}	Damage (Based on Van der Meer [1988])	[-]	2.000	26.430	68.450

TABLE A.9 - INPUT VARIABLES BASED ON SCHIERECK & FONTIJN [1996]

[7] Note that these input values are not based Schiereck & Fontijn [1996], as explained on the previous page.

A.2.2.2 TEST PLAN

With all input variables and constants known, the test plan can be finalized. For constructional reasons from the lab, the first slope to be tested is the 1:15 slope. The slope was constructed in a sturdy way, i.e. the slope is very stiff, such that upon wave impact the slope construction will not significantly vibrate. (see the left picture in Figure A.11, in which the slope construction is partly visible). This way the stones placed on the slope will not be influenced by wave induced vibrations. The layer thickness was indicated with tape on the side of the flume, which was used during the construction of the armor layer as reference for the layer thickness. A plumb rule was used to make sure the same layer thickness was applied over the entire width of the flume. See the middle picture in Figure A.11. Using this methodology, a layer thickness of 2 D_{n50} was constructed, i.e. 32 mm.

Once the slope was fully constructed and aligned to the design layer thickness, the first scan can be made. The scans were made with a 3D laser scanner, a Leica C10. For each profile measurement two scans are made, one before and one after the wave series. This results in two separate pointclouds. These two pointclouds will be fitted together with the use of three especially placed trackers. These trackers will remain in the exact same position, with these stationary points the two pointclouds can be exactly aligned. See Figure A.11 (right picture) with the red square indicating the scanner and the red circles the trackers.

FIGURE A.11 - CONSTRUCTION OF SLOPE (LEFT & MIDDLE) AND SCANNER AND TRACKERS (RIGHT)

With the first scan done, the water can be pumped into the flume. This has to be done slowly in order for the rising water level not to influence the stones on the slope. Once the water level reaches the designated level, i.e. h= 0.65 m, the pumps can be closed. A final check on the position of the wave gauges and the EMS has to be made, in order to verify that all are in the correct position. The setup of the profile measurement tests is depicted in Figure A.11. The wave gauges are represented with the bold vertical lines crossing the water level, whereas the EMS is represented by the dashed line. Furthermore, in Figure A.12 on the next page the Leica C10 laser scanner is depicted by the circle on the left side of the flume.

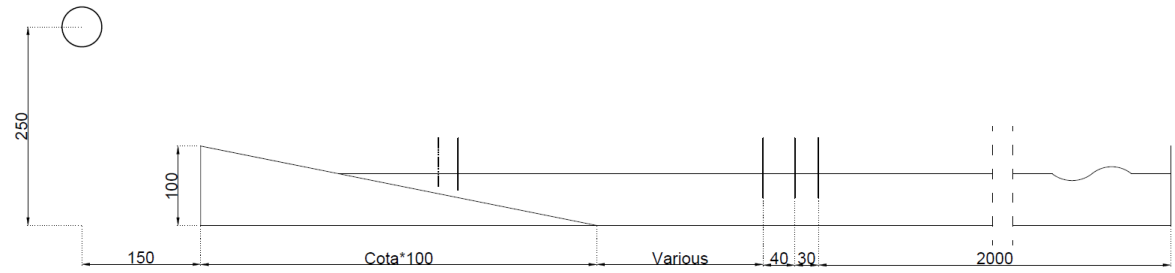

FIGURE A.12 - TEST SET UP FOR PROFILE CHANGE TESTS. (LENGTHS IN CM)

Once this is verified, the wave gauges are calibrated. The calibration is done by moving the gauges 5cm upward and downward over time. The change in voltage can then be used to calculate the ratio volt to centimeter. Which is later used to translate the voltage signal produced by the wave gauge to a wave signal. At last the input values for the wave board are checked before the start of the test.

Once all input values and set up characteristics are checked and verified, the test can commence. The wave board can be activated and the set wave conditions created. A total number of 3000 waves will be created, this represents a Dutch storm event. After the wave series, the flume will be carefully drained, in order to make sure the stones do not move during the draining of the flume.

A.2.2.3 WAVE ANALYSIS

As the waves reflect on the slope and influence the incoming waves, the actual wave height on the slope differs from the input values. Using the three wave gauges, as depicted in Figure A.12, the incoming wave can be split from the reflected wave. For the profile change tests, the following wave characteristics were derived, see Table A.10.

Test		$H_{s;input}$ [m]	$T_{m;input}$ [s]	$H_{m0;output}$ [m]	$T_{m-1.0;output}$ [s]
Slope 1:5	S_{norm}	0.057	1.022	0.054	1.022
	S_{VDM}	0.062	1.065	0.058	1.053
Slope 1:10	S_{VDM}	0.100	1.355	0.939	1.341
	S_{SF}	0.135	1.570	0.129	1.562
Slope 1:15	S_{VDM}	0.133	1.560	0.125	1.559
	S_{SF}	0.200	1.920	0.173	1.942

TABLE A.10 - WAVE CHARACTERISTICS PROFILE CHANGE TESTS

For the further the elaboration the actual wave height and period will need to be used instead of the input values. Van der Meer [1988] uses the highest one third of the waves ($H_{1/3}$), which is different from H_{m0} for shallow water. However, the differences are assumed to be negligible, therefore the derived actual wave heights are implemented in the further research.

A.2.3 BIV/PIV MEASUREMENTS

This part of the test plan is done in order to accurately compare the model XBeach-G with reality. XBeach-G offers the opportunity to use two different formulae in order to determine the sediment transport, i.e. Van Rijn [2007] and Nielsen [2006]. Both formulae can be split into a drag and an inertia part, in other words the drag part is determined by the velocity of the water whereas the inertia is determined by the acceleration. Also from the research of Postma [2016] resulted that the phase lag angle and sediment friction factor in the Nielsen [2006] formula seem to be of great influence on the accuracy of the results. Since these parameters are substituted with standard values in the formula used, this is potentially a factor that could greatly improve the accuracy of the Nielsen [2006] formula.

In order to measure these parameters a BIV/PIV set up has been realized. This will be elaborated below.

A.2.3.1 INPUT

The BIV/PIV measurements have been done on the same slopes as the profile change tests, i.e. slopes of 1:5, 1:10 and 1:15. For all these slopes, one test will be done. Tests will be done around the moment that damage starts, this comes down to the wave height that coincides with the extrapolation made Wit [2015]. Since damage is normally caused by the highest waves of the spectrum, the significant wave height is rewritten into the highest 1% of the waves.

The switch from irregular waves to regular waves is made for the BIV/PIV tests. This is done because in this case the exact same wave will reach the slope, therefore the conditions are constant. And theoretically should be just around the moment that damage starts. To rewrite the JONSWAP spectrum in to a regular wave that represents the highest 1% of the waves in the spectrum a Rayleigh distribution is used. This is presented in equation 2.3.

$$P\{\underline{H} > H\} = \exp\left[-2\left(\frac{H}{H_s}\right)^2\right] \qquad \text{Equation A.12}$$

This results in that the highest one percent of the waves roughly comes down to $H_{1\%} \approx 1.5H_s$. Using this wave height as input for the regular waves of the BIV/PIV tests, whilst keeping the wave steepness constant at 0.04 results in the wave periods per test. The steepness is kept constants to ensure the same type of wave breaking. On the last slope, 1:5, two test have been done. While the wave height is the same, the wave period is adjusted. On the second test for the 1:5 slope, the wave height is raised whereas the wave period is kept constant, physically representing the highest 1% of the spectrum. Whereas the other tests merely represent the wave height of the highest 1% waves. With the second test on the 1:5 slope, the steepness will change and thus the Iribarren value, therefore a different type of wave breaking is simulated.

The BIV/PIV tests are done with a camera, the camera focusses on a certain Field of View (FOV). This location of the FOV is chosen based on the damage profile caused by the profile change tests, together with visual observations of the location of movement of stones. At the location of the FOV and around the FOV the stones are painted black. This is done because the yellow and white stones create too much reflection.

Further input values are summarized in the Table 3.4 As can be noted the same input values have been used for BIV/PIV test series as for the Profile change test series.

Variable			1:5		1:10	1:15
h	Water depth	[m]	0.65		0.65	0.65
d_{n50}	Nominal stone size diameter	[mm]	16.2		16.2	16.2
Δ	Relative density	[-]	1.69		1.69	1.69
s	Steepness	[-]	0.06	0.04	0.04	0.04
P	(notional) Permeability	[-]	0.1		0.1	0.1
ξ	Iribarren value	[-]	0.82	1.0	0.5	0.33

TABLE A.11 - INPUT CONSTANT PARAMETERS

For the wave input the highest one percent waves will be used. Originally with constant steepness, to recreate the same type of wave breaking. Except for the 1:5 slope upon which an extra test will be done, in which physically the highest 1% of the spectrum exactly will be reproduced. See Table A.12 - Input Wave dataA.12.

Wave data			1:5		1:10	1:15
H_{m0}	Significant wave height	[m]	0.062		0.089	0.133
$T_{m-1.0}$	Mean wave period	[s]	0.995		1.266	1.458
H	Highest one percent waves	[m]	0.093	0.093	0.133	0.200
T	Wave period	[s]	0.995	1.220	1.459	1.790

TABLE A.12 - INPUT WAVE DATA

For the BIV/PIV test series the camera plays a significant role in the results. For a successful measurement, the amount of movement of bubbles/particles (i.e. BIV/PIV) should be just right. Too little movement and the difference is hardly noticeable, and too much movement in between frames and the reference in between two frames is lost.

The camera used for this experiment is the 'DFK 23 GP031' from the Imaging source. At a set resolution of 720x480 the camera is capable of shooting video images with a frame rate of 132 frames per second. The camera is to shoot a FOV of roughly 12 cm wide and 9 cm high.

On this camera, a Pentax lens has been used, the lens has an 8mm focal length and an aperture of 1.4. Theoretically this set up should be capable of creating a shallow Depth of Field (DOF). However, analysing the results using this technique has shown differently. 3D effects were visible in the analysed results, indicating a too deep DOF. To counteract this problem, the lighting has been adapted, resulting in a beam of light of roughly 5 cm thick. As outside of this beam nothing is visible the same effect was achieved by applying this method as would be with the lens.

This DOF is one of the factors that creates a measuring error. A larger DOF leads to a higher measuring error. This is because in when a particle shifts in between two frames (n and n+1), it is not known whether the particle was in the front of DOF (close to the camera) or in the back of the DOF (further away from the camera). However, since the particle in the back of the DOF needs to travel further (and thus faster) than the particle in the front of the DOF, in order to have the same result on the recorded image. This error can be calculated by equation

$$Error = \frac{{}^{1}/_{2} \cdot DOF}{L} \cdot 100\% = \frac{{}^{1}/_{2} \cdot 4.5\ cm}{80\ cm} \cdot 100\% = 2.8\% \qquad \text{Equation A.13}$$

With L is the distance from the camera to the FOV. Which results in a 2.8 % error. This principle is schematized in Figure A.13

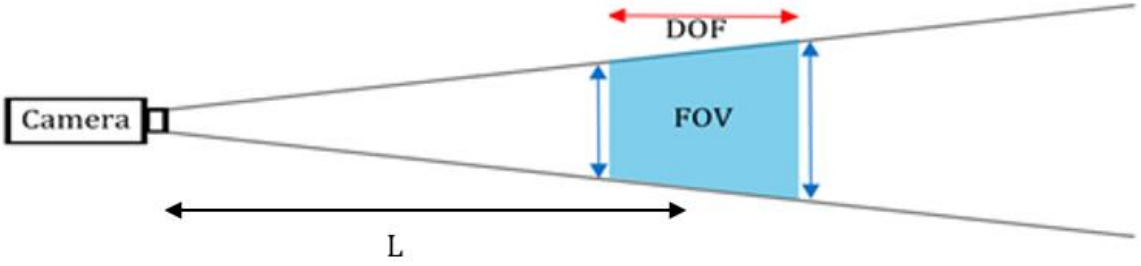

FIGURE A.13 - SCHEMATIC OVERVIEW DOF AND FOV FOR BIV/PIV TESTS

When applying these camera settings and assuming velocities in the order of 1 m/s. This is equivalent with a motion of 1000 mm/s. Combining the resolution with the size of the FOV gives a pixel density of 28 pixels per mm^2 (each pixel is roughly 0.2x0.2 mm). With 132 frames per second that comes down to a movement of 7.6 mm in between frames. This is assumed a good amount of movement to be able to analyse the velocity distribution within the FOV.

Bubbles are not always present in the FOV, for example during the run-down of the wave. A lack of bubbles means there is nothing to measure, this has been solved by adding particles to the water just prior to the test. The particles are suspended in the water and follow the movement of the water. The particles have a size of 100 µm (=0.1 mm) which comes down to 25% of the size of a pixel. This was assumed to be enough to alter the colour signal in the pixel. With this difference in colour the particle can be traced by the software used to analyse frames.

Lights are crucial for a BIV/PIV measurement, as without proper lights the bubbles nor the particles will be visible and distinguishable for the camera. Without the bubbles and particles being properly visible the software can't trace them, and thus no relevant analysis can be made. For this test, multiple lighting set ups have been tested and the lighting set up with the best results has been chosen. Further elaboration on this will be done in the chapter 3, the evaluation of the test plan. For the tests two 50W LED lights have been used.

A.2.3.2 TESTPLAN

For each slope, as soon as all the tests have been finalized for the profile change series the BIV/PIV tests can commence. For this test series, the slope has to be altered slightly, meaning the stones in and around the FOV have to be replaced with black stones. This is done because of the reflection of the lights on the stones.

For the BIV/PIV test series a strip of glued stones is used, this way the stones will not move through the field of measurements. This strip is placed over the FOV. The rest of the black stones will be placed around the strip of glued stones. The stones are spread out and aligned to the exact layer thickness in the same manner as was done in the profile change test series, i.e. with an indication line and a plumb rule. Once all the black stones are placed the lights can be placed. The lights are placed on top of a wooden structure that holds the LED lights into position (see Figure A.14). Next to this wooden structure two other plywood boards are placed over the flume, each of the plywood boards is approximately 1 meter wide.

In front of the flume the camera will be placed 75 cm from the flume. With the FOV 5 centimetres removed from the side of the flume this gives a total distance of the camera to the FOV of 80 centimetres. At this distance the FOV had the desired dimensions. Once the camera is installed the camera was focussed on the FOV. Once focussed the entire set up is covered in a blanket to exclude as much of the external light as possible.

With everything in place, the water can be pumped into the flume. This has to be done slowly in order for the rising water level not to influence the stones on the slope. Once the water level reaches the designated level, i.e. h=0.65 m, the pumps can be closed. A final check on the position of the wave gauges and the EMS has to be made, in order to verify that all are in the correct position. Once this is verified the wave gauges are calibrated, this is done by moving the gauges 5cm upward and downward over time. The change in voltage can then be used to calculate the ratio volt to centimeter.

FIGURE A.14 - DEPTH OF FIELD (LEFT AND MIDDLE) LIGHT SET UP (RIGHT)

Once all this is done, a calibration image of the camera was made. This was done by holding a ruler in the FOV. These images together with the set framerate are later used to transform the vectors from the unit pixel/frame to meter/second.

Once all previous steps have been completed, final step is to check and verify the input for the wave board. With this verified the wave board can be turned on.

Once the waves are rolling and have reached the FOV, carefully the particles can be strewn just in front of the breaking waves and mixed into the water. Once this is done 6 short clips will be made, each clip between of approximately 10 seconds long. As the wave period is in the order of a 1-2 seconds, each video covers will contain 5-8 waves.

For the analysis, the video file will be broken up into separate frames. During the analysis with the software PIVLab, two following (frame n and frame n+1) will be cross-referenced in order to determine the flow velocities in the FOV.

A.2.3.3 WAVE CHARACTERISTICS

Just as with the tests regarding the profile change, reflected waves influence the incoming waves. Therefore, the actual incoming wave height has to be determined. This is done with wave signals of 3 wage gauges, that were set particular distances apart.

Test		H_{input} [m]	T_{input} [s]	H_{output} [m]	T_{output} [s]
Slope 1:5	s=0.04	0.093	1.220	0.088	1.219
	s=0.06	0.093	0.995	0.088	0.995
Slope 1:10	s=0.04	0.133	1.459	0.146	1.55
Slope 1:15	s=0.04	0.200	1.790	0.187	1.79

TABLE A.13 - WAVE CHARACTERISTICS PROFILE CHANGE TESTS

A.3. EVALUATION OF THE TEST PLAN

The evaluation of the test plan is split in to two parts, the profile change tests and the BIV/PIV tests. In this chapter looking back at the test in hindsight, choices are elaborated and reviewed.

A.3.1 PROFILE CHANGE

In hindsight of the test series, the test phase went well. The only issue that cost a lot of time was the switch from 2D to 3D scans. After analysis of the 2D results too much noise was found. Even after smoothing the data greatly, no significant results were retrievable from the data. The results of the 1:15 slope with waves based on the Schiereck & Fontijn [1996] data is presented in Figure A.15.

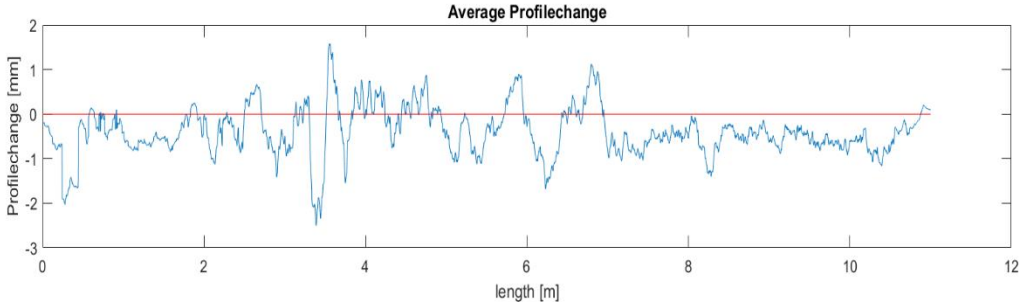

FIGURE A.15 - AVERAGED 2D SCAN RESULTS

When using 2D laser scans on a slope with stones is just not ideal. The laser point is in the order of one tenth of millimetres big. In order to compare the initial profile with the post storm event profile, the exact same line has to be scanned. With only a millimetre difference in position of the laser can lead to a totally different 2D scan. This sensitivity probably explains the results found after the measurements. In order to gain more certainty about the results either a lot more scans will need to be made, to average out the measuring errors. Or a switch to 3D scans can be made.

The use of 3D scans improves the accuracy of the measurements and is quicker than doing numerous 2D scans. For these reasons, the switch to 3D scans was the preferred solution over increasing the number of the 2D scans. See Figure A.16

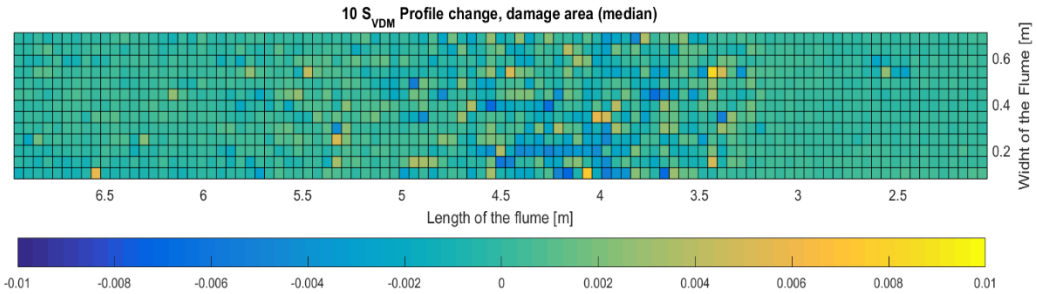

FIGURE A.16 - EXAMPLE OUTPUT 3D SCAN

The scans of the slope were made with a Leica C10 laser scanner, this laser scanner requires quite a bit of skill to operate. Considering the time frame of the test, due to the availability of the wave flume, and the necessity of good results it was decided to have external help for the scans. Yueqian Shen, who is the external help, helped out with the measurement as well as with the pre-processing of the data. Despite the great help that Yueqian Shen gave, the process of profile change

to a useful pointclouds became sort of a 'black-box' transformation. It is advised to learn to operate and pre-process the data yourself when using the scanner, this way you will always know exactly what happens to the data. And therefore, you will be able to declare certain flaws or irregularities in the results better.

Furthermore, with the slope analysis the first idea was to create two scans for each measurement. One from either side of the flume. Than by combining the two pointclouds, a more extensive pointcloud will be gain with a more evenly spread pointcloud density. However, somewhere in the 'black-box' this did not work out, resulting in the use of only one of the two scans. Which is fine, but if one would have known only one scan would be used for each measurement. The placement of the scanner could have been optimized. In future cases, this should be examined. The scanner should than be placed in the location such that the profile change occurs in the area with the highest pointcloud density.

At last create marked points in the scan that serve as reference points. For example, place a reference point at the still water level (SWL). As in the processing of the results it was found that the SWL was hard to determine accurately in the pointclouds. Creating a reference point also a calibration step can be included. For example, by placing an object with known dimensions on the slope in the pre-scan and removing the object for the post wave scan, the exact profile change at the location of the object can be determined.

A.3.2 BIV/PIV

In this paragraph the evaluation of the BIV/PIV tests will be presented, roughly four subjects will be addressed. Firstly, the choice of software and hardware will be elaborated, followed by the determination of the light set up and consequential Depth of Field (DOF). Furthermore, the particles will be addressed followed by at last the output of the camera

A.3.2.1 HARDWARE AND SOFTWARE

For the BIV/PIV firstly was chosen to use the LaVision hardware and software. LaVision is a hardware and software package especially designed for PIV measurements. The hardware consists of a laser beam and special high frequency camera, both laser and camera can be controlled with the software that comes with the system. With set up two successive images can be taken very shortly after each other. You need the accompanying controlled laser to make this happen though. This is necessary because the camera works in the following way.

Two photos are taken within a very short period of time. The first one is taken for example in 1ms, however it takes 10 ms to process the photo. The system covers this by taking photo 2 whilst the photo 1 is processed, consequentially the shutter time for photo 2 becomes 10 microseconds. Therefore, if used constant lighting, the second photo will be overexposed. This is covered by the LaVision system that flashes the laser only for short periods of time (e.g. 0.5ms). Since the rest of the time the view is pitch black (safety measures because of the laser, therefore the whole environment will need to be closed off) only the 0.5ms of the time will be seen on the photo. This way even with a framerate of e.g. 30 frames per second, one can have an interval between two analysed frames in the order of milliseconds.

Despite this favourable set up, problems arose when applying this to BIV. The laser is too intense to use with the bubbles, as when the laser hits a bubble it will overexpose the photo and possibly destroy the camera. For the BIV variant regular light will have to be used. Creating a powerful LED strip that is capable of flashing on an exact timing was deemed possible but time consuming to build and with no guarantees of it working accordingly. This together with the outspoken doubt on success from the assistance available in hydraulic laboratory the choice was made not to continue with LaVision. Prevailing in this decision was the uncertainty regarding the intensity of the lights, possibility regarding the flashing frequency and the colour of light on the available LED strip (green).

A.3.2.2 DEPTH OF FIELD

With this decision made, plan B resulted in continuous lighting with a high frequency camera. The best camera available at this time in the hydraulic lab was the 'DFK 23 GP031', from the Imaging source. This camera has a highest frequency of 132 frames per second at a set resolution of 640x480. This camera is combined with a Pentax 8mm lens with an aperture of 1.4. Using this camera and lens the DOF can be calculated. The DOF is defined as follows, see equation A.14

$$DOF = S - R$$
$$R = \frac{Lf^2}{(f^2 + NLC)}$$
$$S = \frac{Lf^2}{(f^2 - NLC)}$$

Equation A.14

With f is the focal length of the camera focal lens, C is the value of the circle of confusion that depends on the property of the camera, N is the f-number of the camera aperture and L is the length of the distance between the camera and the FOV. The distance between the camera and the FOV is 80 centimetres, the focal length of the camera is 8mm, the f-number of the aperture is 1.4 and finally circle of confusion is 0.0052 mm. This results in a DOF of 14.6 centimetre. This results in an error of 9.1 percent; this is considered too high. Furthermore, during the analysis 3D effects appeared in the output which indicates that the DOF is too big.

Therefore, multiple lighting set ups and camera tweaks have been tested with the aim to improve the quality of the images. Lights shining from above, lights under an angle with the camera axis, and a combination of the previous have been examined. From these tests a quick analysis has been made in order to examine the accuracy of the measurements, which determined which lighting settings and camera settings are the optimal for this case.

However, after this first analysis of the images gained with this camera and the above elaborated settings appear to result in a far larger DOF. This is visible in the raw frames as well as in the processed (with PIVLab) frames. This larger DOF characterizes itself with what appears to be 3D effects in the velocity vector field. At this stage, it is unclear why the DOF appears to be larger than the theory describes, clear however is that this way of measuring results in unreliable results. The results have a high error percentage, however how high is unclear.

Because of this a different lighting set up has been examined. A wooden structure has been built over the flume with a narrow gap (5 mm) in it. By mounting the two LED lights (50W) above this gap (at 30cm height), the lights shine through the gap and create a beam of light. With this set up the beam of light has a width of 4.8 cm. See Figure A.144. Once all is installed and the camera adjusted and focussed on the FOV, the entire set up is covered in a blanket to exclude as much of the external light as possible. With this done, the only thing visible on the camera are the bubbles and particles within this beam of light. Therefore, by altering the set-up, the DOF is controlled in another way than with camera settings. At first there appeared not to be enough light, however

since the DOF is controlled by the beam of light alone the aperture settings don't influence the DOF anymore. After fully opening the aperture there was enough light to make images which can properly be analysed by PIVLab.

A.3.2.3 PARTICLES

At first the idea was to do merely a BIV measurement, i.e. no particles were added to the water. However, after the first results indicated that the measurement was not accurate during the periods of time that no (visible) bubbles were present. Therefore, it was decided to add particles to water, to improve results at the times no bubbles were visually present. Two sizes of particles were available at the fluid mechanic lab of Delft University of Technology, 10 and 100 µm. The size of the particles should be large enough to light up a pixel in the video image. The pixels have the dimensions of roughly 0.2x0.2mm. The smallest particle (10 µm) only cover 0.25% of a pixel, whereas the larger particle an area covers of 25% of the pixel. The latter was therefore applied in the water to improve the BIV measurements. With the particles added the measurements turn in to a combination of Bubble Image Velocimetry (BIV) and Particle Image Velocimetry (PIV). After the first test with the 100 µm particles, the particles were indeed visible in the video image and therefore detectable by the analysing software.

APPENDIX B – TEST RESULTS & ANALYSIS

In this appendix, the transformation from raw data to analyzed results shall be presented. The test procedure was fully elaborated in the previous appendix, therefore merely results and analysis' will be presented here. This is appendix is split into two parts, firstly the profile change tests will be elaborated followed by the analysis of the BIV/PIV tests.

B.1. PROFILE CHANGE

In this chapter of Appendix B, the analysis of the results will be elaborated. Firstly, the general procedure shall be presented in detail. Once the procedure of the analysis is clear, all raw data will be analyzed for each particular test.

B.1.1 GENERAL PRECEDURE

The input data for the profile tests is obtained by a 3D scanner, the Leica C10. This scanner creates a digital pointclouds of the scanned area. These pointclouds are first adjusted in the software program 'CloudCompare'. CloudCompare is a user friendly graphical interface that allows to make some basic adjustments to pointclouds. Per test two scans are necessary, one before and one after the wave series. These two scans are exactly aligned with the help of CloudCompare. Furthermore, from the entire scan, the region of interest (ROI) is cut out from the surroundings, in this case the ROI is the slope. Once the pointclouds have been aligned and cut to the ROI, they can be exported from CloudCompare in to .txt files. These files will form the input for Matlab.

Firstly, the text files containing the data gathered by the Leica C10 (.txt files with XYZ values, RGB values and an intensity value, for this research merely the first three columns are necessary, i.e. the XYZ-values) are imported in Matlab. Since the pointclouds don't have the exact same coordinates, the inner overlapping values are used. This way, both the pre- and post-wave series scan will have the same coordinates. The pointclouds are than fitted into a grid with $\Delta x = \Delta y = 3\ D_{n50}$. This size is chosen to align with the damage description by Hofland et al. [2011], they proposed to take the average over a circle with diameter 3 D_{n50}. For pragmatic reasons a square is used in this research. Per grid the median z-value of all the data points within the grid will be taken, the median is taken instead of the average to exclude the extreme values. Since the scanner scans from 1 single point per scan, the density of the points in the pointclouds decreases with the distance from the scanner. (The scanner creates a data point every 60 µrad, both horizontally and vertically). This is represented in Figure B.1.

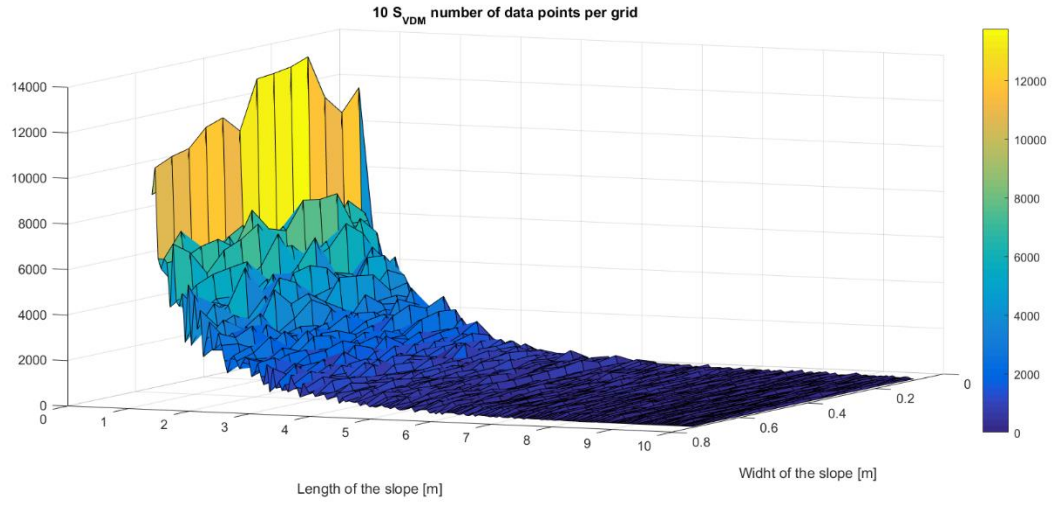

FIGURE B.1 - POINTDENSITY (COTA= 10, WAVES BASED ON VAN DER MEER [1988], PRE-WAVE SCAN)

The scans will be made from the topside of the slop, because the point density is higher close to the scanner than it is further away, see Figure B.1(previous page). This figure represents the point density of the pre-waves scan on the Van der Meer [1988] test on the 1:10 slope. This example will be used throughout the whole description of the procedure. Note that, as is presented in Figure B.2 and Figure B.3, the standard deviation of the value represented in the grid does not depend on the number of data points per grid. It appears therefore that the entire slope is analyzed equally accurate over the entire slope.

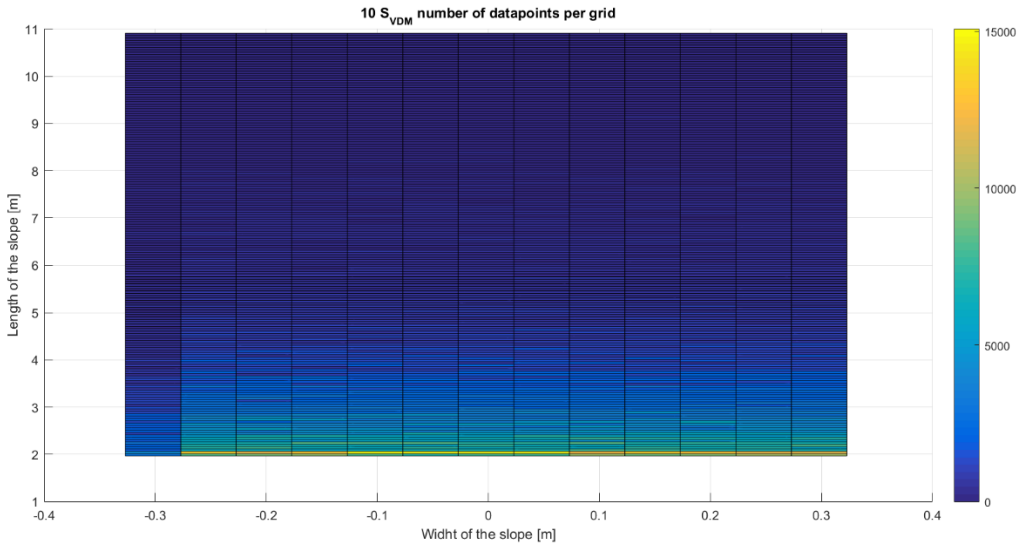

FIGURE B.2 – NUMBER OF DATAPOINTS PER GRID (SLOPE 1:10, WAVES BASED ON VAN DER MEER [1988])

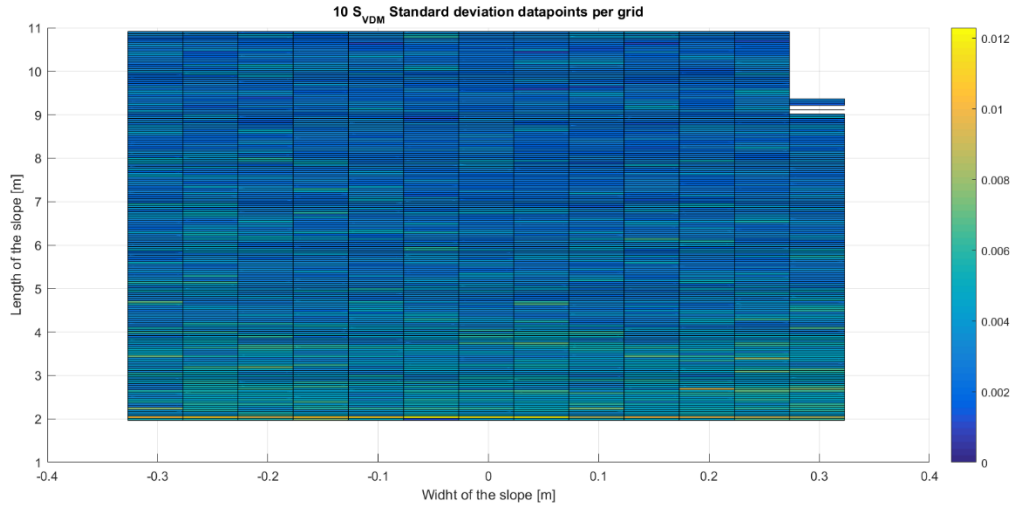

FIGURE B.3 - STANDARD DEVIATION [M] (SLOPE 1:10, WAVES BASED ON VAN DER MEER [1988])

Both scans (pre- and post-waves) have been fitted over the grid, the median of the data per grid is taken for both scans. The post wave series scan is than subtracted from the pre-wave scan. This results in the profile change per grid, this profile change is plotted in a 3D figure, see Figure 3.7 B.4 (next page). The still water level (SWL) is depicted in the figure together with the wave direction.

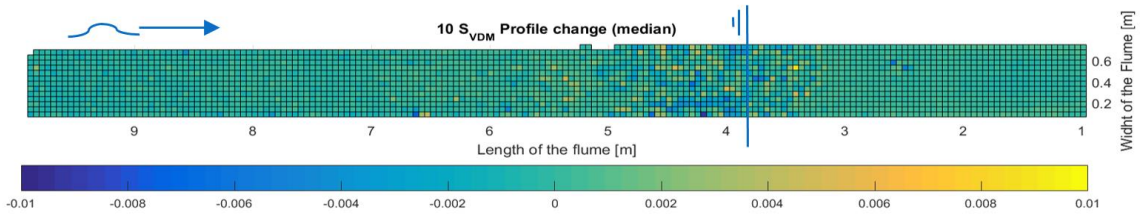

FIGURE B.4 - 3D PLOT PROFILE CHANGE FOR SLOPE 1:10, WAVES BASED ON VAN DER MEER [1988]

If you examine Figure 3.7, you can conclude that all the damage occurs at one specific area. This area is around SWL. The conservation of mass states that the amount of stones will stay the same during the tests, which can be translated to that the sum of the profile change should be zero. The area over which the sum has been taken has been diminished to the area where profile change is found. This results in Figure 3.8 B.5.

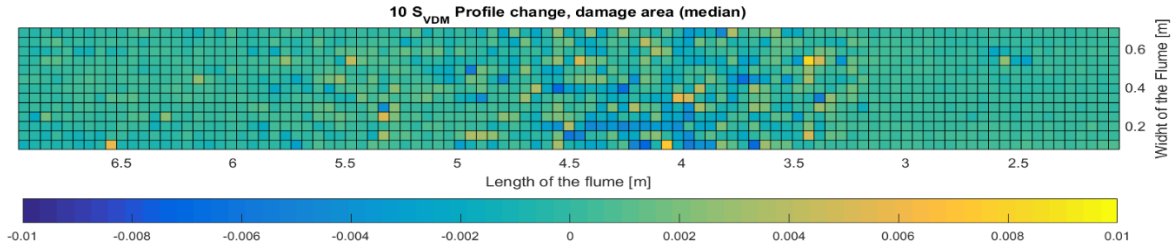

FIGURE B.5 - 3D PLOT PROFILE CHANGE, DAMAGE AREA (SLOPE 1:10, WAVES BASED ON VAN DER MEER [1988])

The profile change is averaged over the width of the flume, resulting in an average profile change over the length of the flume. When integrating the entire averaged profile change, the balance of the profile change should be zero. ($\sum A_e = 0$). In most of the scans the sum of the erosion was however nonzero. In order to account for this, a correction factor (c_f) was applied to the average profile, either shifting the average profile up or down. This was done iteratively until the total erosion area was in the order of 10^{-6} ($=\mathcal{O}(mm^2)$), which is roughly relates to 0 and 4 % of one D_{n50}^2. With these final adjustments, the profile change can be plotted, this is done in B.6.

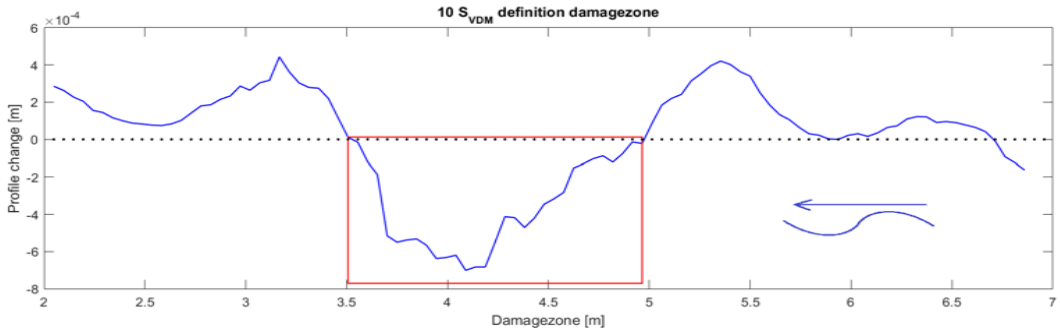

FIGURE B.6 - AVERAGE PROFILE CHANGE AND DEFINITION OF THE DAMAGEZONE (SLOPE 1:10, WAVES BASED ON VAN DER MEER [1988])

In this profile the erosion area can be identified, this erosion area will be called the damage zone as this area will be representative for the derived damage characteristics. The damagezone is defined as a part of the profile, which is *continuously* below zero (i.e. represents merely erosion). The boundaries of the damagezone are marked by the zero crossings of the average profile (i.e. the shift from erosion to accretion and vice versa). In Figure 3.9 this average profile is depicted together with a visualization of the damagezone, the red square.

From the damagezone, as defined in Figure 3.9, the damage characteristics can be derived. From the average profile zoomed in on the damagezone, the total erosion area is determined. This erosion area translates to the damage level 'S' Van der Meer [1988] uses to describe damage. Furthermore, the average and maximum erosion depth are determined. The latter will be related to the nominal diameter of the rock protection, as proposed by Hofland et al. [2011].

The damage characteristics are summarized in Table 3.6. The average erosion depth is defined as the total erosion area of the damagezone (A_e) divided by the length of the damagezone. The maximal erosion depth is maximal erosion depth represented by a grid cell, where each grid cell represents the median of the data points in that grid cell. The size of the grid cell corresponds is a square of 3 x 3 D_{n50}, which corresponds with the by Hofland et al. [2011] suggested damage characteristic damage depth 'E_3'.

Slope	Test	H_{m0} [m]	A_e [m²]	$d_{e;av}$	$d_{e;max}$	S [-]	$d_{e;av}/D_{n50}$ [-]	E_3 [-]
1:10	S_{VDM}	0.094	-5.3 E-4	-3.5 E-4	-7.2 E-3	2.01	2.2%	44.4 %

TABLE B.1 - DAMAGE CHARACTERISTICS (COTA=10, WAVES BASED ON WIT [2015])

In order to compare the test results with the existing Van der Meer [1988] formula, the two damage levels derived per slope will be inter- or extrapolated to derive the wave height corresponding with S=2. This is done by approximating the damage curve with the inter- and extrapolation.

The determined damage levels can be substituted in to the damage curve. The damage curve is derived from the Van der Meer [1988] formulae for plunging waves. Which results in equation

$$S = \left(\frac{H_s}{\Delta \cdot d_{n50} \cdot 6.2 \cdot P^{0.18} \cdot \xi^{-0.5}}\right)^5 \cdot \sqrt{N} \qquad \text{Equation B.1}$$

All input is known and constant per test, except for the wave height and the Iribarren number. Since the wave steepness is constant throughout the test series (s= 0.04), the Iribarren number is only depending on the slope. Per slope two different wave heights have been tested, a wave height based on the results of Schiereck and Fontijn [1996], denoted as Ssf, and on an extrapolation of tolerable damage on milder slopes the Van der Meer [1988] formula done by Wit [2015], denoted as S_{VDM}. Figure B.7 shows respectively shows the results, together with the damage curve based on the Van der Meer [1988] formula.

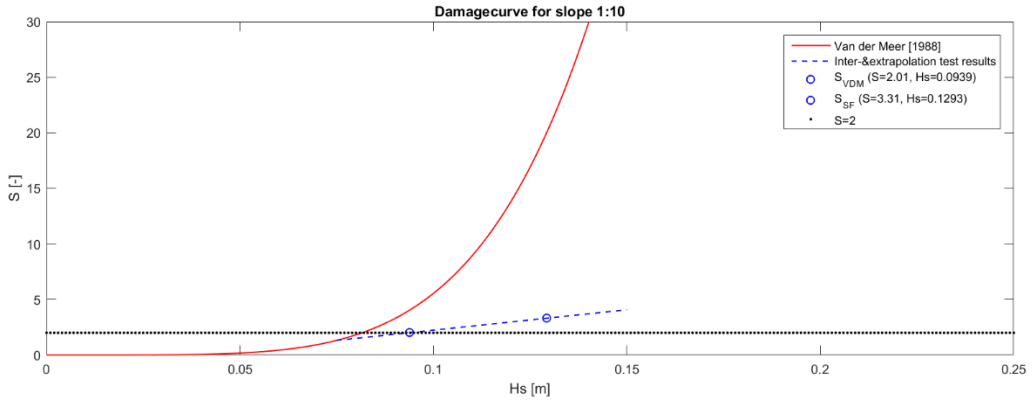

FIGURE B.7 - DAMAGE CURVE AND TEST RESULTS FOR COTA=10

The test results have been inter- and extrapolated, see the blue line in Figure B.7. Two reference points have been used in this inter- and extrapolation, the two test results (S_{VDM} and S_{SF})

Using the inter- and extrapolation of the test results, one can determine the wave height that, based on the test results, is linked to a damage of S=2. For slope 1:10 the wave height that theoretically is responsible for a damage of S=2, based on the extrapolation of our test results, is determined from the intersection of the line S=2 and the inter- & extrapolation curve. For the 1:10 slope this results in a wave height of H_s= 0.0937 meter. With this known the stability parameter ($H_s/\Delta D_{n50}$) based on the test results can be determined. The results of this, together with the results of the other slopes will be plotted in a stability factor against Iribarren number.

Furthermore, the other damage characteristic will be analyzed. The damage depth as proposed by Hofland et al. [2011] will be plotted against the wave height.

B.1.2 PROCESSED RESULTS

The analyzed results will be presented in this paragraph; all analysis will follow the showcase as presented in the previous paragraph. Firstly, the 1:5 slope will be examined, followed by the 1:10 slope and at last the 1:15 slope will be elaborated. Per slope a 3D image, zoomed in on the profile change area, and the average profile change will be plotted. The latter will have the defined damagezone depicted in the same plot. In all the plots the wave direction is added as a reference. At the end of each sub-paragraph the results will be quantitatively elaborated.

B.1.2.1 SLOPE 1:5 – VAN DER MEER [1988], EXTRAPOLATED BY WIT [2015]

This subparagraph elaborates the first test on the 1:5 slope, the test based on the extrapolated tolerable damage by Wit [2015]. See Appendix A, for an elaboration on the extrapolated tolerable damage. From this extrapolation follows a tolerable damage of S=3 for a slope with cotα=5. Rewriting Van der Meer [1988] gives that this damage should theoretically occur under a significant wave height of 6.2 centimeter. This results in the following profile change, which is depicted in Figure B.8.

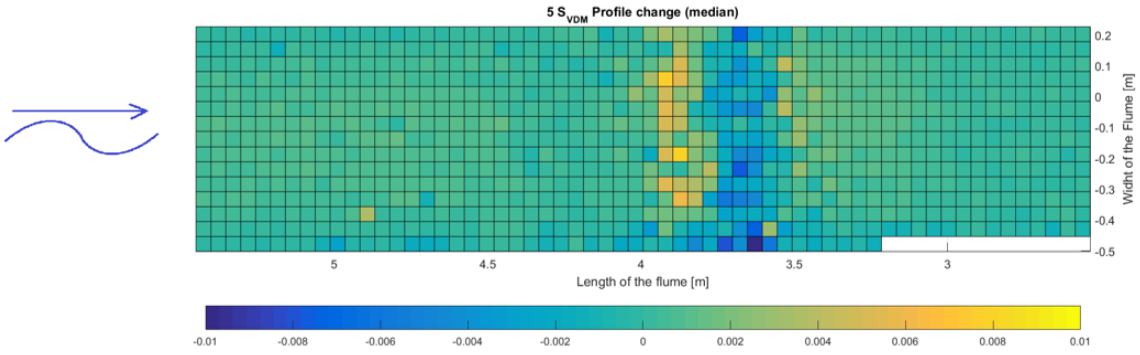

FIGURE B.8 - 3D PROFILE CHANGE (COLORBAR IN METER) (COTA=5, S_{VDM})

In the test results can be seen that the displacement of stones is mainly in the downward direction of the slope. However also very slightly in the upward direction. From this scan, together with visual observations during the test, was concluded that the damage zone is directly under the still water level (SWL).

When averaging the profile change over the x-axis, i.e. the width of the flume, the average cross-section can be determined. From this average cross-section, the damage parameters will be determined. The zone over which the damage is measured is indicated in Figure B.9. In this figure, also the zero-damage line is depicted with the black dotted line, this is denoted in the legend as S=0 as it indicates zero profile change.

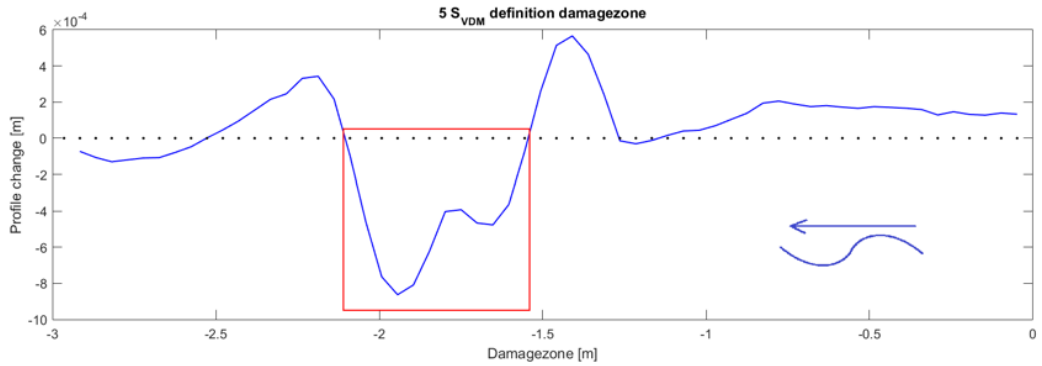

FIGURE B.9 - AVERAGE CROSS-SECTION AND DEFINITION DAMAGE ZONE (COTA=5, S_{VDM})

From Figure B.9, the damage characteristics can be determined. The erosion area is determined by taking the integral over the interval of the damage zone. Furthermore, the maximum eroded depth and the average eroded depth are determined from this damage zone. All damage characteristics are presented in Table A.2. In the last columns several damage denotations are given, the most commonly used damage level 'S', the average erosion depth ($d_{e;average}$) in the damagezone divided by the nominal stone size and the final column represents the maximum erosion depth ($d_{e;max}$) divided by the nominal stone size. The latter is the proposed damage definition by Hofland et al. [2011], E_3.

Slope	Test	H_s [m]	A_e [m²]	$d_{e;average}$	$d_{e;max}$	S [-]	$E_{3;Average}$ [-]	$E_{3;max}$ [-]
1:5	S_{wit}	0.0577	-2.77E-4	-4.82E-4	-0.0102	1.02	3.0%	63.0 %

TABLE A.2 – DAMAGE CHARACTERISTICS (COTA=5, S_{VDM})

B.1.2.2 SLOPE 1:5 – VAN DER MEER [1988], BASED ON S=2

The second test done on the 1:5 slope was with waves that would theoretically create a damage level of exactly 2. This case resulted in significant wave height of 5.7 centimeter. With this wave height, the profile change resulted in Figure B.10.

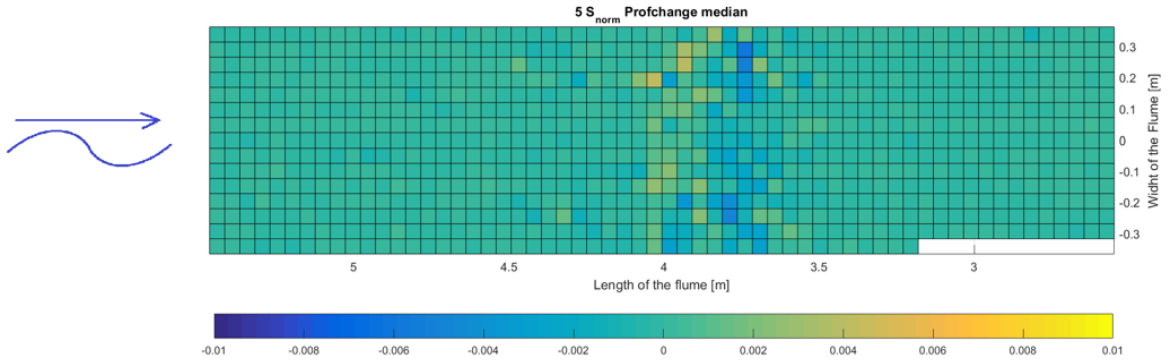

FIGURE B.10 - 3D PROFILE CHANGE (COLORBAR IN METER) (COTA=5, S_{NORM})

One can clearly see, when comparing Figure B.9 with Figure B.10, that as expected for the lower wave quite clearly less profile change occurs. Again, most profile change occurs just under SWL, with mainly downslope movement of stones. After the profile, has been averaged over the width of the flume, the following (see Figure B.11) cross-section appears. In this cross-section, the damage zone has been visualized. The damage zone is determined under the set conditions, i.e. the erosion area around SWL with merely erosion.

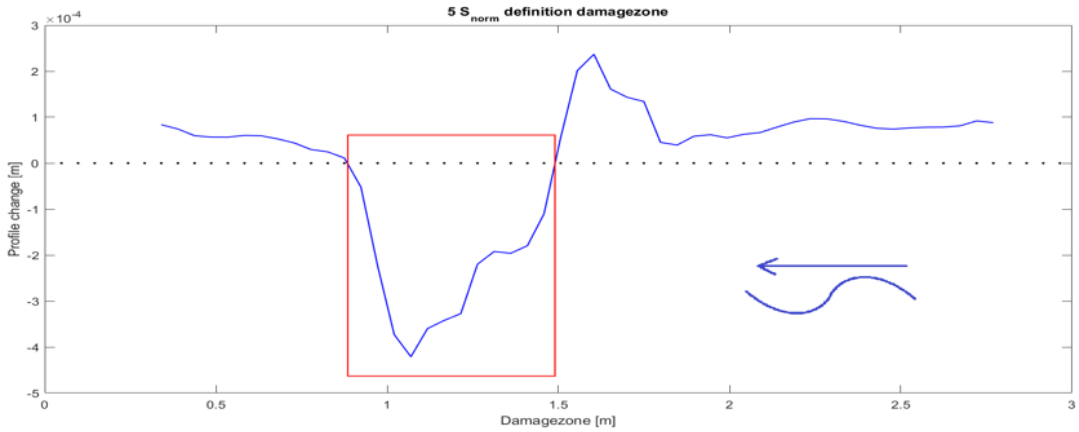

FIGURE B.11 - AVERAGE CROSS-SECTION AND DEFINITION DAMAGE ZONE (COTA=5, SNORM)

From this graph the damage characteristics are derived and presented in Table B.3. In the last columns several damage denotations are given, the most commonly used damage level 'S', the average erosion depth ($d_{e;average}$) divided by the nominal stone size diameter and the final column represents the maximum erosion depth ($d_{e;max}$) divided by the nominal stone size diameter (i.e. E_3)

Slope	Test	H_s [m]	A_e [m²]	$d_{e;average}$	$d_{e;max}$	S [-]	$E_{3;Average}$ [-]	E_3 [-]
1:5	S_2	0.0542	-1.44E-4	-2.09E-4	-5.8E-3	0.55	1.3 %	35.8%

TABLE B.3 - DAMAGE CHARACTERISTICS (COTA=5, S_2)

B.1.2.3 SLOPE 1:10 – VAN DER MEER [1988], EXTRAPOLATED BY WIT [2015]

In this subparagraph, the results for the 1:10 slope with the wave height based on the tolerable damage extrapolation of Van der Meer [1988] done by Wit [2015] will be elaborated. The significant wave height followed from the wave analysis is determined at 0.0939 meter high.

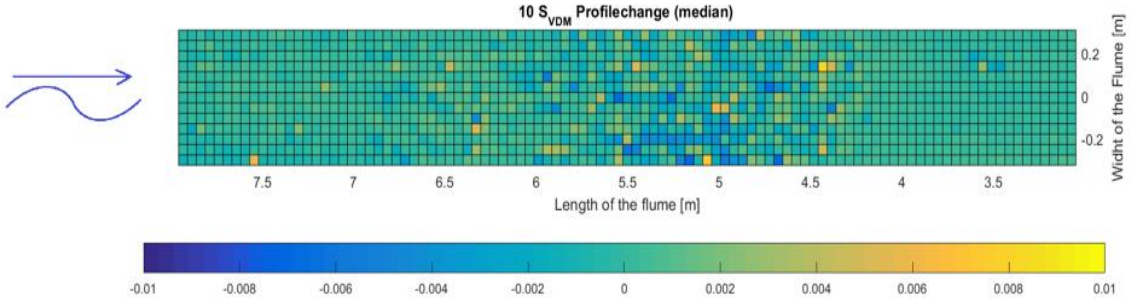

FIGURE B.12 - 3D PROFILE CHANGE (COLORBAR IN METER) (COTA=10, SVDM)

Averaging the profile change presented in Figure B.12 over the width of the flume results in an average profile. In this cross-section, the damage zone is indicated with the red square.

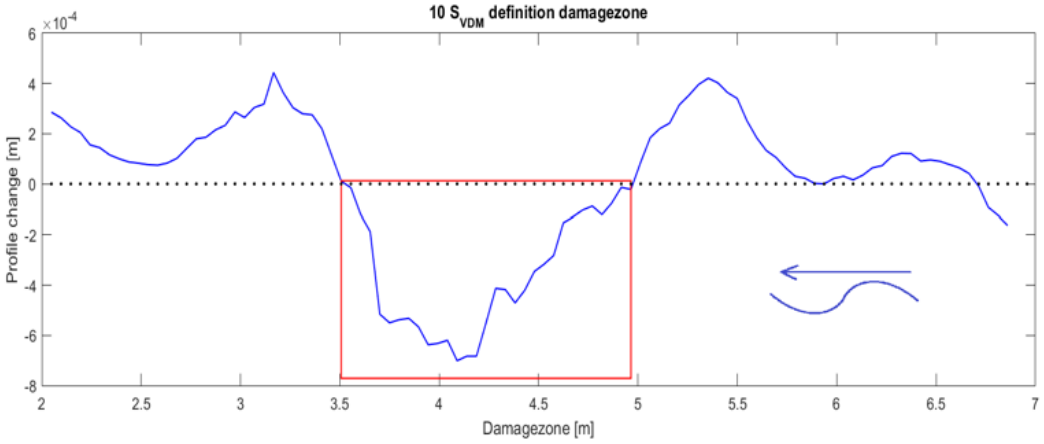

FIGURE B.13 - AVERAGE CROSS-SECTION AND DEFINITION DAMAGE ZONE (COTA=10, SVDM)

During the profile change, stones appear to have moved in both directions. The damage characteristics derived from Figure B.13 are presented in Table B.4. In the last columns several damage denotations are given, the most commonly used damage level 'S', the average erosion depth ($d_{e;average}$) divided by the layer thickness ($t=2d_{n50}=32.4$ mm) and the final column represents the maximum erosion depth ($d_{e;max}$) divided by the layer thickness 't', resulting in the damage depth E_3.

Slope	Test	H_s [m]	A_e [m²]	$d_{e;average}$	$d_{e;max}$	S [-]	$E_{3;Average}$ [-]	E_3 [-]
1:10	S_{wit}	0.939	-5.29E-4	-3.51E-4	-0.0072	2.01	2.2%	44.4 %

TABLE B.4 - DAMAGE CHARACTERISTICS (COTA=10, SVDM)

B.1.2.4 SLOPE 1:10 – SCHIERECK & FONTIJN [1996]

In this subparagraph, the test results from the 1:10 slope, with a significant wave height based on the results of Schiereck & Fontijn [1996] are presented. This derivation of the from Schiereck & Fontijn, see Appendix A, resulted in a significant wave height of 0.135 meter. After 3000 waves this resulted in a profile change that is depicted in Figure B.14.

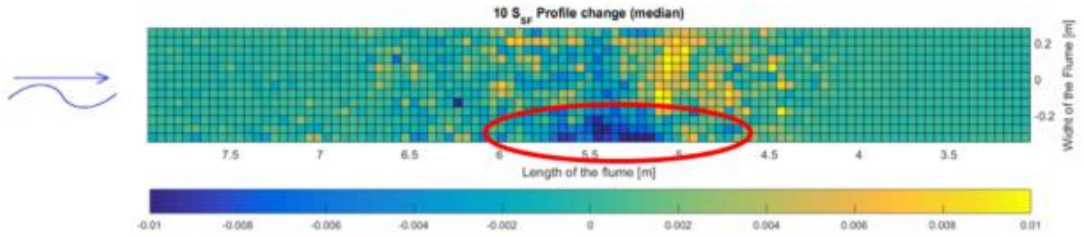

FIGURE B.14 - 3D PROFILE CHANGE (COLORBAR IN METER) (COTA=10, S_{SF}, INCLUDING BOUNDARY EFFECTS)

In Figure B.14 one can see that there appears to be significant boundary effects (see red ellipse in Figure B.14) present in the slope analysis. This can be explained by the sublayer of the physical model used in the flume. The wooden structure, which was used to represent the impermeable sublayer, had a slight gap in between the side of the flume and the structure. Because of this gap and the changing water level (i.e. waves), water rushed in and out through this gap. Causing the stones on that side of the flume to erode. As in this ellipse merely erosion takes place, the stones must have moved cross-slope. This cross-slope movement results in the fact that the balance of stones around water level appears to be intact, see Figure B.15. Furthermore, the movement of the stones almost only is in the upslope direction.

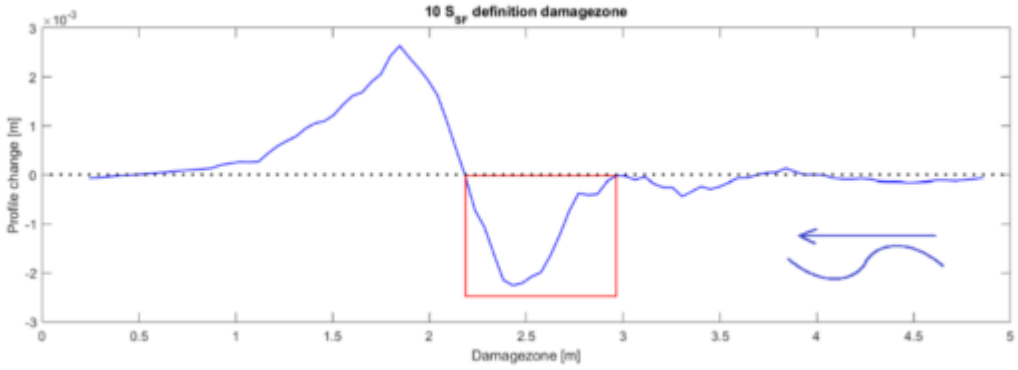

FIGURE B.15 - AVERAGE CROSS-SECTION AND DEFINITION DAMAGE ZONE (COTA=10, S_{SF}, INCLUDING BOUNDARY EFFECTS)

The boundary effects can be dealt with in two ways, firstly by leaving the data grid as is presented in Figure B.14 and secondly by excluding the boundary effects from the results. Both approaches will be presented in this subparagraph. Firstly, the damage over the full data set will be elaborated. This results in the average cross-section as is presented in Figure B.15. The damage characteristics of the full data set, derived from Figure B.15, are presented in Table B.9

Slope	Test	H_s [m]	A_e [m²]	$d_{e;average}$	$d_{e;max}$	S [-]	$E_{3;Average}$ [-]	E_3 [-]
1:10	S_{sf}	0.1293	-9.22E-4	-1.10E-3	-0.0123	3.51	6.8%	75.9 %

TABLE B.5 - DAMAGE CHARACTERISTICS, DERIVED FROM FULL DATA SET (COTA=10, S_{SF})

Second analysis of the results from this test, with reduced data input, which excludes the boundary effects from the analysis results in the following 3D profile change, see Figure B.16. As can been seen in Figure B.16 when comparing with Figure B.14, the significant erosion on the side of the flume with the boundary effects is not taken into account.

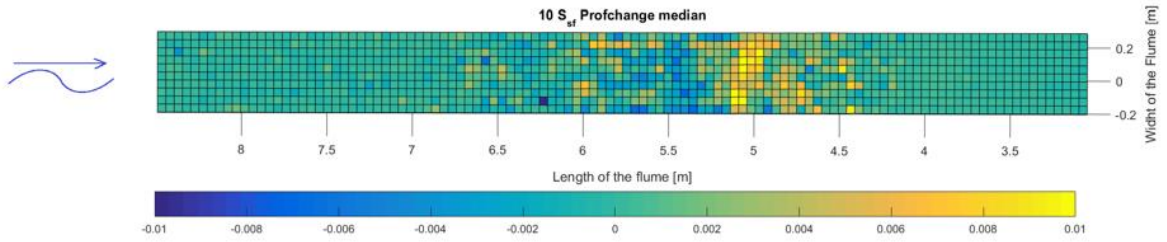

FIGURE B.16 - 3D PROFILE CHANGE (COLORBAR IN METER) (COTA= 10, S_{SF}, EXCLUDING BOUNDARY EFFECTS)

The cross-section of the average profile change along the slope, as depicted in Figure B.17, shows that the accretion is significantly greater than the erosion in down slope of it. This indicates an unbalanced mass balance and it is for this reason that these results are not used in the analysis. This is reinforced by the possibility that the erosion caused by the boundary effect could also be accountable for the decrease of erosion in the rest of the cross-section, i.e. cross-slope transport.

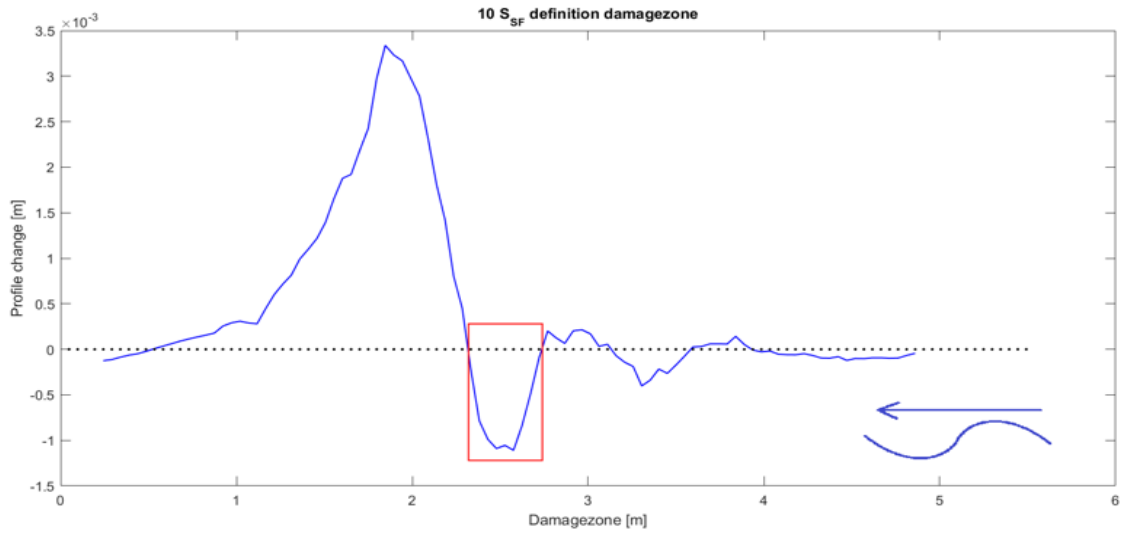

FIGURE B.17 - CROSS-SECTION PROFILE CHANGE AND DAMAGE ZONE DEFINITION (COTA=10, S_{SF})

Rewriting the profile change as derived from Figure B.17 in to the damage characteristics as has been done for all the slopes results in Table B.6 (see next page). As was expected the damage characteristics are significantly lower than, when the entire dataset was used (including the boundary affected region).

Slope	Test	H_s [m]	A_e [m²]	$d_{e;average}$	$d_{e;max}$	S [-]	$E_{3;Average}$ [-]	E_3 [-]
1:10	S_{sf}	0.1293	-3.07E-4	-5.46E-4	-0.0081	1.07	2.1%	50 %

TABLE B.6 -DAMAGE CHARACTERISTICS, ADJUSTED FOR BOUNDARY EFFECTS (COTA=10, S_{SF})

After analyzing both results, the results of the test without boundary effects (Figure B.16) has significantly lower damage characteristics. In fact, even lower than was found for the tests based on the extrapolation of Van der Meer [1988], which had a significantly lower significant wave height (H_s= 0.0939 m compared to 0,1293 meter).

This decrease of damage can be declared by a cross-profile transport, that appears to be present. As in the boundary effected area, the along slope profile change merely is erosion (see red ellipse in Figure B.14) and very little accretion. From that one can conclude that the rock protection will have moved cross-profile. This has decreased the amount of erosion and increased the amount of accretion over the rest of the width.

For the rest of this research, the slope analysis with the boundary effects (i.e. Figure B.14) will be used. This is done because including the area affected by the boundary effects leads to a balanced cross-section, with the integral over the graph being close to zero. Secondly by utilizing the entire data set the upper boundary of the damage is considered, which is considered favorable for a safe design.

B.1.2.5 SLOPE 1:15 –VAN DER MEER [1988] EXTRAPOLATED BY WIT [2015]

The results from the test on the 1:15 slope with waves based on the extrapolation of the tolerable damage of Van der Meer [1988] to mild slopes by Wit [2015] are presented in this subparagraph. After the full waves series, the profile changed appeared as is depicted in Figure B.18.

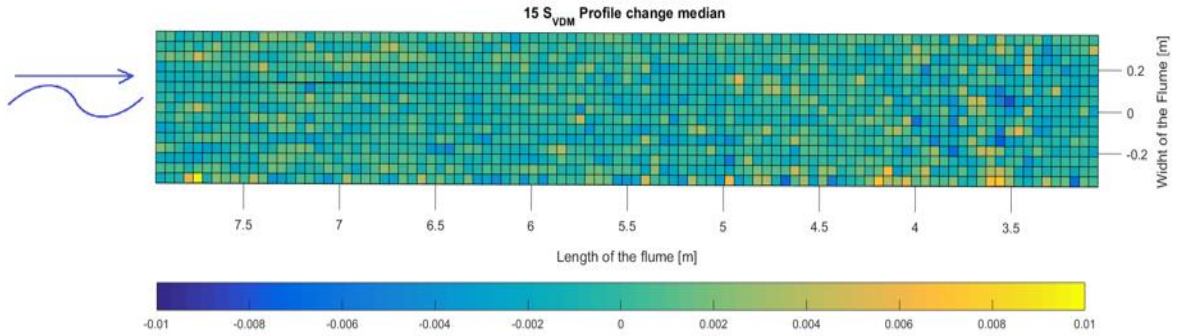

FIGURE B.18 - 3D PROFILE CHANGE (COLORBAR IN METER) (COTA=15, S_{VDM})

The amount of profile change increases in the upslope direction. Visual observations during the test noticed occasional to frequent movement of stones. Stones however did not appear to create a net transport along the slope. Therefore, in the end barely any damage was measured from the profile, while there was definitely significant movement of stones. The profile change is depicted in Figure B.19 (see next page). From this damagezone the following damage characteristics are derived, see Table B.7.

Slope	Test	H_s [m]	A_e [m²]	$d_{e;average}$	$d_{e;max}$	S [-]	$E_{3;Average}$ [-]	E_3 [-]
1:15	S_{VDM}	0.125	-2.76E-4	-1.59E-4	-0.0054	1.05	1.0%	33.3 %

TABLE B.7 -DAMAGE CHARACTERISTICS (COTA=15, S_{VDM})

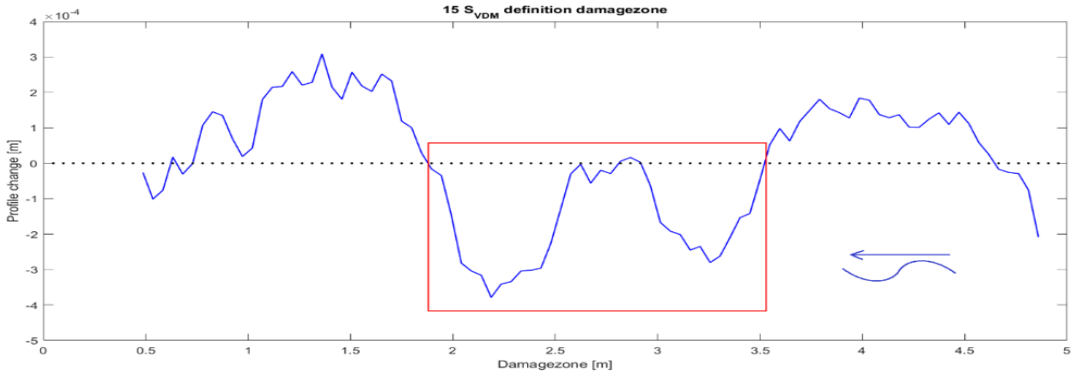

FIGURE B.19 - AVERAGE PROFILE CHANGE AND DEFINITION DAMAGEZONE (COTA= 15, S_{VDM})

B.1.2.6 SLOPE 1:15 – SCHIERECK & FONTIJN [1996]

In this subparagraph, the test results from the last test are presented. In this test the wave height was based on the results as were presented in the research of Schiereck & Fontijn [1996]. Their results have been rewritten on the stability of rock on mild slopes under wave attack were written in a stability parameter, this was translated to a wave height. This is explained in appendix A. After a series of a total of 3000 waves, the profile change was measured. The results are presented in Figure B.20

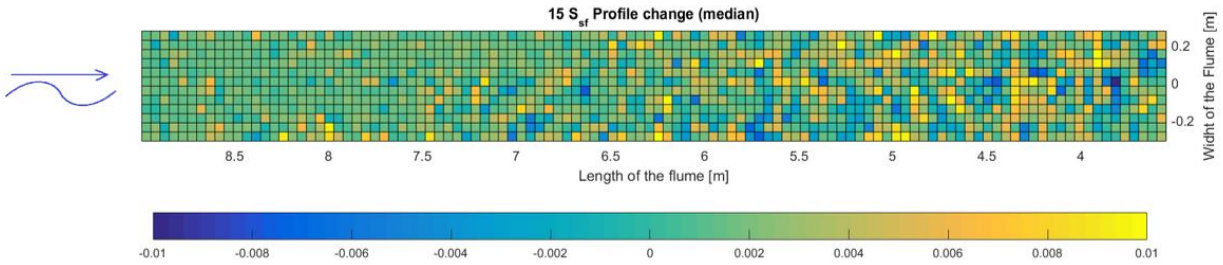

FIGURE B.20 - 3D PROFILE CHANGE (COLORBAR IN METER) (COTA=15, S_{SF})

During the tests, visual observations were done. In these observations, significant displacements of rocks were observed, however without a dominant direction (i.e. up or down the slope). Therefore, even after 3000 waves the profile seems to be rather intact, without the development of a damage zone. These visual observations come back in the 3D plot of the profile change both erosion and accretion are presented in the area around SWL.

The average cross-section for this test is presented in Figure B.21. From the previous plot one can would expect that the average cross-section of this test will lack a distinguished damage zone, however there is a zone with merely erosion. This area of erosion is defined as the damage zone.

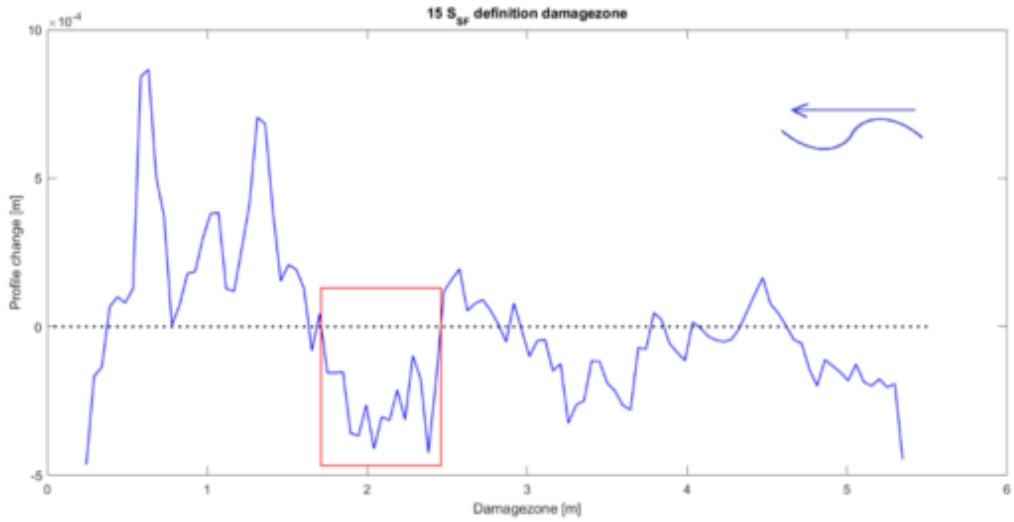

FIGURE B.21 - CROSS-SECTION PROFILE CHANGE AND DAMAGE ZONE DEFINITION (COTA=15, S_{SF})

The analysis of this damage zone results in Table B.8, in this table the damage characteristics are presented as has been done for all the slopes.

Slope	Test	H_s [m]	A_e [m²]	$d_{e;average}$	$d_{e;max}$	S [-]	$E_{3;Average}$ [-]	E_3 [-]
1:10	S_{sf}	0.173	-1.85-4	-2.19E-4	-0.0075	0.70	1.4%	46.3 %

TABLE B.8 - DAMAGE CHARACTERISTICS (COTA=15, S_{SF})

B.1.2.7 CONCLUDING

In this final subparagraph of the processed results, the damage characteristics are summarized. This final summary of results (see Table B.9) forms the main input for the next paragraph, in which the results are analyzed and compared to the existing literature.

Slope	Test	H_s [m]	S_{theory} [-]	A_e [m²]	S_{test} [-]	$d_{e;max}$ [m]	E_3 [-]
1:5	S_{VDM}	0.057	2.00	-2.77E-4	1.06	-1.02E-3	63.0 %
	S_{norm}	0.054	1.47	-1.44E-4	0.55	-5.80E-3	35.8%
1:10	S_{VDM}	0.094	4.04	-5.29E-4	2.01	-7.20E-3	44.4 %
	S_{SF}	0.129	20.02	-9.22E-4	3.51	-1.23E-2	75.9%
1:15	S_{VDM}	0.125	5.98	-2.76E-4	1.05	-5.40E-3	33.3%
	S_{SF}	0.173	30.38	-1.85E-4	0.70	-7.50E-3	46.3%

TABLE B.9 - SUMMARY OF DAMAGE CHARACTERISTICS OF ALL TESTS

B.1.3 ANALYSIS

In this paragraph the processed results from the previous paragraph will be elaborated. These results will be processed following a certain procedure which will be elaborated in subparagraph B.1.3.1. This will be followed by analyzing the processed data from slope 1:5 in subparagraph B.1.3.2, slope 1:10 in subparagraph in B.1.3.3 and slope 1:15 in subparagraph B.1.3.4. With all the slopes analyzed an overall analysis will be done. In the last subparagraph, the results will be reviewed.

B.1.3.1 GENERAL PROCEDURE

The determined damage levels can be substituted in to the damage curves. The damage curve is derived from the Van der Meer [1988] formulae for plunging waves. Which results in Equation B.2

$$S = \left(\frac{H_s}{\Delta \cdot d_{n50} \cdot 6.2 \cdot P^{0.18} \cdot \xi^{-0.5}} \right)^5 \cdot \sqrt{N} \qquad \text{Equation B.2}$$

All input is known and constant per test, except for the wave height and the Iribarren number. Since the wave steepness is constant throughout the test series (s=0.04), the Iribarren number is only depending on the slope. Per slope two different wave heights have been tested, a wave height based on the results of Schiereck and Fontijn [1996], denoted as S_{SF}, and on the extrapolation of Van der Meer [1988] as was done by Wit [2015], denoted as S_{VDM}. All damage curves and the measured damage levels for all the slopes have been plotted in Figure B.22. All the damage levels are on the right side/under the damage curves that were derived from Van der Meer [1988], indicating that in all cases there occurred less damage than the according to the Van der Meer [1988] formula one would expect.

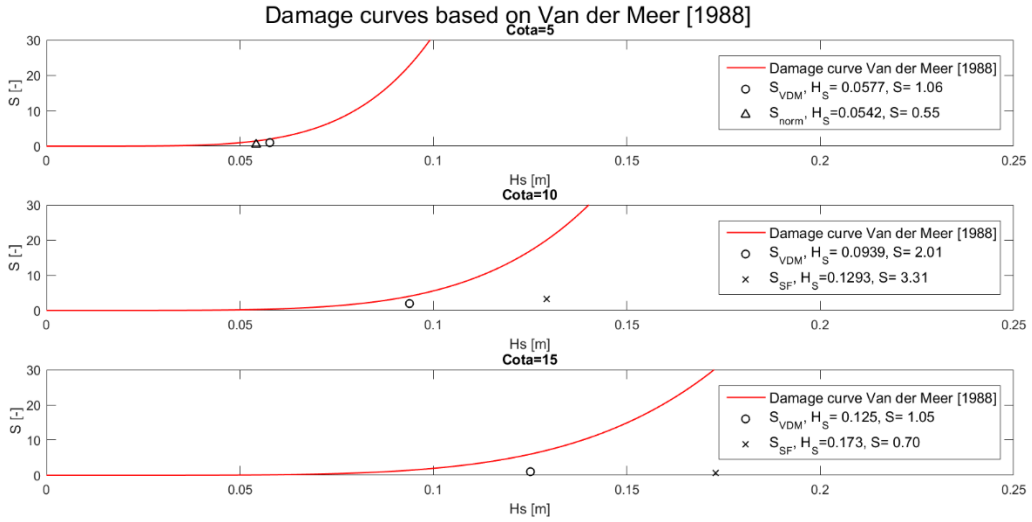

FIGURE B.22 - DAMAGE CURVES AND MEASURED DAMAGE LEVELS FOR ALL SLOPES

The test results will be inter- and extrapolated. Two reference points will be used in this inter- and extrapolation, the two test results (S_{VDM} and S_{SF}). A linear interpolation will be used.

Using the inter- and extrapolation of the test results, once can determine the wave height that, based on the test results, is theoretically related to a damage of S=2. With this known the stability parameter ($H_s/\Delta D_{n50}$) based on the test results can be determined. The results of this, together with the results of the other slopes will be plotted in a stability factor against Iribarren number plot. This will be presented in subparagraph B.1.3.5

B.1.3.2 ANALYSIS SLOPE 1:5

In this subparagraph, the results from the tests on the 1:5 slope will be analyzed, following the procedure as described in the previous subparagraph. Firstly, the two measured damage levels are plotted in the same figure as the theoretical damage curve as was derived from the Van der Meer [1988] formula.

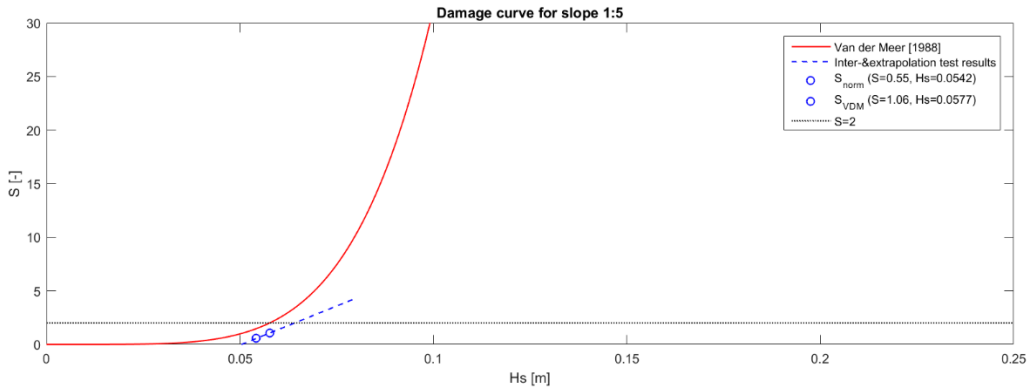

FIGURE B.23 – DAMAGE CURVE ANALYSIS OF TEST RESULTS OF SLOPE 1:5

In Figure B.23 one can see the measured damage levels, plotted against their respective wave height. Both S_{VDM} and S_{norm} are situated under/to the right of the red damage curve, which indicates that the measured damage levels are lower than the damage that was theoretically expected when applying the Van der Meer [1988] formula.

Retrieving the coordinates of the cross section of the plot of the interpolation with the line for S= 2, gives the wave height under which, according to the test results, a damage of S= 2 can be expected. The linear extrapolation methodology results in a wave height of H_S= 0.0642 m. Van der Meer estimated that a wave height of 0.057 would result in a damage level of 2 after 3000 waves. This means that the stability number based on our test is roughly 12.6 % higher than van der Meer [1988] derived.

The damages that were found are much lower than the Van der Meer [1988] suggests. S_{VDM} only results in 53.0% of the expected damage (S= 1.06 in the test, compared to S= 2 which was expected). As only a damage level of S= 0.55 was measured for the S_{norm} test, merely 37.4 % of the expected damage level of 1.47 was measured.

B.1.3.3 ANALYSIS SLOPE 1:10

The slope 1:10 will be evaluated in the same manner as the previous slope. Since the Iribarren number for this slope will be lower in for this slope the damage curve will slightly change, see Figure B.22. The damage levels as well as the inter- and extrapolation will be plotted in the same figure, Figure B.24.

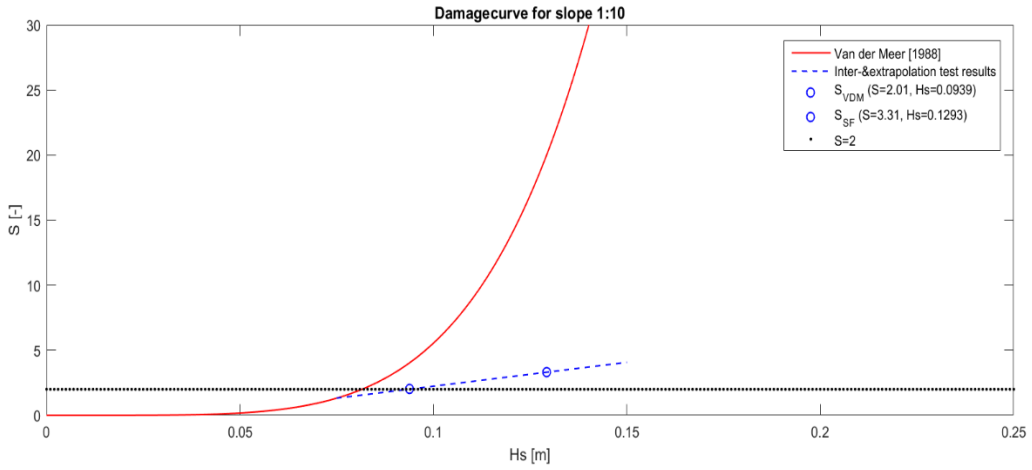

FIGURE B.24 – DAMAGE CURVE ANALYSIS OF TEST RESULTS OF SLOPE 1:10

In Figure B.24 the damage curve is plotted in red, this curve is based on the damage that one would theoretically expect when applying the formula of Van der Meer [1988]. Furthermore, the measured damages are plotted in the figure, the damage based (S_{SF}=3.31) on the wave height derived van from Schiereck and Fontijn [1996]. Whereas the other blue circle indicates the damage measured (S_{VDM}=2.01) after the test with the wave height based on the extrapolation of Van der Meer [1988] done by Wit [2015].

The inter- and extrapolation curve crosses the S=2 line at a wave height of 0.0937 meter. Van der Meer [1988] estimates that a wave height of 0.082 meter will resolve in a damage level of 2 after 3000 waves. This means that the stability number, derived from the tests is roughly 14.3% higher.

The damages that were measured for the test are significantly lower than the Van der Meer [1988] theory suggests. For the test with the wave height based on the extrapolation of Van der Meer [1988] as was done by Wit [2015], leads to a damage of S= 2.01 which is only 49.7 % of the damage that would occur according to theory. For the test based on the data used by Schiereck and Fontijn [1996] even only 17.5% of the damage occurs.

B.1.3.4 ANALYSIS SLOPE 1:15

At last the 1:15 slope results will be analyzed. On this slope, the results of the S_{VDM} test (i.e. a significant wave height of 0.125 meter) show a higher damage level than the results of the S_{SF} test (i.e. a significant wave height of 0.173 meter). The results are plotted in Figure B.25. As the inter- and extrapolation curve shows, the results suggest that no intersection with the line S=2 is obtained.

From visual observations during the test series, was noticed that significantly more stones were in movement during the S_{SF} test. However, what was also noticed, and mentioned in the previous

paragraph, is that the stones do not appear to have dominant direction. Stones frequently move up and down the slope, but without a net transport.

This leads to a scattered profile change plot (see Figure B.20). Where significant profile change is measured, but when the profile change is averaged over the width of the flume it goes to zero

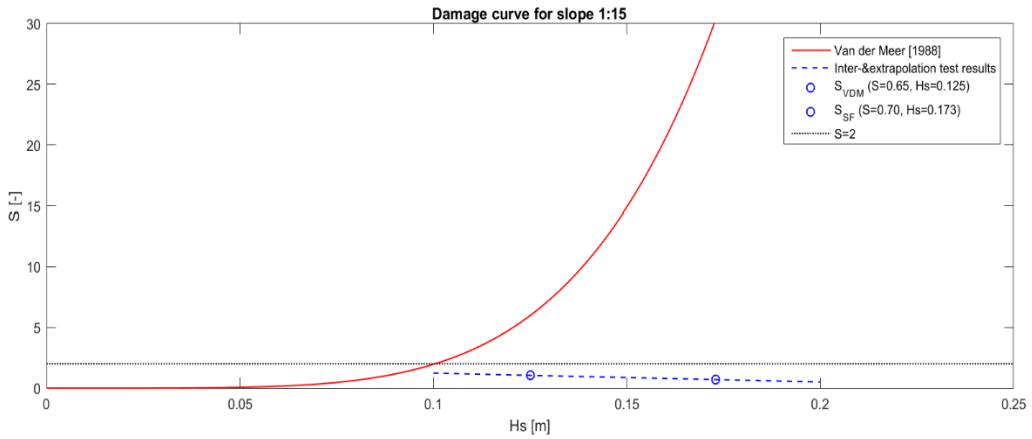

FIGURE B.25 – DAMAGE CURVE ANALYSIS FOR TEST RESULTS OF SLOPE 1:15

From this plot, no interpolated wave height can be derived, that would theoretically (based on the test results) concur with a damage level of 2. This will not be done as the interpolation line has a negative inclination, indicating that for higher waves the damage level will decrease. It appears that the definition of damage level on mild slopes does not suffice.

For the tests on the 1:15 slope very low damages were measured. For the test with the waves based on the Van der Meer [1988] extrapolation as was done by Wit [2015], only 17.6% of the expected damage level was measured. For the test with the waves based on the results that were used by Schiereck & Fontijn [1996], merely 2.3% of the theoretically predicted damage occurred.

B.1.3.5 CONCLUDING ANALYSIS

In the previous subparagraphs, the results from the scans are elaborated. Finally resulting in a wave height that would theoretically be responsible for a damage of S=2, based on the results of the tests. After rewriting these results in stability parameters, the results can be directly compared with the results of both Van der Meer [1988] and Schiereck and Fontijn [1996]. In this plot the data on which Schiereck and Fontijn [1996] has been approximated and depicted together with extrapolation of the Van der Meer [1988] formula (for S=2) for plunging waves in Figure B.26. Furthermore, the results from the tests have been plotted in this figure. The results from the 1:15 slope have not been plotted, as they did not lead to suitable results for this plot.

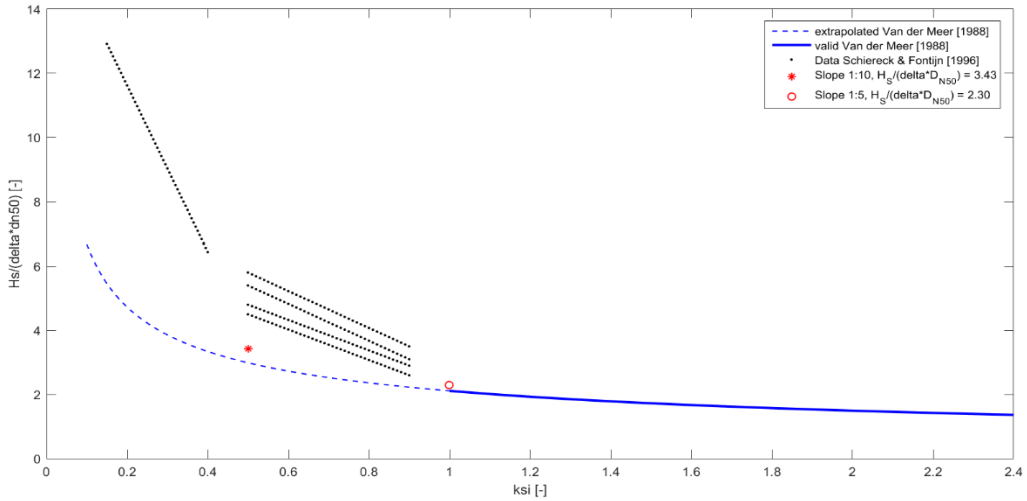

FIGURE B.26 – STABILITY PARAMETER VS. IRIBARREN PLOT.

The results in Figure B.26 are based on the design damage level S= 2, however as this research suggests that these damage levels are too conservative. Higher damage levels are ought to be acceptable, which resulted in the extrapolation by Wit [2015] of the tolerable damage based on Van der Meer [1988] (denoted as S_{extrap}). Using the higher damage levels, gives different results. The blue lines in Figure B.26, will shift upward, indicating higher stability.

Firstly, the extrapolated value for the stability has to be adjusted. The inter- and extrapolated curve's intersection with the line 'S= S_{extrap}' instead of 'S= 2'. The damage levels respective wave height is determined in the same fashion as was done in the previous paragraph. The intersection of the extrapolation of the test results line with the line of constant damage, S_{extrap} has been taken. For slope 1:5, see

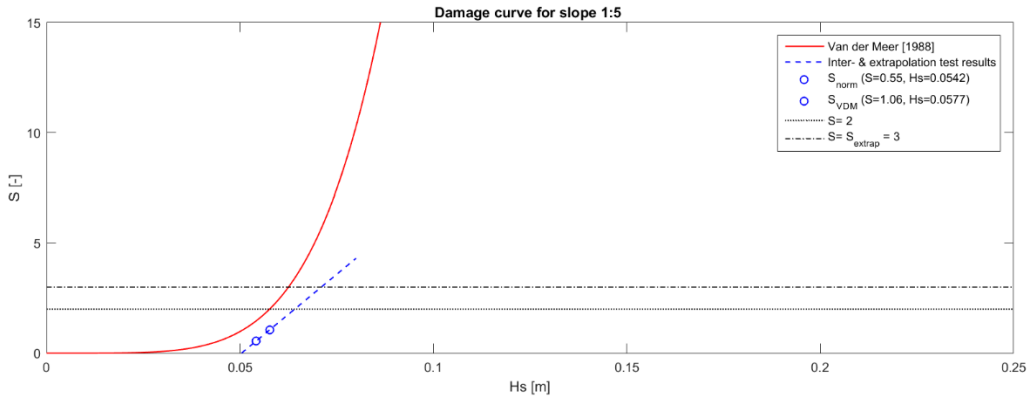

FIGURE B.27 - DAMAGE CURVE ANALYSIS FOR EXTRAPOLATED DAMAGE LEVEL (SLOPE 1:5)

For this slope the damage level, S_{extrap}= 3, intersect the extrapolation of the test results at a wave height of H_s=0.071. Translating this to the stability parameter results in a stability parameter of $H_s/\Delta D_{n50}$= 2.60.

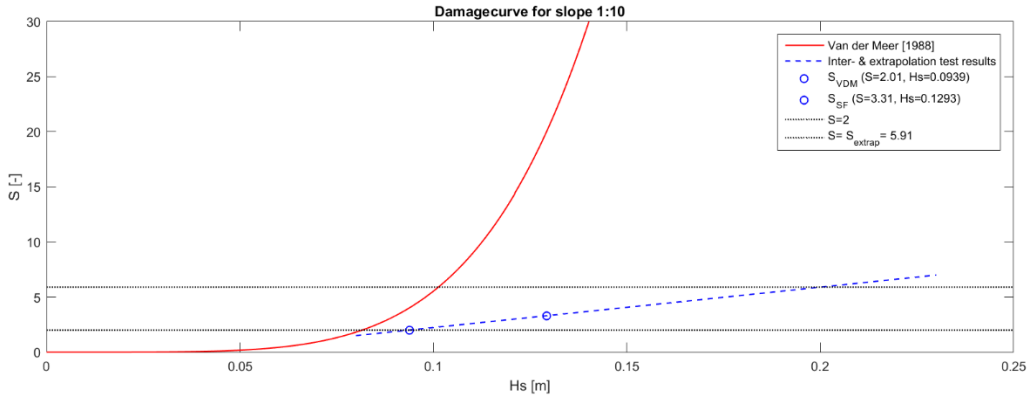

FIGURE B.28 - DAMAGE CURVE ANALYSIS FOR EXTRAPOLATED DAMAGE LEVEL (SLOPE 1:10)

For this slope the damage level, S_{extrap}= 5.91, intersect the extrapolation of the test results at a wave height of H_s=0.202. Translating this to the stability parameter results in a stability parameter of $H_s/\Delta D_{n50}$= 7.33. For the final slope (1:15) the extrapolation is not made, because the applied method of analysis is insufficient. For further elaboration on this, see the previous paragraph.

Combining all the previous results and implementing in a stability parameter vs. Iribarren number plot results in Figure B.29. The blue line (solid) represent the conventional Van der Meer [1988] approach with S= 2, this formula is extrapolated (blue dashed line) outside its validity region. The black circles represent test results Van der Meer [1988] based his results on. The black dots indicate the test results Schiereck & Fontijn [1996] based their research on. Furthermore, the inter- & extrapolated results from this results are represented with the asterisks. The blue asterisks represent the extrapolation to S= 2, and the red asterisks represent the extrapolation to S= S_{extrap}.

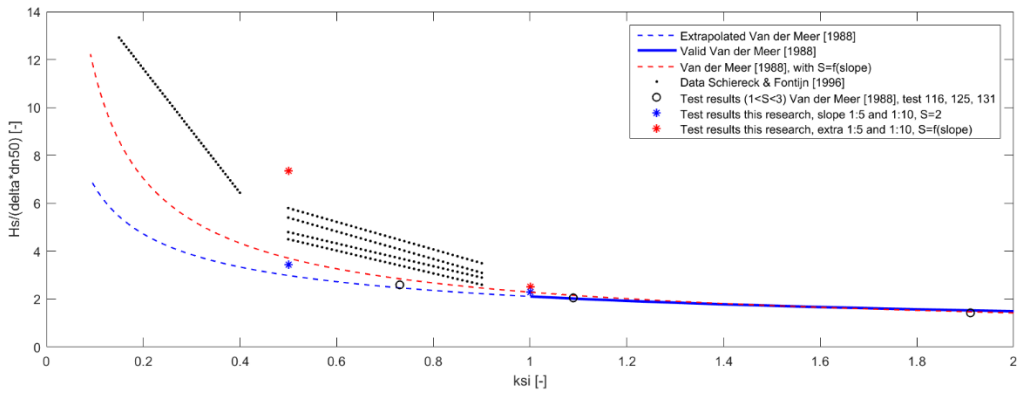

FIGURE B.29 – STABILITY PARAMETER VS IRIBARREN NUMBER PLOT, WITH DAMAGE LEVEL AS FUNCTION OF THE SLOPE

Based on these results one can conclude that the stability of the stones on mild slopes is higher than the Van der Meer [1988] formula for plunging waves suggests. Significantly lower damage levels were measured in the test series. All test results are more stable than the extrapolation of the Van der Meer [1988] formula suggests.

Apart from the damage level 'S', also other damage characteristics were elaborated. As Hofland et al [2011] proposed the damage depth, which is defined as $E_3 = \frac{\langle d_e \rangle_{3dn50}}{D_{n50}}$.

The eroded depth, denoted as d_e, was the average depth taken in a circle of $3D_{n50}$. In this research, for pragmatic reasons the median depth over a square with sides of $3D_{n50}$. These results appear to give reasonable results, even for the 1:15 slope. The results are plotted in Figure 4.6. The different shapes indicate different test inputs, which are specified in the legend of the figure. Subscript 'norm' indicates the test on slope 1:5 with the normal damage level S=2. The subscript 'VDM' represent the test based on the extrapolation of Van der Meer [1988] as was done by Wit [2015] and at last the subscript 'SF represents the test based on the data that was used by Schiereck & Fontijn [1996].

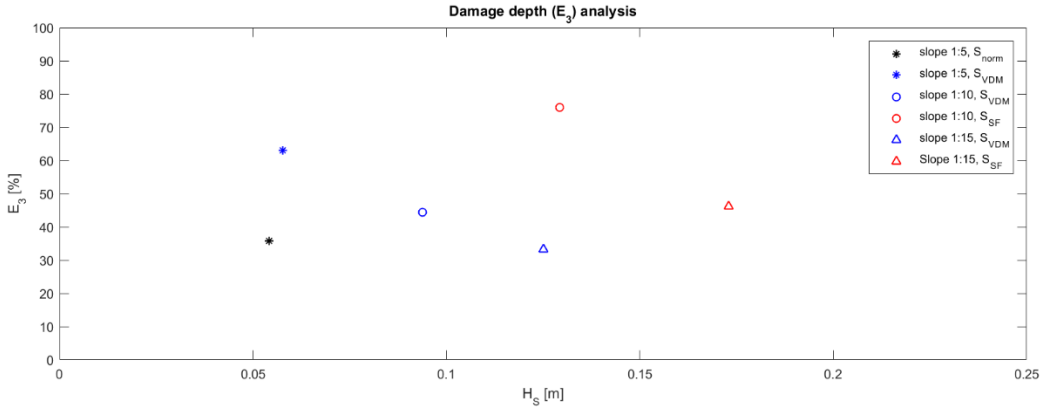

FIGURE B.30 - DAMAGE DEPTH VS. THE SIGNIFICANT WAVE HEIGHT.

When closely examing Figure 4.6, and relating the damage depth to the slope angle. A trendline can be drawn through the data points per slope, resulting in one trendline for each slope. This is presented in Figure 4.8B.32. One can see that the influence of the waveheight, with respect to the damage depth, decreases for milder slopes.

This can be explained by the spreading of the wave energy. Under constant steepness, the type of wave breaking changes with the changing of the slope angle. The different type of wave breaking are related to the surf simularity parameter or Iribarren number 'ξ'.The energy dissipation of waves can be significantly different, as is sketched in Figure 4.7.

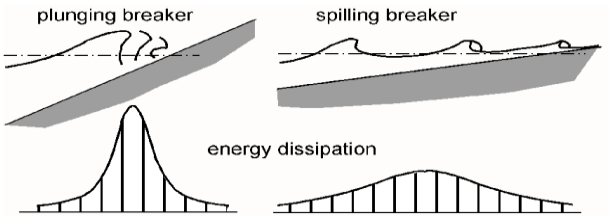

FIGURE B.31 - ENERGY DISSIPATION UNDER PLUNGING AND SPILLING WAVES (SCHIERECK ET AL. [2012])

Therefore on one particular slope, the damage depth increases with increasing wave height. However this ratio is different per slope angle. This difference in ratio can be explained by the spreading of the wave energy (which is defined as $E_{wave}=1/8 \cdot \rho \cdot g \cdot H^2$). More tests should be done to derive a proper trend line through the data.

As a first indication, trendlines for each slope have been drawn through the testdata. The influence of the waveheight diminishes for milder slopes, i.e. the inclination of the trend line decreases, see Figure B.32.

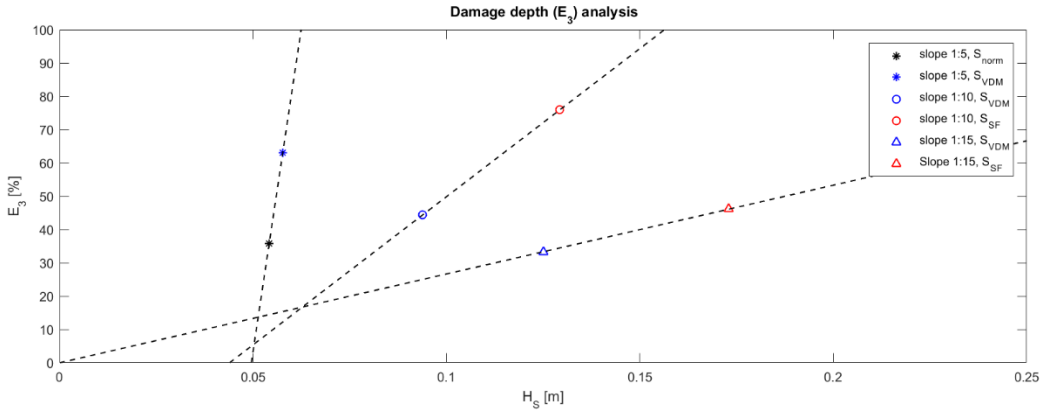

FIGURE B.32 - DAMAGE DEPTH VS WAVEHEIGHT WITH TRENDLINES PER SLOPE

When multiplying the results with the tangent of the slope all the results cluster together, see Figure B.33. This appears to represent that the damage depth is a function of the wave height times the tangent of the slope angle ($E_3 = f(H_S \cdot \tan\alpha)$). Noted should be that the effect of the slope still is represented in the trendlines, as the milder slopes have a lower inclination than the steeper slopes. Further research should be done in order to determine the shape of this formula, in which more variables should be examined.

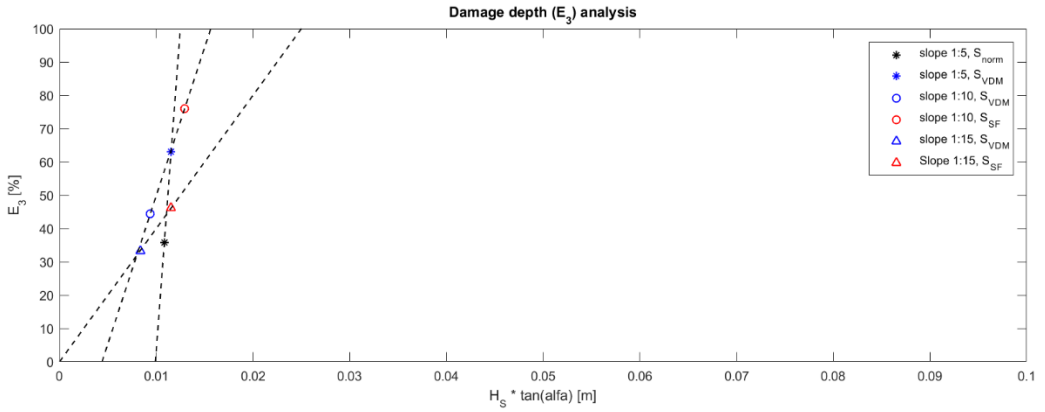

FIGURE B.33 - DAMAGE DEPTH VS WAVEHEIGHT * TAN(ALFA)

B.2. BIV/PIV

Chapter B.2 of this appendix will elaborate on the results of the BIV/PIV measurements. This is done in the same fashion as the previous chapter, i.e. firstly elaborating on the general procedure, followed by the analyzed results and at last elaborating the trends that come forward from the analyzed results.

B.2.1 GENERAL PRECEDURE

In this paragraph the procedure regarding the processing of the raw data for the BIV/PIV tests will be elaborated. For an elaboration on the test program and the test set up, see Appendix A. In the first paragraph, merely the processing of the video image will be presented. The images are processed by the means of PIVLab, a plugin for Matlab. This is a graphical user interface application, which can be downloaded and implemented in Matlab. PIVLab has been developed by Thielicke [2014], for his PhD research. In his PhD thesis, all tools within PIVLab are elaborated and explained.

B.2.1.1 VIDEO TO FRAME

In Appendix A, the camera and lighting set up has been elaborated. With this set up merely a small beam of light has been used, in order to create a narrow Depth of Field (DOF). There within the Field of View (FOV) only the bubbles and particles within the DOF are lit and therefore visible. The camera shoots a video with a resolution of 720*480 pixels and a frame rate of 132 frames per second (fps).

In order to analyze the video with PIVLab, the video has to be broken up into separate frames. This was done by writing a Matlab script, that reads an .avi file and returns .bmp files. The extension .bmp has been chosen as this image extension does not compress the data within a single frame, whereas for example .jpg or .jpeg do compress the data. All separated frames are numbered in chronological order, such that they are easily implemented in PIVLab.

B.2.1.2 IMAGE PRE-PROCESSING

PIVLab allows for a couple image pre-processing tools. Firstly, a mask will be drawn over part of the image. This mask excludes the selected area from the analysis. The mask is drawn over the part of the image where the stones are, as there will be no detectable water movement. Reducing the area that has to be processed by PIVLab reduces the calculation time.

Apart from the mask, image enhancement is also done in the pre-processing phase. Three types of image enhancement are used for this research. Firstly, CLAHE (Contrast Limited Adapted Histogram Equalization) has been applied to all the frames. This enhancement technique optimizes separate tiles (areas of 20x20 pixel in this research), this is favorable over optimizing over the entire frame at once because the FOV will not be uniformly exposed (i.e. different light intensities throughout the FOV). CLAHE spreads the most frequent intensities of the tiles over the full range of the data. Because the tiles are used instead of the full frames, the areas with different light intensities are optimized separately. After this optimization, the tiles are interpolated to create a smooth transition between the tiles.

Secondly, an intensity high pass is used. Due to reflections and light scattering, for example due to the breaking of light at the transition of air to water (and vice versa), bubbles and particles can be lit up. Because of this inhomogeneous lighting the results can be disturbed significantly, therefore an

intensity high pass is used. This entails that the background effects, that are caused by the inhomogeneous lighting, are ignored in the processing. The filter size here is also 20x20 pixels.

The final image enhancement is the 'intensity capping'. White intense spots in the FOV tend dominate the vector determination, intensity capping limits the intensity and therefore reduces their significance. This decreases their dominance in the vector determination, which leads to a more balanced input.

The principles of the above-mentioned image enhancement tools have been depicted in Figure B.34.

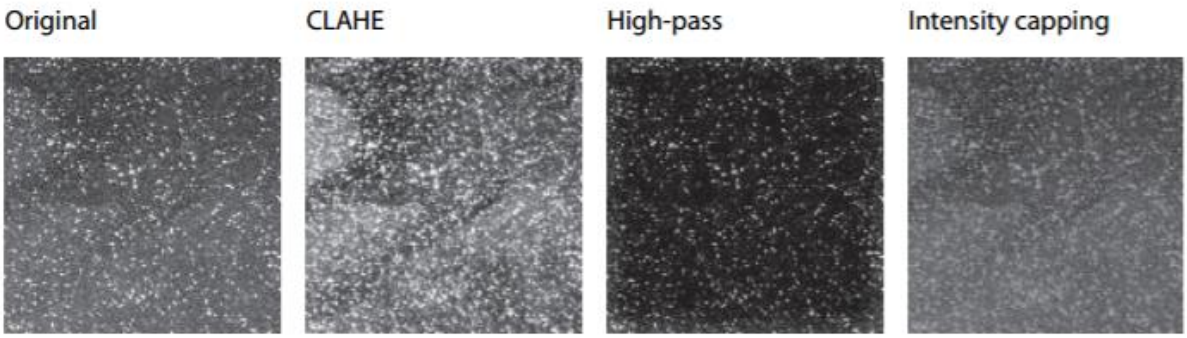

FIGURE B.34 - IMAGE ENHANCEMENT TOOLS - THIELICKE [2014]

B.2.1.3 PIV SETTINGS

The frames can be processed can be in two different sequences, (1-2, 3-4, 5-6… and 1-2, 2-3, 3-4…), the latter is chosen in this research. This is because than both velocity and acceleration can be calculated with the same step size (Δt).

Two options for the PIV algorithm are available in PIVLab, the DCC (Direct Cross-Correlation) and the DFT (Discrete Fourier Transform). Thielicke [2014] states that the DFT algorithm in most scenarios delivers the most accurate results, furthermore the DFT is stated to be the methodology with the lowest computational time. Therefore, the DFT option is used for the analysis of the data.

The frame analysis is done in three passes, firstly a rather large interrogation area has been used. This results in a reliable first estimate of the displacement, with a high signal-to-noise ratio. The higher this ratio is the more dominant the signal output is over the noise in the image. Since this large interrogation area results in a low vector density, multiple passes will be used. The displacement information of the first pass, forms the offset of the second pass. The same applies for the third pass. By using three passes (128x128 pixel, 64x64 pixel and finally 32x32 pixel) results in a high vector resolution but remains reliable with a high signal-to-noise ratio.

With these setting the frames can be analyzed.

B.2.1.4 POST PROCESSING

After the frames have been analyzed, the output of the vectors is in the dimension pixel per frame. To translate this to the vectors with the dimension meters per second, the results will have to be calibrated. This is done by the means of an external calibration image; this image has been shot with the same camera that has been used for the BIV/PIV measurement. This calibration image has been taken from the exact same distance with the exact same settings as the measurement have been done.

Therefore, they will have the exact same FOV. This calibration results in the translation from number of pixel to distance in meter, the time calibration is done by the means of the framerate. The framerate is set at 132 frames per second (i.e. Δt = 7.576 ms). See Figure B.35 (left), for an image on the matter.

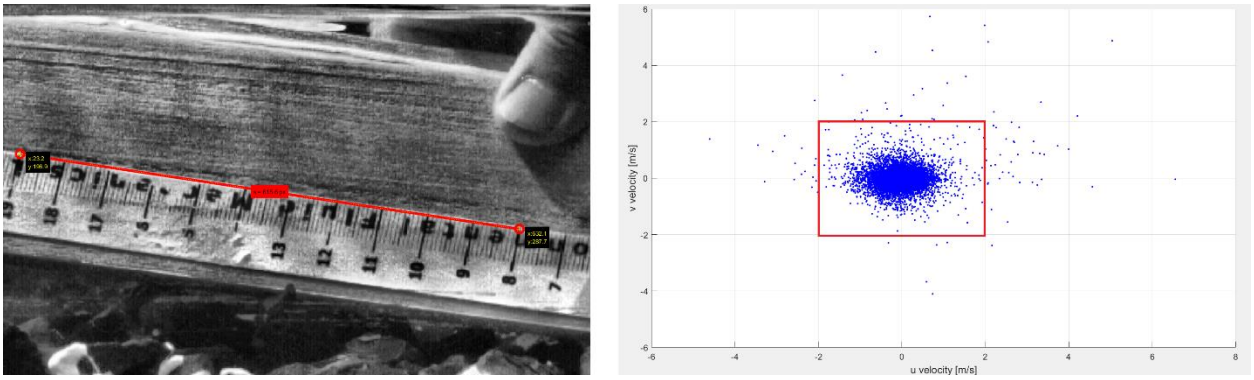

FIGURE B.35 - CALIBRATION METHOD (LEFT) & VECTOR VALIDATION (RIGHT)

From the calibrated velocity vectors a scatterplot can be made, see Figure B.35 (right). This scatter plot has the horizontal velocity on the x-axis and the vertical velocity on the y-axis. In Figure B.35 (right) all the vectors are plotted from all the frames (roughly 1200) in the analysis. As this research is interested in the flow field rather than the extreme values, the vectors with u components between -2 and 2 m/s have been validated. The same is done for the v components, those are also validated between -2 and 2 m/s.

Finally, the vectors are set to represent the velocity magnitude. The vectors have been slightly smoothed and the background is transformed in a color graded map, with the color spread between 0 and 2 m/s. Areas where data is lacking, PIVLab interpolates the vectors, these vectors are indicated in red, whereas the vectors based on the data from the image are represented in black. An example is given in Figure B.36.

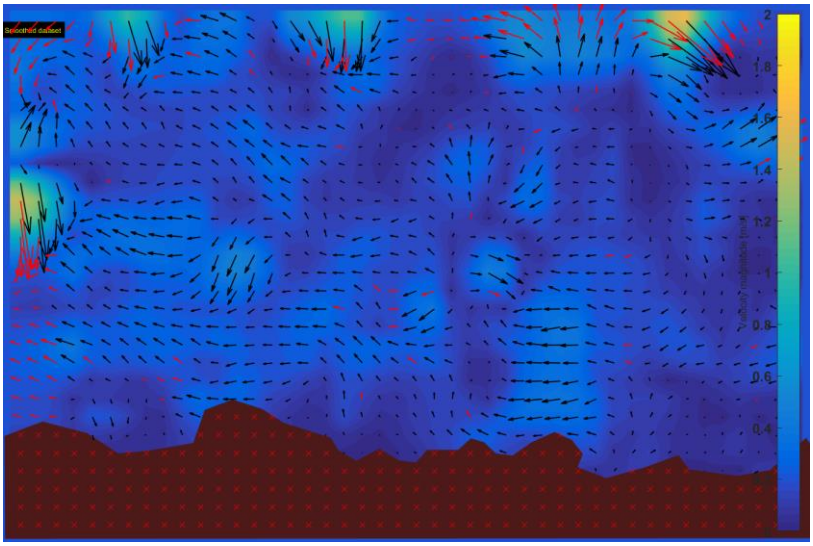

FIGURE B.36 - OUTPUT PIVLAB.

B.2.1.5 PIVLAB OUTPUT

Since PIVLab results in vector fields per time step, the output needs to be processed further. Outside of the boundaries of PIVLab. Therefore, the results from PIVLab are exported in .mat files, such that the files can be further processed. As this research is interested in the stability of the stones on the slope, the PIVLab output is further processed. From the PIVLab results, see the vector field in Figure B.36, a Region of Interest (ROI) is chosen. The ROI is determined just above the stone layer, as the velocity and acceleration in this area influences the stability of the stone. The area has a width of 2 D_{n50} (1d_{n50} upslope of the center of the ROI, and 1 D_{n50} downslope) and a height of 1 D_{n50}. The ROI for the tests on the 1:10 slope is depicted in Figure B.37.

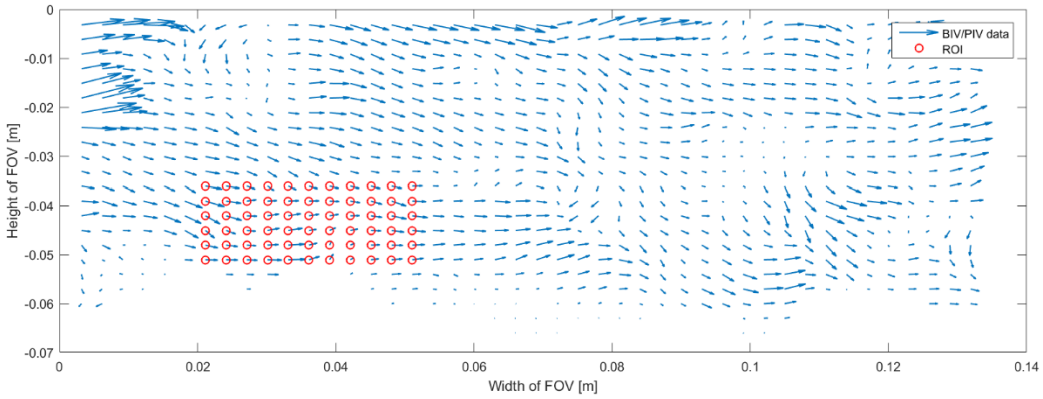

FIGURE B.37 – VISUALIZATION OF THE REGINO OF INTEREST (ROI)

Over the ROI the horizontal velocity U is averaged per frame, i.e. per vector field. By doing so for each frame, i.e. time step Δt, a time signal of the respective velocities can be determined. Furthermore, the total magnitude of the velocity and acceleration can be derived.

The vertical velocities are not taken into account in the rest of the research. Because of the use of both BIV and PIV the vertical initial velocity will differ between bubbles and particles (due to the difference in buoyancy between the bubbles and particles). Therefore, the output signal will create too much noise, which will lead to inaccurate and unreliable output. With merely the horizontal velocities and accelerations left, the results as were derived from the ROI over time and smoothed. A smoothing spline function was applied in Matlab with a smoothing parameter of 0.99 for both the velocity. From the obtained velocity signal the derivative has been taken to gain the acceleration du/dt. This results in a smooth time signal for both the velocity and acceleration, see Figure B.38.

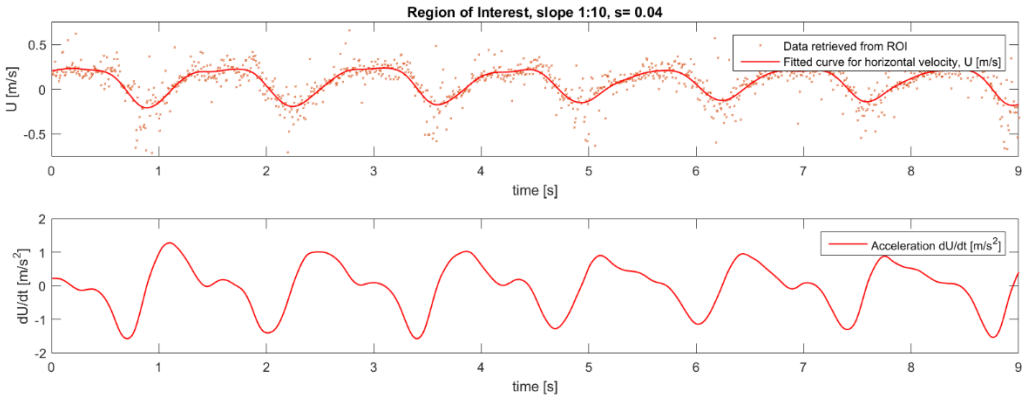

FIGURE B.38 – VELOCITY AND ACCELERATION SIGNAL FOR THE ROI, SLOPE 1:10.

Apart from the FOV the free stream velocity is approached. The free stream velocity can be approached by the means of a cross section of the FOV, in other words a velocity profile from the bottom to the water level. By plotting this for several points in time, with respect to the wave period (e.g. t=0, t=0.1T, t=0.2T, ….) one can derive from where the bottom layer effects are negligible and the velocity profile becomes rather constant.

For the 1:10 slope the free stream velocity can be approached. However, for the 1:5 slopes the free stream velocity cannot be derived. As the FOV is placed at the location of the damage zone, and the damage zone is very close to SWL, the water level fluctuations (i.e. waves) are directly in the FOV, see Figure B.0.39.

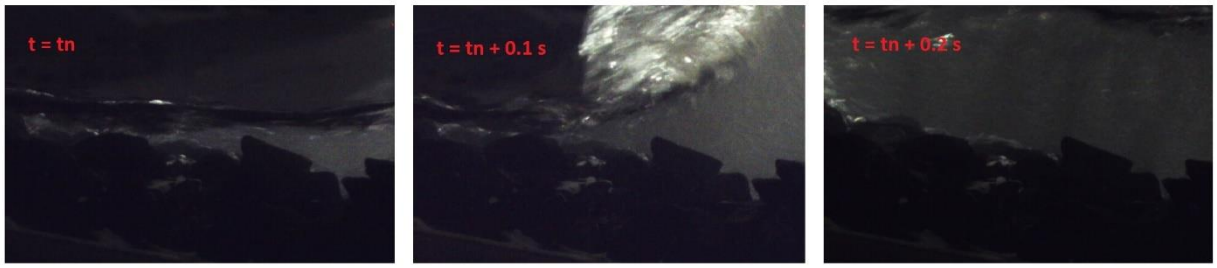

FIGURE B.0.39 - WATERLEVEL FLUCTUATION AT FOV FOR SLOPE 1:5

For the 1:10 and 1:15 slopes where the damagezone is further away from the SWL, the remaining water level under a trough of a wave is ought to be still significant enough to derive a free stream velocity. The location of the derivation of the free stream velocity should however account for the fluctuating water level. The height at which the free stream velocity occurs is determined by the boundary layer. The boundary layer is described by Figure B.40. Under waves, the boundary layer grows in time but is therefore restricted by the wave period (i.e. flow reversal). By finding the height at which the velocity signals approximately become constant, the boundary layer can be determined.

Above the boundary the free stream velocity is found, therefore by retrieving the average velocity above the boundary layer the free stream velocity can be approximated. In the figure the thickness of the boundary is depicted by δ, furthermore the velocity profile of the horizontal velocity u is depicted.

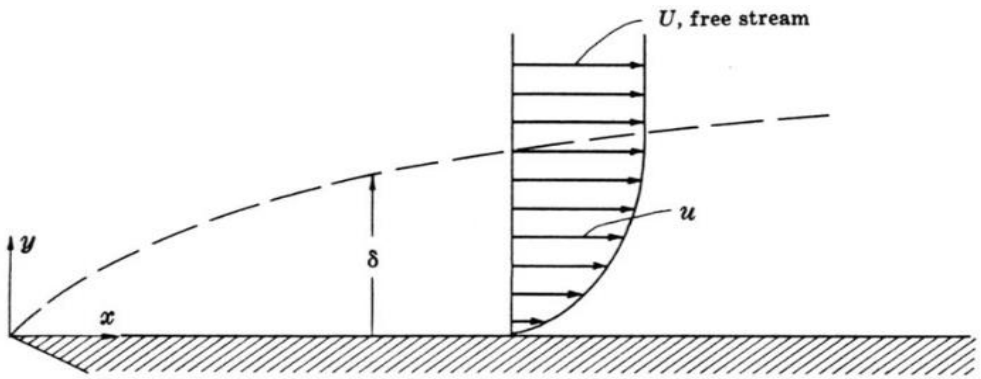

FIGURE B.40 - BOUNDARY LAYER AND FREE STREAM VELOCITY

In order to smooth the profile slightly, the average over 3 vectors in width is taken, the vectors used for the derivation are depicted in Figure B.41. represents the vector field of an arbitrary moment in time of the BIV analysis for the 1:10 slope.

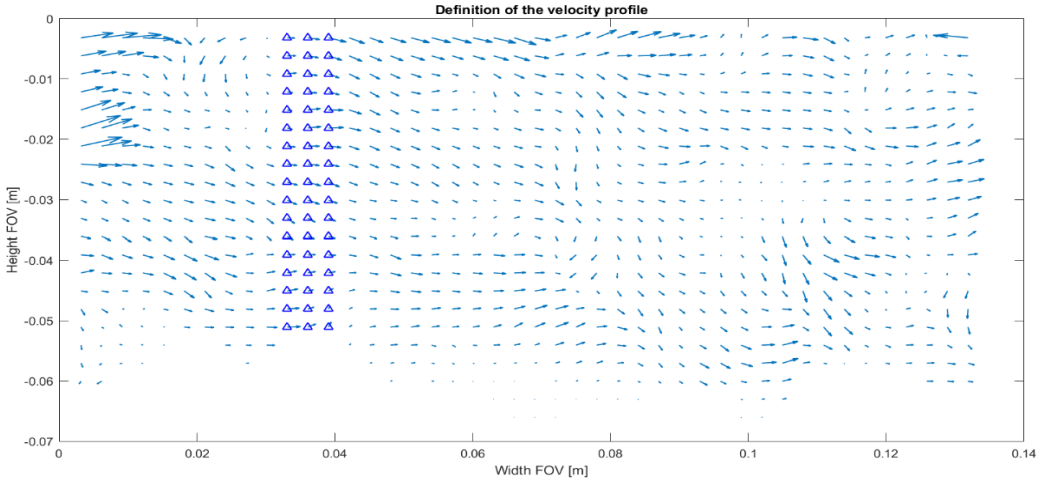

FIGURE B.41 - DEFINITION OF VELOCITY PROFILE DERIVATION

From this region, the velocity profile is derived for every tenth of a wave period. Staying with the example of the 1:10 slope, the different velocity profiles can be plotted for different time steps, this is presented in Figure B.42. Note that a negative velocity represents upslope movement of the particles/bubbles and thus the water. The velocity scale is set to –1 to +1 meter per second, except for the t=0.6T, which for this case represents the uprush of the wave.

From Figure B.38 and Figure B.42 one can conclude that the velocity profile is skewed. The upward motion of the water is briefer and more abrupt than the downslope movement of the water.

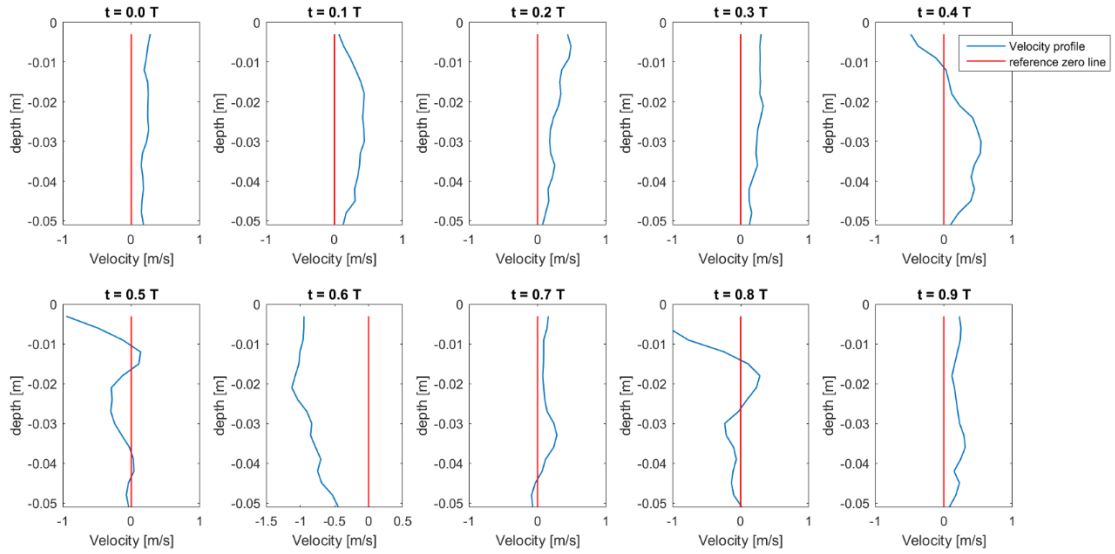

FIGURE B.42 - VELOCITY PROFILES FOR EVERY TENTH OF A WAVE PERIOD, FOR SLOPE 1:10.

Furthermore, from Figure B.42 the location for the best approximation of the free stream velocity will be made. Considering the water level fluctuation, the region of the approximated of the free stream velocity will have to be below the lowest water level. After video analysis, the lowest water level is set at -1cm, therefore the region of the approximation of the free stream velocity will be just below this level. The size of the region will be the same as has been arbitrarily used for the ROI, i.e. 2 d_{n50} wide and 1 d_{n50} high. This results in the following region, see Figure B.43.

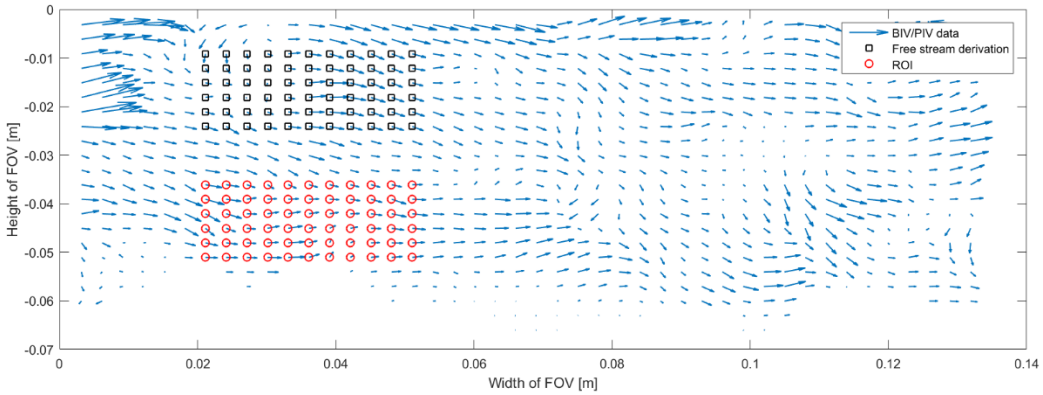

FIGURE B.43 - ROI AND REGION FOR THE APPROXIMATION OF THE FREE STREAM VELOCITY, FOR SLOPE 1:10

From the region for the approximation of the free stream velocity, i.e. the black squares in Figure B.43, the velocity and acceleration signal is derived. This is done in the same manner as was done for the ROI. This entails, that for each vector field, the average value over the region is determined. Each vector field represents a moment in time, therefore deriving the average vector for all vector fields (i.e. time steps) creates a time signal. The results are scattered and therefore fitted into a smoothed curve. For the acceleration, the derivative of the scattered data is taken, these results are also smoothed with the same factor as the velocity signal.

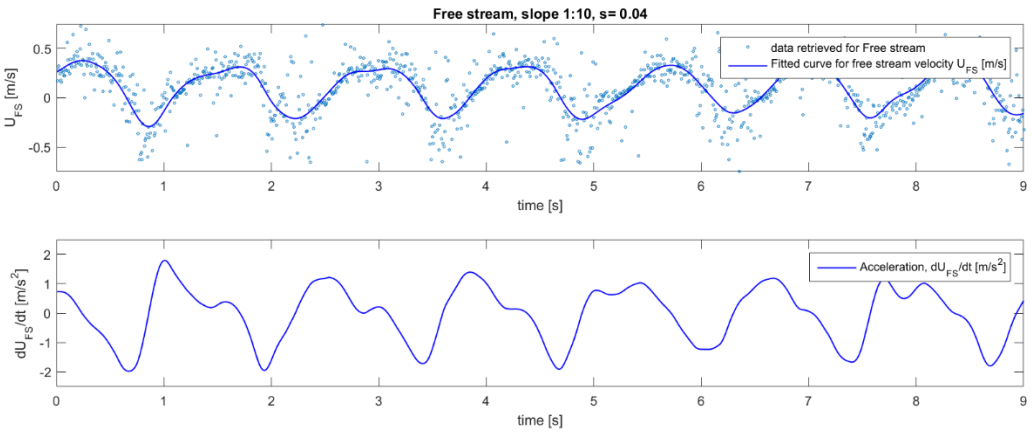

FIGURE B.44 - VELOCITY AND ACCELERATION DERIVED FOR THE APPROXIMATION OF THE FREE STREAM VELOCITY, FOR SLOPE 1:10

The signals clearly indicate the different waves with the oscillating velocity. This is considered a confirmation that the results indeed still represent the wave signal. The difference become clear when both are plotted in the same figure, see Figure B.45.

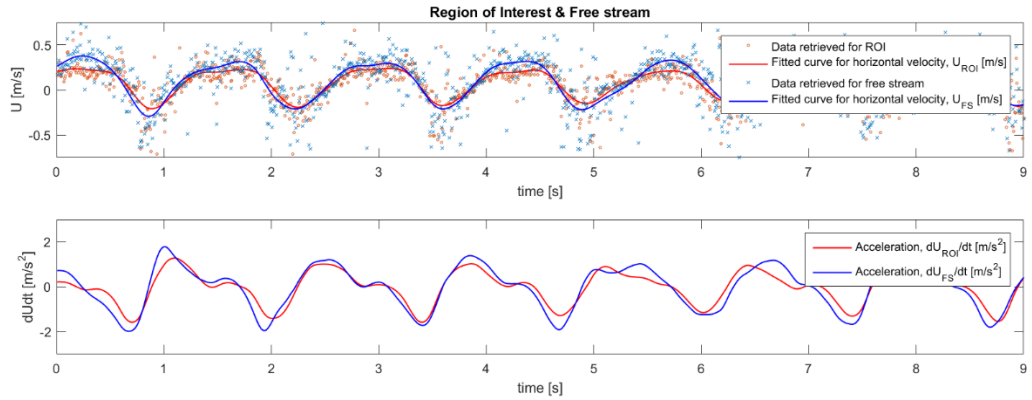

FIGURE B.45 - VELOCITY AND ACCELERATION SIGNAL FOR ROI AND THE APPROXIMATION OF FREE STREAM VELOCITY, FOR SLOPE 1:10

The blue smoothed line represents the approximation of free stream velocity whereas the red smoothed line indicates the ROI. The free stream approximation data for the velocity as well as the acceleration is of greater magnitude, this aligns with the theory. As the friction effects reduce further away from the bottom. At some distance from the bottom, the free stream velocity is reached and the boundary layer (i.e. layer influenced by the bottom) has no influence on the velocity.

B.2.1.6 DERIVATION PARAMETERS

The velocity and acceleration signal will be substituted in the different physical methodologies which are applied in XBeach-G, i.e. Van Rijn [2007] and Nielsen [2006]. Both methods are combined with a Shields [1936] approach to determine the initiation of motion. This approach is modified to account for the slope effect. As both the Van Rijn [2007] and the Nielsen [2006] approach are used in this form, they can be directly compared. Both approaches are elaborated in chapter 2, Literature.

A brief recap of the formulae will be given, with the values for the parameters. The slope correction factor is derived by the hand of the research of Fredsøe and Deigaard [1922].

$$\theta' = \theta \cdot \cos\beta \cdot \left(1 \pm \frac{\tan\beta}{\tan\emptyset}\right) \qquad \text{Equation B.3}$$

The slope angle 'β' obviously changes per slope, whereas the angle of repose is assumed at 40°. As the same stones are used for all the tests, the angle of repose remains the same for all test. Therefore, the correction factor is merely a function of the slope angle. The correction factor is greater than 1 for downslope direction and smaller than 1 for the upslope direction. The results of the analysis are presented in Table B.10

Slope correction factor	Slope 1:5	Slope 1:10	Slope 1:15
Upslope direction	0.747	0.877	0.919
Downslope direction	1.214	1.113	1.077

TABLE B.10 - SLOPE CORRECTION FACTORS BASED ON FREDSØE AND DEIGAARD [1922]

VAN RIJN [2007]

XBeach-G applies the Van Rijn [2007] formula in the following way, see equation B.4 and B.5

$$\theta = \frac{\tau_b}{\rho g \Delta D_{50}} \cdot \cos\beta \cdot \left(1 \pm \frac{\tan\beta}{\tan\emptyset}\right) \qquad \text{Equation B.4}$$

$$\tau_b = \tau_{bd} + \tau_{bi} = \underbrace{c_f \rho \frac{u|u|}{h}}_{drag} + \underbrace{\rho c_m c_v c_n D_{50} \frac{\partial u}{\partial t}}_{inertia} \qquad \text{Equation B.5}$$

The velocity and the acceleration over time are derived from the BIV/PIV analysis. The rest of the parameters still need to be determined, for the Van Rijn [2007] formula this results in the following parameters.

C_f - the friction factor. In XBeach-G McCall [2015] rewrites the friction factor to compensate for the infiltration and exfiltration effects. This is not measured during the test in the flume, therefore this compensation is not accounted for in this research. Ignoring the infiltration and exfiltration effects, the Van Rijn [2007] methodology uses the method of Kobayashi et al. [1987].

$$c_f = \frac{g}{\left(18 \log\left(\frac{12h}{k}\right)\right)^2} \qquad \text{Equation B.6}$$

$$with\ k = 3\ d_{90}$$

Since the depth at the location of the FOV is different for each slope, the friction factor differs with this depth. The depths at the location of the FOV are respectively

With a D_{90} of 25 mm this results in three friction factors of 0.054 for the 1:5 slope and 0.031 and 0.025 for slope 1:10 and 1:15 respectively.

Test	1:5, s= 0.04	1:5, s= 0.06	1:10, s= 0.04	1:15, s= 0.04
Friction factor – c_f [-]	0.054	0.054	0.031	0.025

TABLE B.11 - FRICTION FACTORS VAN RIJN [2007] FORMULA

ρ_s – the density of the stones. The density of the stones has been determined by the means of a serie of tests, elaborated in Appendix A. From those tests followed that he density of the stones was 2685 kg/m^3.

h – the water depth. The water depth is measured at the location of the ROI in the FOV. The FOV is located at the location of the most significant erosion after the irregular waves series. As the wave height changed per slope, so did the location of the erosion compared to SWL. See

Test	1:5, s= 0.04	1:5, s= 0.06	1:10, s= 0.04	1:15, s= 0.04
Water depth at ROI – h [m]	0.035	0.035	0.059	0.077

TABLE B.12 - WATER DEPTHS FOR THE BIV TESTS

c_x – coefficients. Three coefficients, apart from the friction coefficient, are used in the Van Rijn [2007] approach. For convenience, the shape of the stones is considered spherical. The coefficient for the added mass is defined as $c_m = 1 + c_a$, with c_a is 0.5 for spheres with zero autonomous acceleration. The volume shape factor c_v is $\pi/6$ for spheres. At last the coefficient for the number of grains (i.e. stones) that is influenced by the acceleration per unit of area. All these coefficients can also be replaced with one calibration coefficient $c_i = c_m \cdot c_v \cdot c_n \approx \mathcal{O}(1)$.

g – gravitational acceleration. The gravitational acceleration is constant at 9.81 m/s^2 in the Netherlands, which is taken as the representative in this research.

Δ– relative effective weight of the stones. The effective weight can be calculated by the standard formula $\Delta = \rho_s - \rho_w / \rho_w$. Note that McCall [2015] uses Δ_i, which accounts for the through bed flow effects. As those effects are not accounted for in this research, the regular effective weight is used.

D_{50} – the characteristic stone size. The characteristic stone size in this research is 19.2 mm, as follows from the sieve curve presented in Appendix A.

The derived parameters are presented in Table 4.4.

Parameter	C_f [-]	ρ [kg/m^3]	h [m]	C_m [-]	C_v [-]	C_n [-]	g [m/s^2]	Δ_i [-]	D_{50} [m]
Value	variable	2685	variable	1.5	0.52	1	9.81	1.685	0.0192

TABLE B.13 - PARAMETERS VAN RIJN [2007] METHODOLOGY

Furthermore, according to Tromp [2004], the stability of rock on mild slopes could be described by a Morison-like formula. This formula is a form of the Van Rijn [2007] description, which is integrated over the stones on a particular slope. This integration gives a force on the stones instead of the shear stress on the bed. Therefore, this formulation is depending on the characteristics (protrusion, stone size etc.) of one single stone. This is approach is not further elaborated, as the Van Rijn [2007] methodology describes the same process, just in a more general form.

NIELSEN [2006]

Xbeach-G uses the Nielsen [2006] formula in the following way, see equation B.7 and B.8.

$$\theta = \frac{u_*^2}{\Delta g D_{50}} \cdot \cos\beta \cdot \left(1 \pm \frac{\tan\beta}{\tan\emptyset}\right) \qquad \text{Equation B.7}$$

$$u_* = \sqrt{\frac{f_s}{2}}\left(\cos\varphi \cdot u + \frac{T_{m-1.0}}{2\pi}\sin\varphi\frac{\partial u}{\partial t}\right)$$

$$u_* = \underbrace{\sqrt{\frac{f_s}{2}} \cdot \cos\varphi \cdot u}_{velocity} + \underbrace{\sqrt{\frac{f_s}{2}} \cdot \frac{T_{m-1.0}}{2\pi}\sin\varphi\frac{\partial u}{\partial t}}_{acceleration} \qquad \text{Equation B.8}$$

The velocity and acceleration are derived from the BIV/PIV analysis, the rest of the parameters are derived in below and will be summarized in Table 4.8.

f_s - sediment friction factor. This value can be calculated by the means of the standard wave friction factor. In the research of Postma [2016], he used the sediment friction factor provided by Xbeach-G ans was kept constant at f_s=0.025. However, with the BIV/PIV measurements it this friction factor can be determined. This is done by the means of equation

$$f_s = \exp\left(5.5\left(\frac{2{,}5\, d_{50}}{A}\right)^{0.2} - 6.3\right)$$

$$with\ A = \frac{\sqrt{2}}{\omega_p}\sqrt{var\ \{u_\infty(t)\}} \qquad \text{Equation B.9}$$

The angular peak frequency is known, as regular waves are used during the BIV/PIV analysis, T_p=T. With this the angular velocity is defined as 2π/T. Since the wave characteristics alter per slope, the angular velocity also changes. The variance of the free stream velocity follows a Matlab analysis. This results in values of f_s, see Table 4.5.

Test	1:5, s= 0.04	1:5, s= 0.06	1:10, s= 0.04	1:15, s= 0.04
Var {u_∞(t)}	0.0284	0.0355	0.0846	0.0430
Sediment friction factor -f_s [-]	0.3611	0.3215	0.2091	0.2914

TABLE B.14 – SEDIMENT FRICTION VALUES FOR NIELSEN [2006] FORMULA.

The suggested value of Xbeach-G for the sediment friction factor is set at f_s = 0.025. The values found with the BIV/PIV tests are about a factor 10 higher.

φ – Phase shift angle. The phase shift angle is defined as the phase difference between the free stream velocity and the shear velocity. This value is determined by plotting both the free stream velocity and the shear velocity on the same time scale. For each zero crossing (up- and downward) the phase lag of the shear velocity is determined in seconds. The phase lag for all zero crossings are summed and divided by the number of zero crossings.

The phase lags are then transferred to degrees by dividing the phase lag (in seconds) by the wave period and multiplying by 360°. An example of a plot of both the shear velocity and the free stream velocity is presented in Figure 4.10.

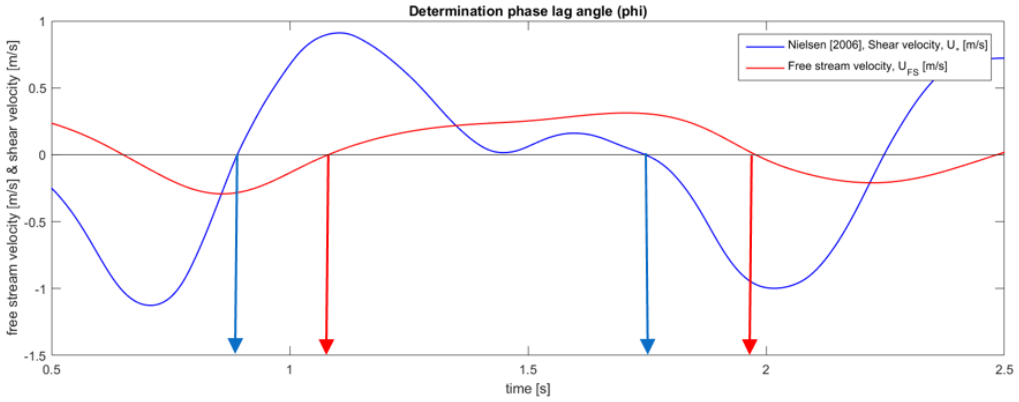

FIGURE B.0.46 - DETERMINATION OF THE PHASE LAG ANGLE (ARBITRARY EXAMPLE OF SLOPE 1:10)

Figure B.0.46 shows two arbitrary determination of the phase lag of the shear velocity compared to the free stream velocity. The blue arrow represents the zero crossing of the shear velocity, whereas the red arrow represents the zero crossing of the free stream velocity. The time difference is here roughly 0.15 seconds. This method is applied for all zero crossings (up- and downward) for each BIV/PIV analysis and then divided by the number of zero crossings. This results in Table B.15.

Test	1:5, s= 0.04	1:5, s= 0.06	1:10, s= 0.04	1:15, s= 0.04
Phase shift – φ_{time} [s]	0.247	0.195	0.280	0.346
Phase shift angle – φ [°]	72.8	70.5	65.0	69.6

TABLE B.15 - PHASE SHIFT ANGLE VALUES FOR NIELSEN [2006] FORMULA

Note that this phase lag is significantly higher than the value used as standard by Xbeach-G, who used a value of 25°. Physically the higher phase lag angles indicate that the drag term (i.e. velocity term) of Nielsen [2006] formula becomes less dominant and the inertia term (i.e. acceleration term) becomes more dominant. (cos φ → 0 and sin φ → 1 for higher values of φ).

$T_{m-1.0}$ – spectral wave period. As regular waves were used, the spectral wave period is equal to the mean wave period which has been derived for all tests and presented in Table B.16

Test	1:5, s= 0.04	1:5, s= 0.06	1:10, s= 0.04	1:15, s= 0.04
Wave period – T [s]	1.2196	0.9948	1.5503	1.7900

TABLE B.16 - WAVE PERIOD VALUES FOR NIELSEN [2006] FORMULA

Summarizing the previously presented values for the Nielsen [2006] formula results in Table B.17Table 4.8. all the variable parameters are specified in their respective tables, as presented above.

Parameter	f_s [-]	φ [rad]	$T_{m-1.0}$ [s]	g [m/s²]	Δ [-]	D_{50} [m]
Value	variable	Variable	variable	9.81	1.685	0.0192

TABLE B.17 - PARAMETERS NIELSEN [2006] METHODOLOGY

B.2.1.7 SUBSTITUTION

In this sub-paragraph the final step of the BIV/PIV analysis is presented. The constant parameters and the derived velocities and accelerations are substituted in the two physical formulae. Both the Nielsen [2006] and the Van Rijn [2007] formulae have been elaborated. The results will be elaborated per BIV/PIV test. The Van Rijn [2007] approach can be split in a drag and an inertia part (i.e. a velocity and acceleration term). The Nielsen [2006] approach can also be split in a velocity and an acceleration term. For both formulae, both terms have been plotted in Figure B.47. From this one could derive the relative importance of velocity with respect to acceleration. See Figure B.477

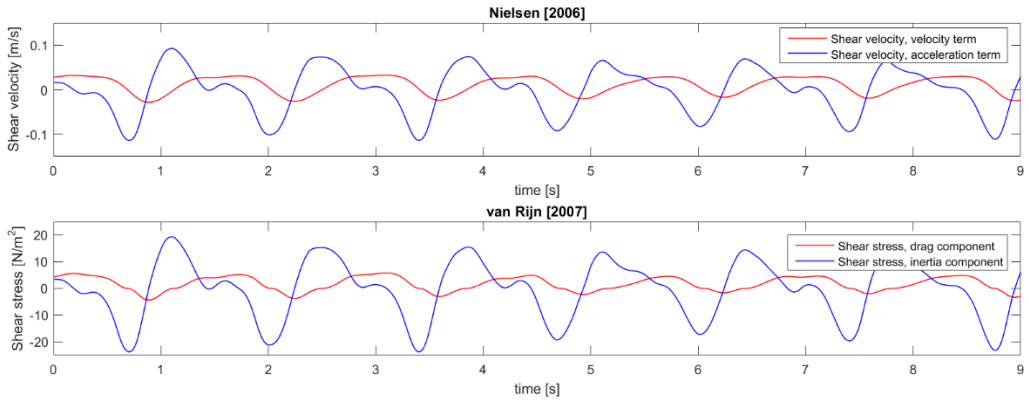

FIGURE B.47 – VELOCITY AND ACCELERATION TERM COMPONENT PLOTTED IN TIME, FOR BOTH NIELSEN [2006] AND THE VAN RIJN [2007] APPROACH

For both the Nielsen [2006] and the Van Rijn [2007] approach the acceleration term is also dominant compared to the velocity, however the velocity term still plays a significant role.

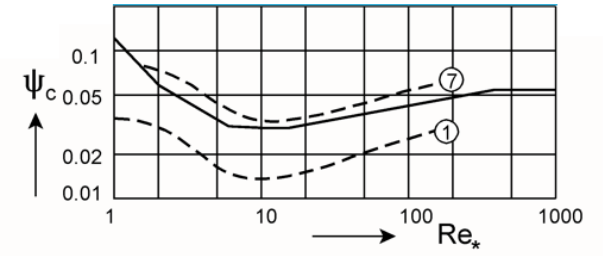

FIGURE B.48 - QUALITATIVE PLOT OF SEVEN STAGES OF MOVEMENT WITH RESPECT TO THE CRITICAL SHIELDS VALUE (SCHIERECK ET AL. [2012])

Seven different stages of movement can be described, starting from 0. no movement at all, to 1. occasional movement at some locations, to 2. Frequent movement at some locations… to eventually 6. Continuous movement of at all location and 7. General transport of grains.

The Shields values have been plotted qualitatively in Figure B.48. From this plot one can derive that grains can start moving once the Shields value exceeds a critical value based on level 1. This value approximated at a critical Shields value of 0.03-0.04.

Furthermore, both the Nielsen [2006] and the [2007] have been rewritten into the shields parameter, this way the formulae can be directly compared. In this graph both the formulae have been adjusted for slope effects. Also for this sub-paragraph, the slope 1:10 is used as an example. This is depicted in Figure B.49. Negative values are based on the upslope velocity and acceleration, whereas the positive values indicate downslope direction of both velocity and acceleration.

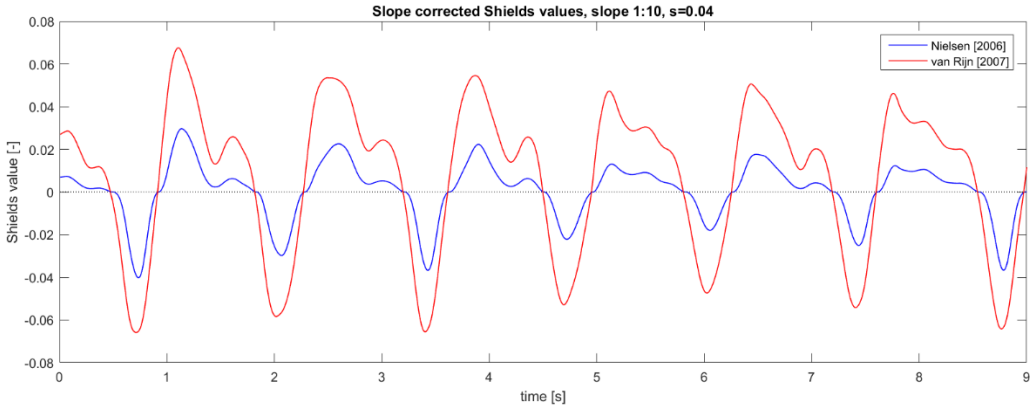

FIGURE B.49 - SHIELDS VALUES PLOTTED AGAINST THE TIME, FOR BOTH THE NIELSEN [2006] AND THE VAN RIJN [2007] APPROACH

In Figure B.49 one can see that the Nielsen [2006] and Van Rijn [2007] are in the right order of magnitude, with respect to the different stages of movement as defined by Shields. From Figure B.48 we know that the first stages of movement coincide with a Shields value of 0.035-0.04, the highest peaks of the Nielsen [2006] approach result in.

Van Rijn [2007] gives absolute Shields values of approximately 0.05-0.06. These values indicate a stage 6 motion of stones, which is described as continuous movement at all locations. However, as the waves in the BIV/PIV tests are based on the highest 1% of the spectrum used in the irregular wave profile change tests this movement would only occur 1% of the waves and thus result in little damage. Therefore, this agrees with the results found in these tests.

B.2.2 ANALYZED RESULTS

In this paragraph the analyzed BIV/PIV results will be presented. This is done by the means of the time signals of both the velocity and acceleration, as are depicted in Figure B.38. Furthermore, the characteristics, i.e. the mean, maximum and minimum value will be elaborated. Furthermore, the drag and inertia part of both the Nielsen [2006] and the Van Rijn [2007] formula will be examined. At last both Nielsen [2006] and Van Rijn [2007] will be rewritten in to the Shields value and multiplied with the slope correction factor of Fredsøe and Deigaard [1922]. The paragraph will be divided in the different test set ups.

B.2.2.1 TEST 1: COTA= 5, S= 0.04, H= 0.0874 M, T= 1.2196 SEC

After the pre-analysis, has been done as is presented in the previous paragraph, the velocity and acceleration signal for U are derived, see Figure B.50. In the signal the velocity U and the acceleration dU/dt are plotted against the time. In Figure B.50, one can see the red circles plotted as the raw input for the model, whereas the red line represents the fitted curve that represents the velocity and the acceleration.

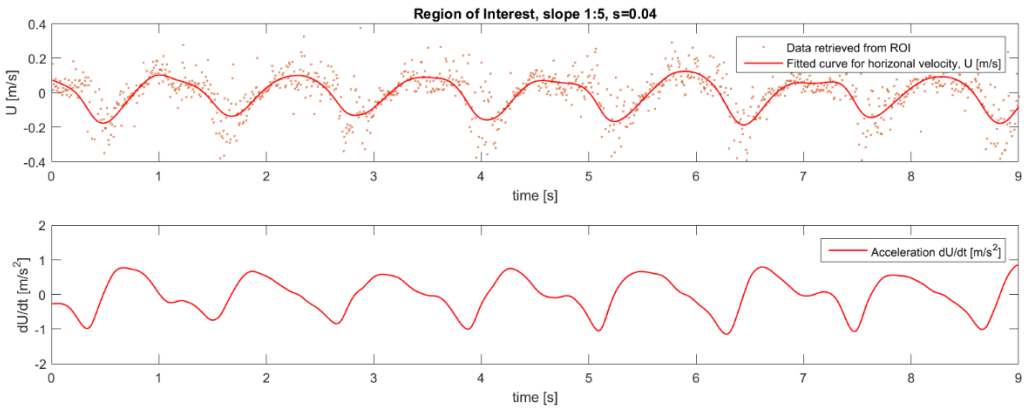

FIGURE B.50 - VELOCITY & ACCELERATION SIGNAL FOR SLOPE 1:5, S=0.04

From this signal the velocity and acceleration characteristics are derived. For both the velocity and the acceleration the mean, the minimal value and the maximum value have derived from the time signal. This results in Table B.18.

	Velocity U [m/s]	Acceleration dU/dt [m/s²]
Mean	-0.008	-0.001
Max	0.124	0.872
Min	-0.187	-1.146

TABLE B.18 - VELOCITY & ACCELERATION CHARACTERISTICS BASED ON FITTED CURVE, SLOPE 1:5 AND WAVE STEEPNESS 0.04

From the plot in Figure B.50 and the characteristics in Table B.18 can be derived that the minimal velocity is greater in magnitude than the maximal velocity. As negatives velocity values represent the upslope movement of water, and the positive values represent the downslope water movement.

To check whether the velocities measured are reasonable, linear wave theory is used to compare. Linear wave theory for states the horizontal particle movement in shallow water can be determined by

$$u = \frac{1}{2} \cdot H \cdot \sqrt{g/h} \cdot \sin(\omega \cdot t) \qquad \text{Equation B.10}$$

As we compare the extreme values, sin (ωt)=1 or -1, we find that the velocity according to the linear wave theory should be u=0.778. This agrees very well with the minimal result, derived from the raw data (u_{min}=0.824 m/s). The fact that maximum value (i.e. downslope movement of water) is lower can be declared by friction effects and wave energy absorption. *Note that the fitted curve is a fitted line, that does not follow the extreme values, and thus is considerably lower than the derived extreme values.*

Whit the derivation of the velocity and the acceleration done, these derivations can be substituted in both the Nielsen [2006] and Van Rijn [2007] formula. Both formulae consist of a velocity term and an acceleration term, for Van Rijn [2007] denoted as respectively drag and inertia terms. Both terms have been derived and plotted for both Nielsen [2006] and Van Rijn [2007] formula in Figure B.51.

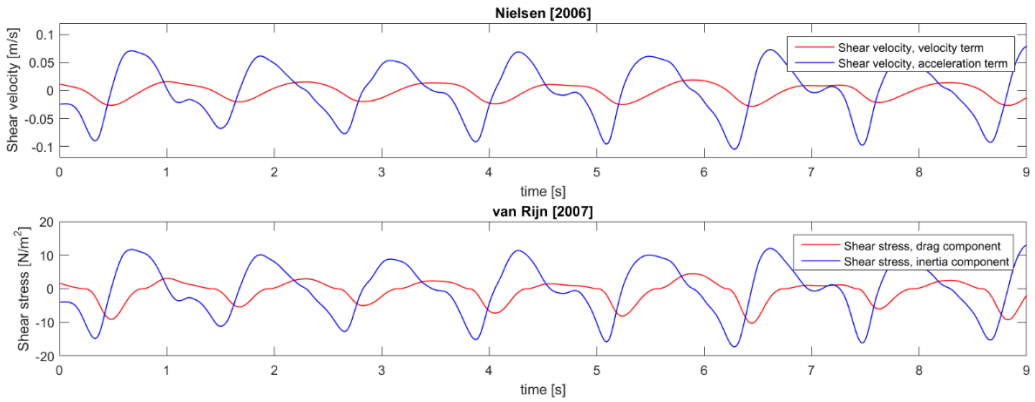

FIGURE B.51 – VELOCITY AND ACCELERATION PART OF BOTH NIELSEN [2006] AND VAN RIJN [2007] FORMULA, BASED ON THE RESULTS OF SLOPE 1:5, S= 0.04.

In Figure B.51, the velocity and acceleration term of the Nielsen [2006] and Van Rijn [2007] formula have been depicted. In both cases one can see that the blue graph, i.e. the acceleration (i.e. inertia for Van Rijn [2007]) term is dominant. Meaning that the acceleration plays a more significant role than the velocity in this test.

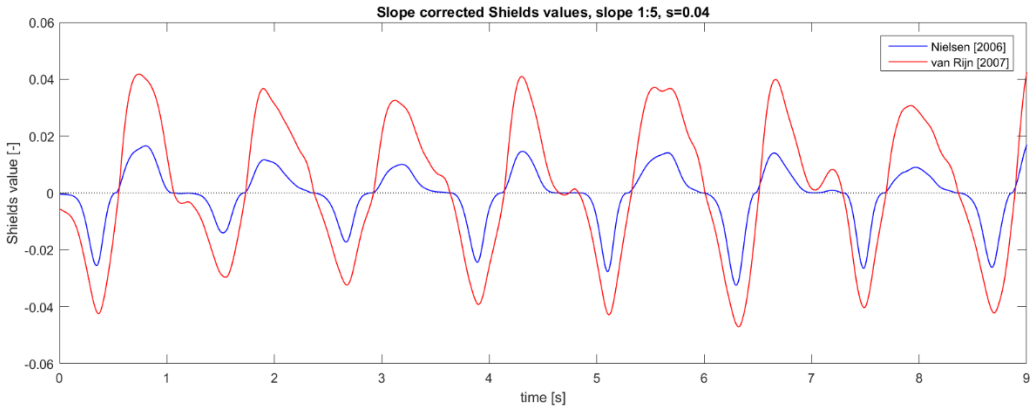

FIGURE B.52 – SLOPE 1:5 CORRECTED SHIELDS VALUES FOR BOTH NIELSEN [2006] AND VAN RIJN [2007]

The characteristic values of derived Shields value are presented in Table B.19. As can also be seen in the graph the negative values (i.e. up slope direction) are dominant. Note that the extreme values are represented in Table B.19 and the graph in Figure B.52 merely represents a fitted curve, which does not include the extreme values.

Shields value based on :	Nielsen [2006]	Van Rijn [2007]
Mean	-1.135×10^{-4}	-0.0025
Max	0.0207	0.0470
Min	-0.0324	-0.0482

TABLE B.19 - CHARACTERISTIC SHIELDS VALUES FOR BOTH NIELSEN [2006] AND VAN RIJN [2007], FOR TEST 1: SLOPE 1:5, S=0.04

In Figure B.52, the slope corrected Shields values for both Nielsen [2006] and Van Rijn [2007] are plotted. Shields stated a critical value at which stones would start to move, for this research this critical Shields value is 0.055. Shields defined different stages of movement, the critical value most

commonly used (0.055) is based on stage 6. Stage 6 is defined as continuous movement at all locations. The lowest stage of Shields, that indicates movement of stones is stage 1, which is defined as occasional movement at some locations. The critical value for this stage is 0.035.

Based on these results, with respect to the irregular wave tests, it appears that the Van Rijn [2007] results in the most realistic Shields values. The Shields values that results from the Nielsen [2006] approach are too low to represent the movement. Because that the waves used for the test represent the highest one percent waves of the wave spectrum used in the irregular wave test.

The fact that the movement of the stones in the 1:5 irregular waves tests was dominantly in the downward direction of the slope, might strike odd when looking at the graph. As the graph presented in Figure B.52, indicates the high Shields values in both directions also in the negative, which indicate upslope velocities and accelerations. Noted should be that, the shields value merely indicates the movement of stones and not the direction. It is therefore reasonable that, the peak of the Shields value breaks the stone free out of the profile, but the soon after followed downward velocities drag the stone down. This is caused by the phase difference between the velocity and the shear stress. At last, the role of gravity which most likely still plays a significant role in the displacement direction of the stones. As the peak of the Shields value indicates a start of movement. Once the stones are 'broken' out of the armor layer gravity force is no longer compensated by the interlocking effects on the slope. This leaves the stone free to move down-slope.

B.2.2.2 TEST 2: COTA= 5, S= 0.06, H= 0.088 M, T= 0.9948 SEC

In this test scenario, the same slope as test 1 has been used, with the same wave height. Merely the wave period, and thus the steepness has been adjusted. To physically exactly represent the highest 1 % of the waves, based on the extrapolation of tolerable damage of Van der Meer [1988] done by Wit [2015]. Following the same methodology of the previous subparagraph, the smoothed results of the second test are plotted in Figure .

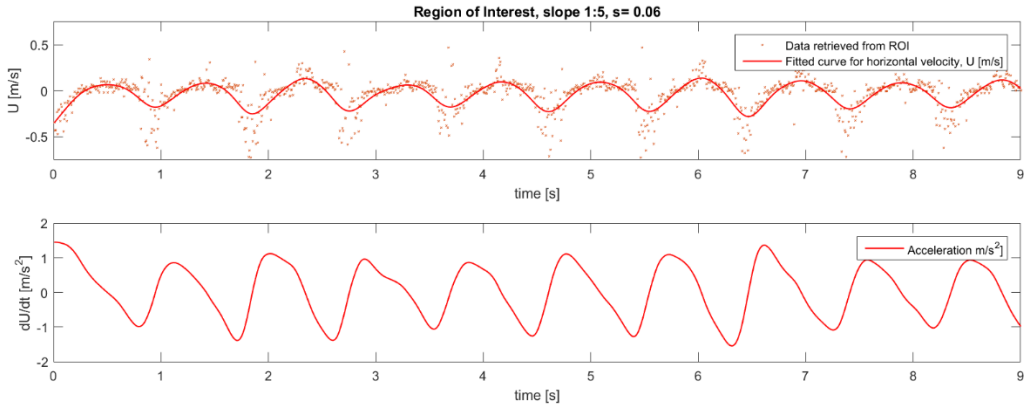

FIGURE B.54 - VELOCITY & ACCELERATION SIGNAL FOR TEST SLOPE 1:5, S= 0.06

Deriving the characteristics from the presented velocity and acceleration signal results in Table B.20. Just as the previous analysis 5 waves have been analyzed in order to gain the following characteristics.

	Velocity U [m/s]	Acceleration dU/dt [m/s²]
Mean	-0.0417	-0.0427
Max	0.1378	1.4534
Min	-0.2513	-1.5433

TABLE B.20 - VELOCITY & ACCELERATION CHARACTERISTICS FOR TEST 2: SLOPE 1:5, S=0.06

Using the linear wave theory to check velocity magnitudes gives, the horizontal particle velocity is the same as for the previous test (i.e. 0.778 m/s) because the wave height and depth are the at the FOV are the same. This agrees with the measured extreme values (the data points in Figure), however note that the input values are based on the fitted curve. The velocity is equal to the derived fitted curve, and the acceleration is the derivative of the velocity. The curve is fitted using a 'smoothingspline' function with a smoothing parameter of 0.99.

The Nielsen [2006] and Van Rijn [2007] both consist of a velocity and an acceleration term. As both the velocity and the acceleration have increased with respect to Test 1, this is visible in the balance between drag and inertia. See Figure B.53.

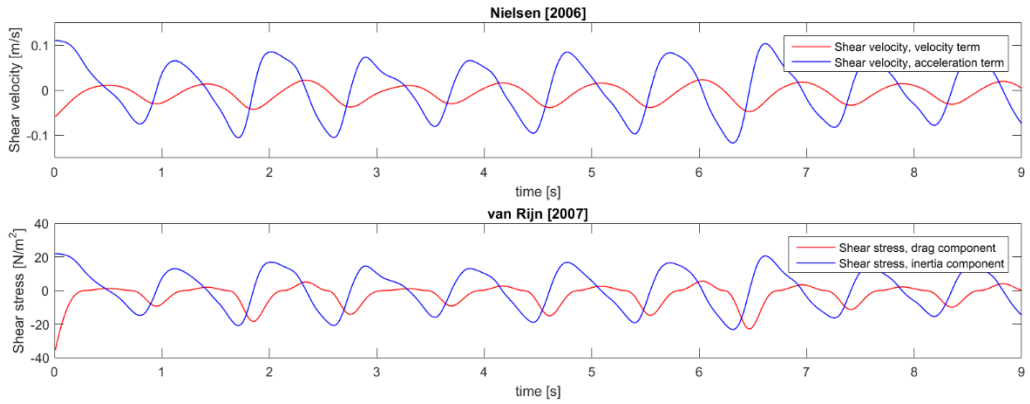

FIGURE B.53 – VELOCITY AND ACCELERATION TERM FOR BOTH THE NIELSEN [2006] AND VAN RIJN [2007] FORMULA, BASED ON THE RESULTS OF SLOPE 1:5, S= 0.06

With both terms for both the Nielsen [2006] and Van Rijn [2007] formula determined, the Shields values can be calculated. The shields values have been corrected for the slope according to the slope correction factor of Fredsøe and Deigaard [1922]. The results are plotted in Figure B.54.

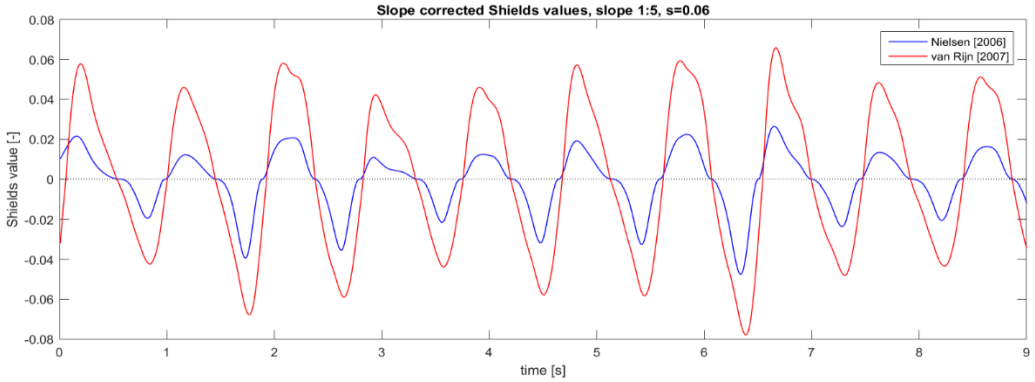

FIGURE B.54 - SLOPE 1:5 CORRECTED SHIELDS VALUES FOR BOTH NIELSEN [2006] AND VAN RIJN [2007]

The characteristic values of derived Shields value are presented in Table B.21. As can also be seen in the graph the negative values (i.e. up slope direction) are dominant.

Shields value based on :	Nielsen [2006]	Van Rijn [2007]
Mean	-0.0006	-0.0014
Max	0.0264	0.0659
Min	-0.0475	-0.0779

TABLE B.21 - CHARACTERISTIC SHIELDS VALUES FOR BOTH NIELSEN [2006] AND VAN RIJN [2007], FOR TEST 2: SLOPE 1:5, S=0.06

Comparing the results of this test (test 2, slope 1:5, s= 0.06) with the test results of test 1 (slope 1:5, s= 0.04), one can see that the Shields values have increased. The higher steepness of test 2 results in higher accelerations, as the wave remains the same the velocities have increased only slightly. The higher accelerations increase the acceleration term in Nielsen [2006] methodology and the inertia term in the Van Rijn [2007] approach.

Comparing the test results with the visual observations during the tests, the Shields values based on Van Rijn [2007] are more realistic. Considering that the highest one percent of the waves of the spectrum used in the Irregular wave tests, one would expect movement of stones under each of these waves. The Shields values based on Nielsen [2006] are indicate a stage 2-3 movement (based on Shields stages of movement) at most, this does not represent the irregular wave tests.

Just as for the previous test, the movement of the stones in downward direction can be explained by the fact that Shields merely indicates a start of movement. The velocity profile has a phase lead over the shear velocity, leading to a shift in velocity just after the peak of the shear velocity. Furthermore, the downslope movement of the stones is reinforced by the gravity.

B.2.2.3 TEST 3: COTA= 10, S= 0.04, H= 0.146 M, T= 1.5503 SEC

For this test the slope angle is altered to 1:10, the waves are based on the highest one percent waves based on the extrapolation of tolerable damage made by Wit [2015]. The wave steepness is kept is set at s=0.04 to create the same type of wave breaking on the slope. The BIV/PIV analysis resulted in a velocity and acceleration signal for 5 waves, as presented in Figure B.55.

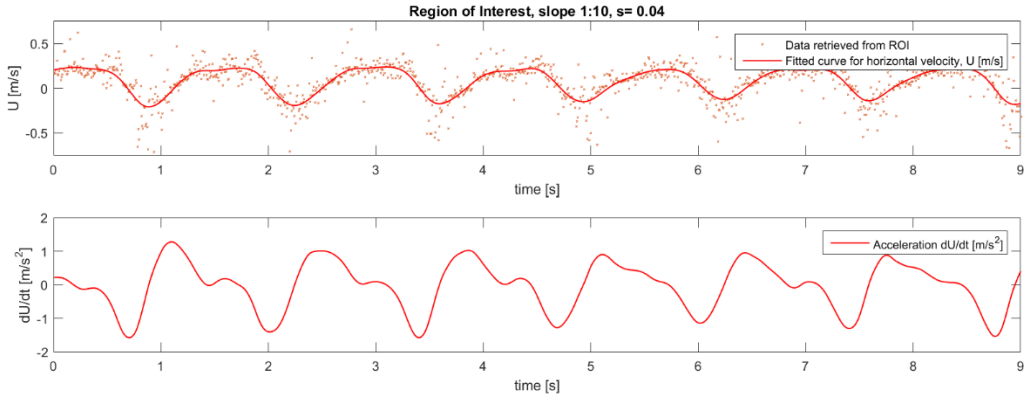

FIGURE B.55 - VELOCITY & ACCELERATION SIGNAL FOR SLOPE 1:10

From these profiles the velocity and acceleration characteristics are derived and presented in

	Velocity U [m/s]	Acceleration [m/s²]
Mean	-0.0019	-0.0005
Max	0.2381	1.2817
Min	-0.2075	-1.5738

TABLE B.22 - VELOCITY & ACCELERATION CHARACTERISTICS FOR TEST 3

The downslope velocity, U_{max}, has increased and is roughly 10 % higher than the upslope velocity of the wave. The difference however is not as significant as was the case on the 1:5 slope, where the upslope velocity was in the order of 50-100% higher. The acceleration however is still higher (roughly 25%) in the upslope direction.

From the derived signals, the velocity and acceleration term of both the Nielsen [2006] and Van Rijn [2007] formula have been determined. Both are depicted in Figure B.56.

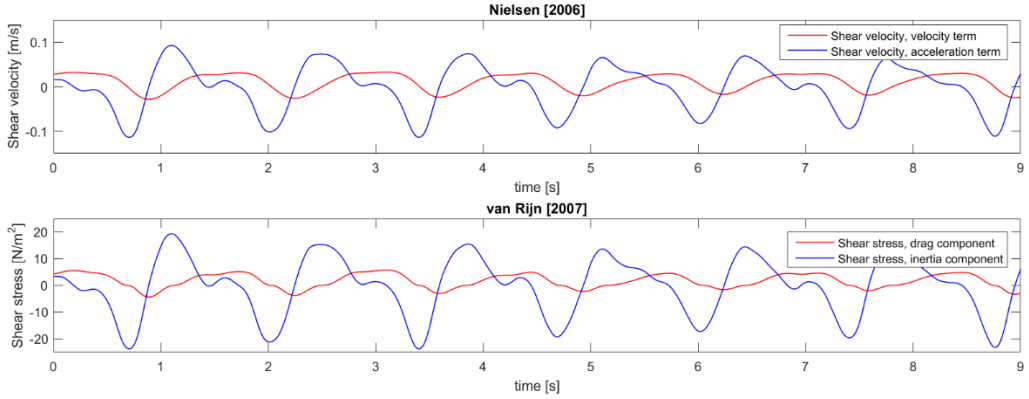

FIGURE B.56 - VELOCITY AND ACCELERATION TERM FOR BOTH NIELSEN [2006] AND VAN RIJN [2007]

Again, the velocity (i.e. inertia) term is the dominant term in the equation, for both the Nielsen [2006] and the Van Rijn [2007] approach. Furthermore, the dominance of the downslope velocity is also visible in the velocity (i.e. drag) term. For both Nielsen [2006] and Van Rijn [2007] the drag and the inertia term have been summed and transferred to Shields values. Furthermore, the slope correction factor has been applied. The results have been plotted in Figure B.57.

In the plot one can see that the order of magnitude for the Shields values of based on both the uprush and down rush of the wave is almost equal, almost even favored for the down rush. As both directions, up- and downslope (i.e. respectively negative and positive) appear to be equally dominant movement in two directions is expected. Noted should be that the gravity has less influence on this milder slope.

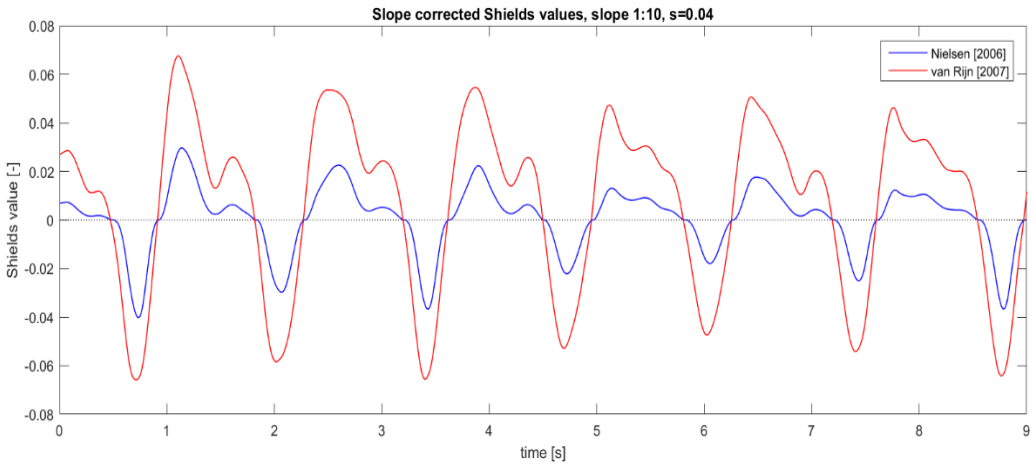

FIGURE B.57 - SLOPE 1:10 CORRECTED SHIELDS VALUES FOR BOTH NIELSEN [2006] AND VAN RIJN [2007]

The characteristic values of derived Shields value are presented in Table B.23. As can also be seen in the graph the negative values (i.e. up slope direction) are dominant

Shields value based on :	Nielsen [2006]	Van Rijn [2007]
Mean	0.0013	0.0087
Max	0.0297	0.0676
Min	-0.0402	-0.0658

TABLE B.23 - CHARACTERISTIC SHIELDS VALUES FOR BOTH NIELSEN [2006] AND VAN RIJN [2007], FOR TEST 3: SLOPE 1:10

The waves used in this test represent the highest one percent of the waves used in the irregular wave test with waves based on the extrapolation of tolerable damage of Van der Meer [1988] done by Wit [2015] (S_{VDM}). Therefore, significant displacement of stones may be expected during these waves. Based on the Shields values derived from this BIV/PIV test, Van Rijn [2007] appears to give the most realistic Shields values. Furthermore, just like the other slope, the Shields values based on Nielsen [2006] are too low.

B.2.2.4 TEST 4: COTA= 15, S= 0.04, H= 0.1872, T=1.790 SEC

For the final test the slope angle is set at 1:15. The waves are based on the extrapolation for tolerable damage made by Wit [2015]. The steepness is kept constant, just like the other tests, at s=0.04. This results in wave period of 1.79 seconds. Analyzing the BIV/PIV test data results in the following velocity and acceleration signal, see Figure B.58. The velocity signal is derived from the data points gathered by the BIV/PIV analysis by fitting a curve through the data. The 'smoothingspline' function of Matlab has been used with a smoothing parameter of 0.99.

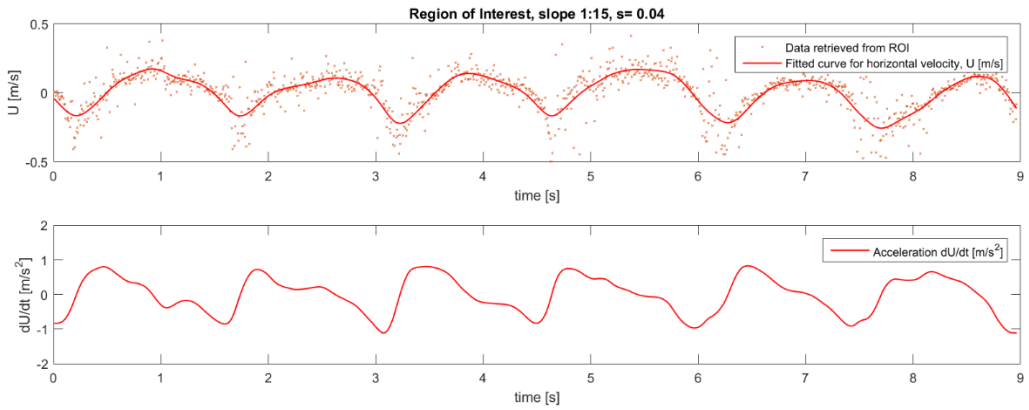

FIGURE B.58 - VELOCITY & ACCELERATION SIGNAL FOR TEST 4

The velocity and acceleration characteristics as presented in Table B.24. The velocity signal is also approximated with the linear wave theory, resulting in a maximum velocity of 1.056 m/s. Based on this approximation, the velocity signal considered a reliable representation of the horizontal velocity. The theory describes the maximum values for the data points, however the smoothed function is used for the analysis. Its characteristics are presented in Table B.24.

	Velocity U [m/s]	Acceleration [m/s²]
Mean	-0.0019	-0.0084
Max	0.1726	0.8278
Min	-0.2577	-1.1111

TABLE B.24 - VELOCITY & ACCELERATION CHARACTERISTICS FOR SLOPE 1:15

The upward velocity is roughly 50 % higher than the downstream velocity, for the acceleration this is roughly 35% higher. The velocity and the acceleration signal are substituted in the Nielsen [2006] and Van Rijn [2007] formulae. As has been done in the analysis of the tests on the steeper slopes, the Nielsen [2006] and Van Rijn [2007] formulae have been split up in their drag and inertia component. This is depicted in Figure B.59.

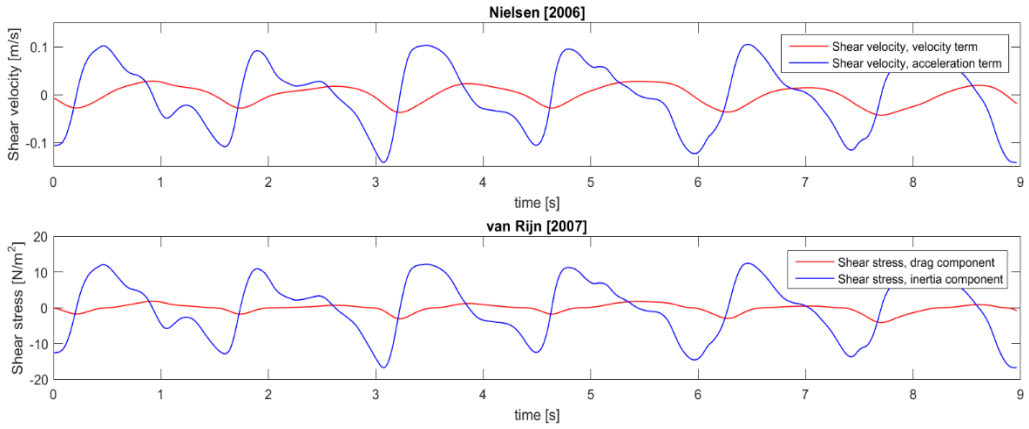

FIGURE B.59 - DRAG AND INERTIA TERM FOR BOTH NIELSEN [2006] AND VAN RIJN [2007]

Firstly, the when comparing the magnitude of the velocity and acceleration term (i.e. drag and inertia term), the acceleration term still is the most dominant term. Furthermore, the order of magnitude of the both components appears to be equal to the test with slope 1:10, only more spread out in time due the increase in wave period.

The drag and inertia term have been added together, for both the Nielsen [2006] and Van Rijn [2007]. Furthermore, the both the Nielsen [2006] and Van Rijn [2007] formulae have been corrected for the slope effects, by the means of the slope correction factor of Fredsøe and Deigaard [1922]. This results in Figure B.60

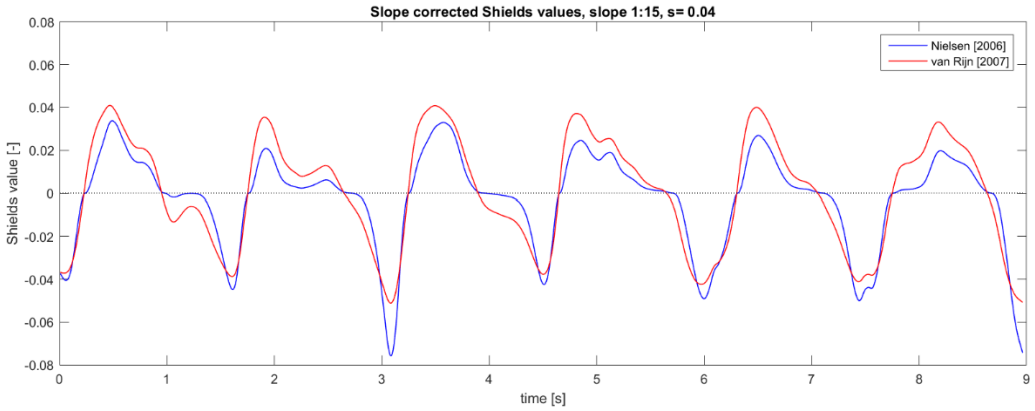

FIGURE B.60 – SLOPE 1:15 CORRECTED SHIELDS VALUES FOR BOTH NIELSEN [2006] AND VAN RIJN [2007]

When examining Figure B.60, firstly one notices that the methodology based on both Nielsen [2006] and Van Rijn [2007] give reasonably good results. Nielsen [2006] however has a significantly lower Shields value for the downslope movement (i.e. positive Shields values), and for the upslope direction (i.e. negative Shields values) both methodologies have Shields values in the same order of magnitude. Except for two solitary peaks, where the acceleration has the lowest values. The fact that the Shields values for both up- and down rush are in the same order agrees with the profile changes found in the irregular wave tests, in which displacement of stones was found in both directions. Furthermore, the influence of the gravity on the direction of the displacement of the stones decreases further.

The characteristic values of derived Shields value are presented in Table B.25. As can also be seen in the graph the negative values (i.e. up slope direction) are dominant.

Shields value based on :	Nielsen [2006]	Van Rijn [2007]
Mean	-0.0025	-0.0008
Max	0.0338	0.0410
Min	-0.0758	-0.0511

TABLE B.25 - CHARACTERISTIC SHIELDS VALUES FOR BOTH NIELSEN [2006] AND VAN RIJN [2007], FOR TEST 4: SLOPE 1:15

B.2.3 CONCLUDING ANALYSIS

In order to get a good oversight of the meaning of the measurements that are made, firstly the derived Shields value characteristics will be presented. Finally, a conclusion will be made whether there is a preference between the Nielsen [2006] and the Van Rijn [2007] methodology.

Nielsen [2006]	Slope 1:5		Slope 1:10	Slope 1:15
	s=0.04	s=0.06	s=0.04	s=0.04
Mean	-0.0001	-0.0005	0.0013	-0.0025
Max	0.0207	0.0264	0.0297	0.0338
Min	-0.0324	-0.0475	-0.0402	-0.0758

TABLE B.26 – SHIELDS VALUE CHARACTERISTICS, BASED ON NIELSEN [2006] FOR ALL TESTS.

Van Rijn [2007]	Slope 1:5		Slope 1:10	Slope 1:15
	s=0.04	s=0.06	s=0.04	s=0.04
Mean	-0.0025	-0.0014	0.0087	-0.0008
Max	0.0482	0.0659	0.0676	0.0410
Min	-0.0470	-0.0779	-0.0658	-0.0511

TABLE B.27 - SHIELDS VALUE CHARACTERISTICS, BASED ON VAN RIJN [2007] FOR ALL TESTS.

Shields described seven different stages of movement can be described, starting from 0. no movement at all, to 1. occasional movement at some locations, to 2. Frequent movement at some locations… to eventually 6. Continuous movement of at all location and 7. General transport of grains. These values have been plotted qualitatively in Figure B.61.

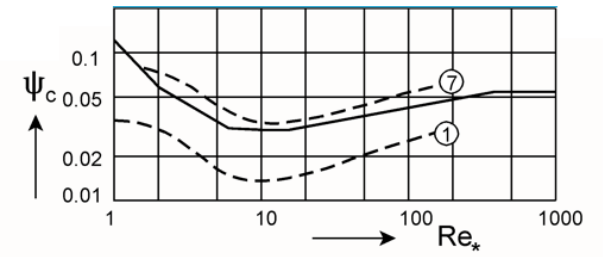

FIGURE B.61 - QUALITATIVE PLOT OF SEVEN STAGES OF MOVEMENT WITH RESPECT TO THE CRITICAL SHIELDS VALUE (SCHIERECK ET AL. [2012])

From this plot one can derive that grains can start moving once the Shields value exceeds a critical value based on level 1. This value approximated at a critical Shields value of 0.035. This coincides with the peaks found in the plots of the Shields value in time. Indicating that the Shields value that is derived from the BIV/PIV measurements indeed suggest that there is movement of stones. The fact this value is only just found, agrees with the fact that the moment of incipient motion is modelled.

Plotting the characteristics that are presented in Table B.26 and Table B.27, results in Figure B.62. The Iribarren values are defined as

$$\xi = \frac{\tan \alpha}{\sqrt{s}} \qquad \text{Equation 1.4}$$

This results in the Iribarren values of 1.0, 0.82, 0.5 and 0.33 for respectively test 1, test 2, test 3 and test 4. (i.e. Slope 1:5 with s=0.04, slope 1:5 with s=0.06, slope 1:10 and at last slope 1:15). The results are presented in Figure B.62, where the red shapes indicate the characteristic values for the Van Rijn [2007] approach, and the blue shapes represent the approach based on Nielsen [2006]. The approach based on Van Rijn [2007] almost always has the more extreme values, except for during uprush (i.e. negative Shields values) on the 1:15 slope (ξ= 0.33).

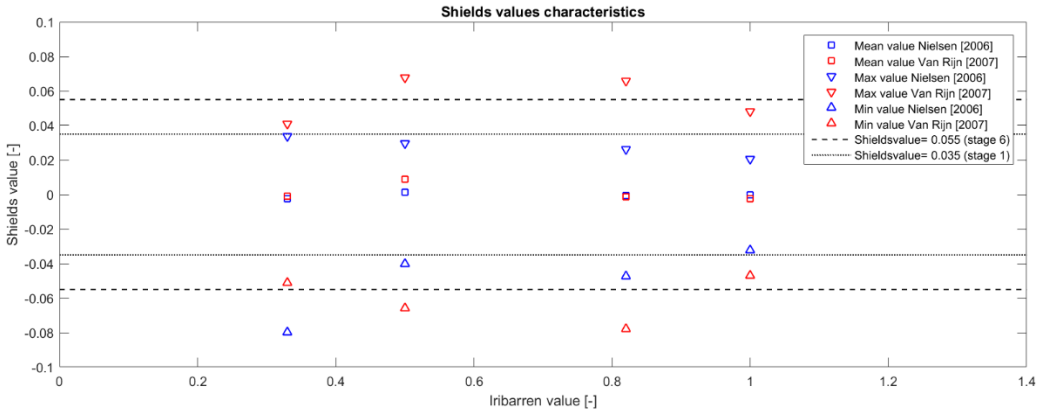

FIGURE B.62 - CHARACTERISTIC SHIELDS VALUES VS. IRIBARREN VALUE

The Van Rijn [2007] approach gives Shields values of roughly 0.055, which coincides with Shields's stage 6 transport. Whereas the approach based on Nielsen [2006] results in Shields values of around 0.035 (i.e. Shields's stage 1). This would indicate occasional movement at some locations.

When comparing the order of magnitude of the Shields values, with the damage that occurred during the profile change tests and the visual observations that were done during the tests. Significant movement was seen under the highest waves in the spectrum. The wave height in the BIV/PIV tests is based on the highest one percent waves of the spectrum, that was used in the S_{VDM}[8] tests. Therefore, the BIV/PIV roughly represent the waves under which incipient motion is found.

The Nielsen [2006] approach results in Shields value just around the Shields's first stage of movement, which is an underestimation of the displacement. This conclusion is based on the visual observations during the profile change tests, in which significant movement was observed during the highest waves of the spectrum. The Van Rijn [2007] approach does describe this type of movement and therefore, based on the visual observations together with test results, gives the most reliable results.

Furthermore, note that Nielsen [2006] and Van Rijn [2007] only this similar when Nielsen [2006] applies accurate parameters, for the phase lag angle (φ) and the sediment friction coefficient (f_s). As is presented in Figure B.63, in which both Nielsen [2006] and van Rijn [2007] are plotted with the correct parameters, derived from the BIV/PIV measurement. Furthermore, in Figure B.63, in the plot Nielsen [2006] with the standard parameters (φ = 25° and f_s=0.025) is presented. The example is given for the 1:10 slope, as has been done throughout this research.

[8] The used spectrum, was based on the extrapolation of tolerable damage of Van der Meer [1988], as was done by Wit [2015], denoted as S_{VDM}

However, in all test results the accuracy of the parameters used in the Nielsen [2006] approach is as significant as presented in Figure B.63.

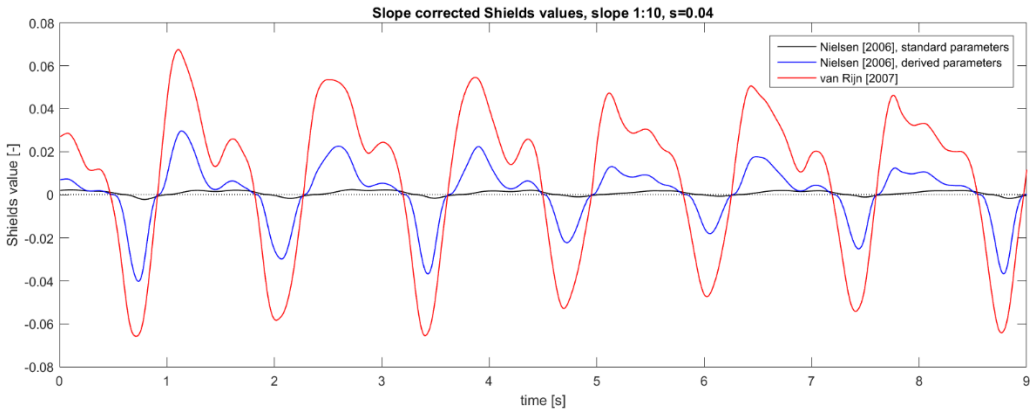

FIGURE B.63 - THE ACCURACY OF NIELSEN [2006] WITH STANDARD PARAMATERS.

From the plot in Figure B.62 one can derive that both the Nielsen [2006] and Van Rijn [2007] appear to give equally reasonably accurate results, with the accurate parameters. However, this is only the case when the parameters in the Nielsen [2006] formula can be accurately determined. Since these parameters have such a significant influence on the accuracy and thus the reliability of the results, this is crucial (see Figure B.636). For the Van Rijn [2007] formula, the dependency on the accuracy of the parameters is most likely equally important, however for the Van Rijn [2007] formula the parameters easily determined and can thus be derived for any slope situation under which only basic details are known.

Therefore, based on the results from this study, it seems that the Van Rijn [2007] approach to describe the stability is the most accurate. Furthermore, the constants in the Van Rijn [2007] are derivable from merely basic details of the slope.